8-9-2006

The Mineralogy, Geochemistry and Phosphate Paragenesis of the Palermo #2 Pegmatite, North Groton, New Hampshire

James Nizamoff
University of New Orleans

THE MINERALOGY, GEOCHEMISTRY & PHOSPHATE PARAGENESIS OF THE PALERMO #2 PEGMATITE, NORTH GROTON, NEW HAMPSHIRE

A Thesis

Submitted to the Graduate Faculty of the
University of New Orleans
in partial fulfillment of the
requirements for the degree of

Master of Science
in
Geology and Geophysics

by

James W. Nizamoff

B.A., University of Maine at Farmington, 1996

August 2006

Acknowledgements

I'm gratefully indebted to Dr. William "Skip" Simmons, Alexander U. Falster and Dr. Karen Webber for their support, patience and all the wonderful opportunities provided to me at UNO. Thank you so much for your friendship and all the great experiences. Special thanks to Al Falster for always being there and helping to keep me sane during trying times. I can't really say how much I appreciate everyone from the MP^2 crew without writing a Falster-sized acknowledgement.

Thanks to Dr. Michael "Mike" Wise for introducing me to pegmatites in a scientific sense and for imparting unto me some of his great knowledge. Thanks to Mike for also realizing that pegmatites rule.

Special thanks to R.W. "Uncle Bob" Whitmore for providing me a great pegmatite to study as well as introducing me to and getting me hooked on phosphate mineralogy. Bob's support of mineralogical research interests is unmatched and greatly appreciated by all the people who have been fortunate enough to work with him.

I owe a great many thanks to Chandra Dreher who has contributed significantly to the quality of this work. Chandra has spent many hours helping with illustrations, tables and formatting. Her support and love are greatly appreciated!

I'd like to thank the many members of Bob Whitmore's "volunteer" slave mining crew at Palermo (especially Steffen Hermanns, Scott Higgins, Gordon Jackson and Rob Lawrence) for their help with sample collection, logistics, lodging, beverages, etc. in the field.

Special thanks to Jace Pearson for his assistance in the field, for providing me a place to sleep during my numerous trips to Maine and being a great friend.

Several colleagues deserve special mention (as they enjoy phosphates almost as much as I do) for their assistance and valuable discussion regarding phosphate mineralogy. Thanks to Dr. Alessandro Guastoni and soon to be Dr. Fernando Colombo for all the stimulating conversation and insight regarding pegmatites. I would also like to thank Dr. André-Mathieu Fransolet and Dr. Frédéric Hatert of the Université de Liège, Belgium for their helpful suggestions and constructive comments regarding my research.

Thanks to Cathe Brown for her assistance with XRF analyses at the Smithsonian, for harassing Mike Wise, and making my time spent at PegCamp a more enjoyable experience.

Special thanks to Ray Sprague for actually selling me a piece of montebrasite from the Emmons Quarry. Also thanks for running the Maine Pegmatite Workshop and giving me a hard time for all these years.

I would also like to thank Mary and Dudy Groves for providing a wonderful facility to learn about pegmatites. I learned a great deal of what I know about pegmatites while staying at Poland Mining Camps.

Thanks to the many students at UNO that have had the fortitude to discuss and/or study pegmatites with me: Brian S. Giller, Morgan and Pam Masau, Peter Tice, Roberta Johnson, Brenda Yawn, Julie Pertuit, Michelle Abraham, Randy Elder, Tabitha Hensley and others.

I'd also like to thank my parents Anne and William Nizamoff for their support and patience. Thank you for allowing me the chance to do this, I couldn't have done without you.

Table of Contents

List of Tables

List of Figures

Abstract

An investigation of the beryl-phosphate subtype Palermo #2 pegmatite, located in the Grafton pegmatite field of New Hampshire, has revealed a large number of phosphate species. Late-stage, carbonate-bearing aqueous fluids have metasomatically altered primary phosphates producing a suite of nearly forty species of secondary phosphates.

The secondary phosphates at Palermo #2 are a result of alteration of primary phosphates and associated silicate, carbonate, sulfide, arsenide and oxide minerals locally present in the core margin. Concomitant alteration of these associated minerals contributes the necessary ions to the hydrothermal fluids responsible for the formation of the diverse suite of secondary phosphates. Alteration of the mineral assemblage occurring in a given area creates a collection of secondary phosphates characteristic of that specific assemblage, whereas a completely different collection of secondary phosphates may appear only a few centimeters away. Thus, each suite of secondary phosphates is the product of its specific microenvironment of alteration.

Introduction

The Palermo #2 granitic pegmatite is located approximately one and one-half miles west-southwest of the village of North Groton, New Hampshire and along with numerous other pegmatites in the vicinity, is part of the Grafton pegmatite field of west central New Hampshire (Figure 1). The Palermo #2 pegmatite and related pegmatites of the Grafton field may be classified as weakly- to moderately-evolved beryl type rare-element pegmatites (Černý and Ercit 2005, Černý 1991a). Černý and Ercit further divide the beryl type into beryl-columbite and beryl-columbite-phosphate subtypes. Pegmatites of the beryl-columbite-phosphate subtype typically display enrichment of beryllium, phosphorus and a greater abundance of niobium versus tantalum. The lack of abundant columbite-tantalite and presence of great quantities of phosphate minerals in the Grafton field suggests that the majority of these pegmatites should be classified as beryl and beryl-phosphate subtypes.

Francis *et al*. (1993) states that no significant field or geochemical studies have been done on the Grafton pegmatite field. Relatively few comprehensive studies of pegmatites belonging to the beryl-phosphate or beryl-columbite-phosphate subtypes exist. However, with the important contributions to the body of knowledge regarding phosphates made by P.B. Moore and coauthors during the 1970's, pegmatite phosphate mineralogy and geochemistry has received more attention from researchers in the last thirty years. Numerous significant works (Moore, 1971; Moore 1973, Moore *et al*., 1975; Mücke 1981; Moore, 1982; London and Burt 1982; Shigley and Brown 1985; Campbell and Roberts 1986; Fransolet *et al*.1986; Keller and Von Knorring 1989; Roda *et al*. 2004) involving the description and geochemistry of phosphate mineral

assemblages in granitic pegmatites have been published in the last thirty years. The current study has been devised based on the objectives and results of those works listed above.

In the Grafton pegmatite field the beryl-columbite-phosphate and beryl-phosphate pegmatites are the most mineralogically evolved pegmatites exposed in the field. Primary pegmatitic phosphates such as triphylite-lithiophilite and montebrasite-amblygonite frequently suffer one or more alterative processes resulting from interaction with postmagmatic aqueous fluids (London and Burt 1982). Alteration of primary phosphates by the processes of cation/anion leaching, oxidation/reduction, hydroxylation, hydration, and cation addition/exchange may generate a wide range of secondary phosphate species (Moore 1973). Approximately 200 secondary phosphates have been identified from pegmatites, indicating that highly variable and complex chemical interactions must take place to form such a wide range of species. Careful examination of phosphate paragenesis may help elucidate the nature of the interactions resulting in the formation of secondary phosphates.

The geochemistry and petrogenesis of beryl-columbite-phosphate and beryl-phosphate pegmatites is not well known as most research has focused on descriptive mineralogy. The two main objectives for this investigation include: 1) detailed description of the mineralogy of the Palermo #2 with emphasis on the phosphate mineralogy, geochemistry and paragenesis; and 2) the identification of geochemical fractionation trends in individual mineral phases and whole-rock samples.

Previous Work

The Grafton pegmatite field has been the subject of relatively little scientific work aside from the description of the unusual mineralogy present in several pegmatites. The Palermo #1 pegmatite has had much attention focused on the wealth of phosphate minerals that occur there. No less than sixty-nine phosphate minerals occur at Palermo #1, eleven of which were first described from the location (Segeler *et al*. 1981; Francis *et al.* 1993). However, most research has pertained to the description of new mineral species. Investigations covering broader topics including mineral paragenesis and geochemical fractionation trends are lacking. Geochemical data for pegmatites from the Grafton field is extremely limited with the exception of a few small sets of analyses by Moore (2000), London *et al*. (1990) and others. No large scale geochemical and/or petrogenetic investigations have been undertaken regarding the pegmatites of the Grafton field.

The Palermo #2 pegmatite in particular has been overlooked scientifically since it does not contain gigantic crystals and masses of primary phosphate minerals comparable to those found at the Palermo #1. The Palermo #2 has also experienced much less mining in terms of tonnage removed than the Palermo #1. Significant portions of the core/core margin that contain the most evolved mineral assemblages are accessible at Palermo #1 while very little of these zones is exposed at Palermo #2.

The Palermo #2 mine was opened between 1888 and 1890 by the Palermo Mining Company, Syracuse, New York which leased the property from 1886-1888. The company later bought the property outright and owned it from 1888-1898. A relatively small open cut was made during this time to assess the mica potential of the pegmatite.

In 1900 the General Electric Company of Schenectady, New York purchased the mineral rights to the Palermo #2 and surrounding pegmatites. A small amount of work was done at the Palermo #2 mine between 1914 and 1918 to provide mica during World War I. Palermo #2 saw a period of inactivity between 1919 and 1941 (Whitmore personal communication 2002). With the outbreak of World War II and corresponding increase in the demand for mica, General Electric started work at Palermo #2 in 1942 under the supervision of Leon Churchill (McNair 1943). The existing small open cut was enlarged to dimensions of approximately 50 meters in length, 10 meters in width and a depth of 3-14 meters and two inclines (~ 13 m in depth) running parallel to the general strike of the pegmatite were sunk (McNair 1943). As part of the U.S. Geological Survey's Pegmatite Investigations program from 1942-1945, the mine was visited periodically by D.M. Larrabee and L.R. Page during 1942-43 and mapped by A.H. McNair and J.H. Chivers in May 1943. Additional maps updating the progress of mining were made by V.E. Shainin and E.N. Cameron during 1943-44. General Electric ceased mining in July 1944 and in April 1945 the mine was remapped by McNair and F.H. Main (Cameron *et al*. 1954). Cameron *et al*. (1954) reported that the Palermo #2 pegmatite is approximately 400 meters in length and varies from 7 to 50 meters in width. The pegmatite strikes N 20º E and dips E-SE at 80-85º. Cameron *et al.* (1954) also contains a description of the zonation and mineralogy of the pegmatite. A border, wall, outer intermediate, core margin and core zone were observed. Major minerals reported were quartz, plagioclase, muscovite, perthite, biotite, schorl, beryl, triphylite and vivianite. In 1958 Mountain Mining Company of Spruce Pine, North Carolina purchased the mineral rights to the property and mined mica from 1958 until 1961

(Whitmore and Lawrence, 2004). In 1961 the U.S. government ended mica subsidies effectively causing the cessation of mica mining in the area (Whitmore personal communication 2002).

From 1996 to present R.W. Whitmore of Weare, New Hampshire has been working the Palermo #2 for beryl and phosphate mineral specimens. Nizamoff *et al*. (1998) and Nizamoff *et al*. (2002) provided an updated account of phosphate mineral descriptions and associations revealed by the recent mining activity that were previously unknown from the Palermo #2 pegmatite.

The age and timing of emplacement for the pegmatites of the Grafton field is a still unanswered question. No detailed geochemical and field studies to determine the petrogenetic origin of the pegmatites have been undertaken in the Grafton field. Several Acadian to post-Acadian orogeny granitoids of the New Hampshire Plutonic suite outcrop within 10 km of the Palermo #2 pegmatite and may have served as the parental source for the pegmatites of the Grafton field. Page (1937) proposed a genetic relationship between pegmatites in the Rumney quadrangle and the various intrusives present (Concord granite, Bethlehem granodiorite and Kinsman granodiorite); reporting pegmatites relating to each intrusive. Page ultimately suggested the majority of said pegmatites were derived from the Concord granite. Cameron *et al*. (1954) suggested the pegmatites could be related to a member of the Concord suite of granitic plutons of the syn- to post-tectonic New Hampshire Plutonic Suite given the pegmatites display no readily discernable deformation or cross-cutting relationships with the Concord granite. Francis *et al*. (1993) also proposed an apparent genetic relationship between the Palermo #1 pegmatite of the Grafton field and the Concord granitic plutons based on

the observations of Cameron *et al*. (1954). Field work was conducted by the author in order confirm these observations and possibly add new data to those already existing.

Background

The Grafton pegmatite field (Francis *et al*. 1993) of west central New Hampshire has an areal extent of approximately 700 km^2 and is composed of several hundred granitic pegmatites occurring in generally northeasterly trending linear belts (Cameron *et al*. 1954) (Figure 1).

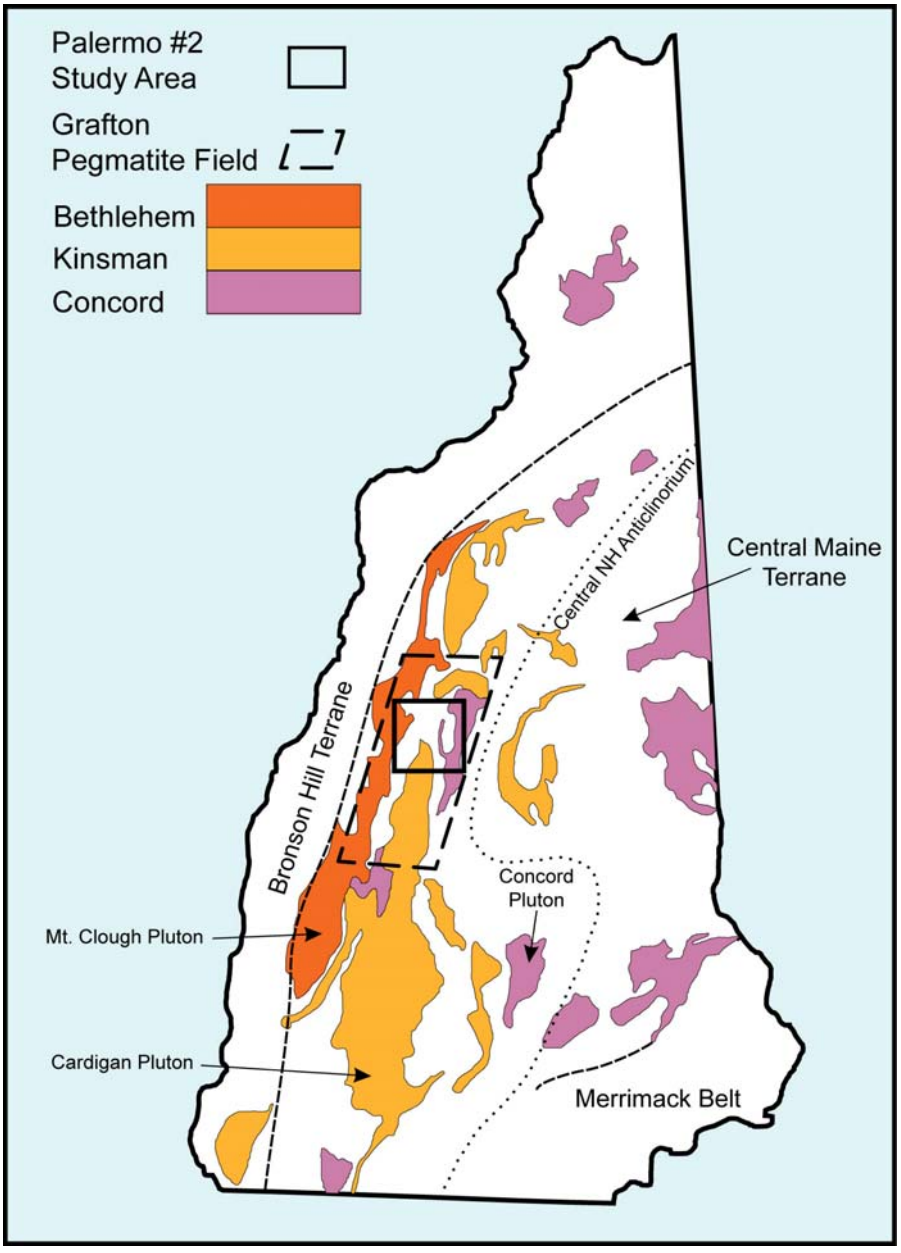

Figure 1: Map delineating the Grafton Pegmatite Field and the Palermo #2 study area, Grafton County, New Hampshire. Syn- and post-Acadian plutonic granitoids are highlighted (Modified from Dorais, 2003).

The Grafton field is known for pegmatites that are generally considered to display low to medium degrees of geochemical and mineralogical evolution (barren; beryl; beryl-phosphate and beryl-columbite-phosphate subtypes). Several pegmatites in the Grafton field are world renowned for producing a wide variety of primary and secondary phosphate minerals (Palermo #1 mine, Fletcher mine, Charles Davis mine).

The Palermo #2 (N 43º 45.137' W 71º 53.632', elevation ~ 538 m) and at least fifty-seven related granitic pegmatites in the immediate area are located in the extreme southern portion of the Rumney 15 minute quadrangle in Grafton County, New Hampshire.

The Rumney 15 minute quadrangle is located within the Acadian orogenic belt of the New England Appalachians. The New England Appalachians were formed by the Taconic and Acadian orogenic events that commenced during the early Paleozoic. The first stage of the building process of the Appalachians, the Taconic orogeny, involved the three continental masses of Laurentia, Gondwana and Baltica. These three blocks collided resulting in the formation of the Caledonides in Europe and Greenland and in the formation of the Appalachians of eastern North America. The New England Appalachians were created by the collision of Laurentia and the northwestern portion of Gondwana (Osberg *et al.* 1989).

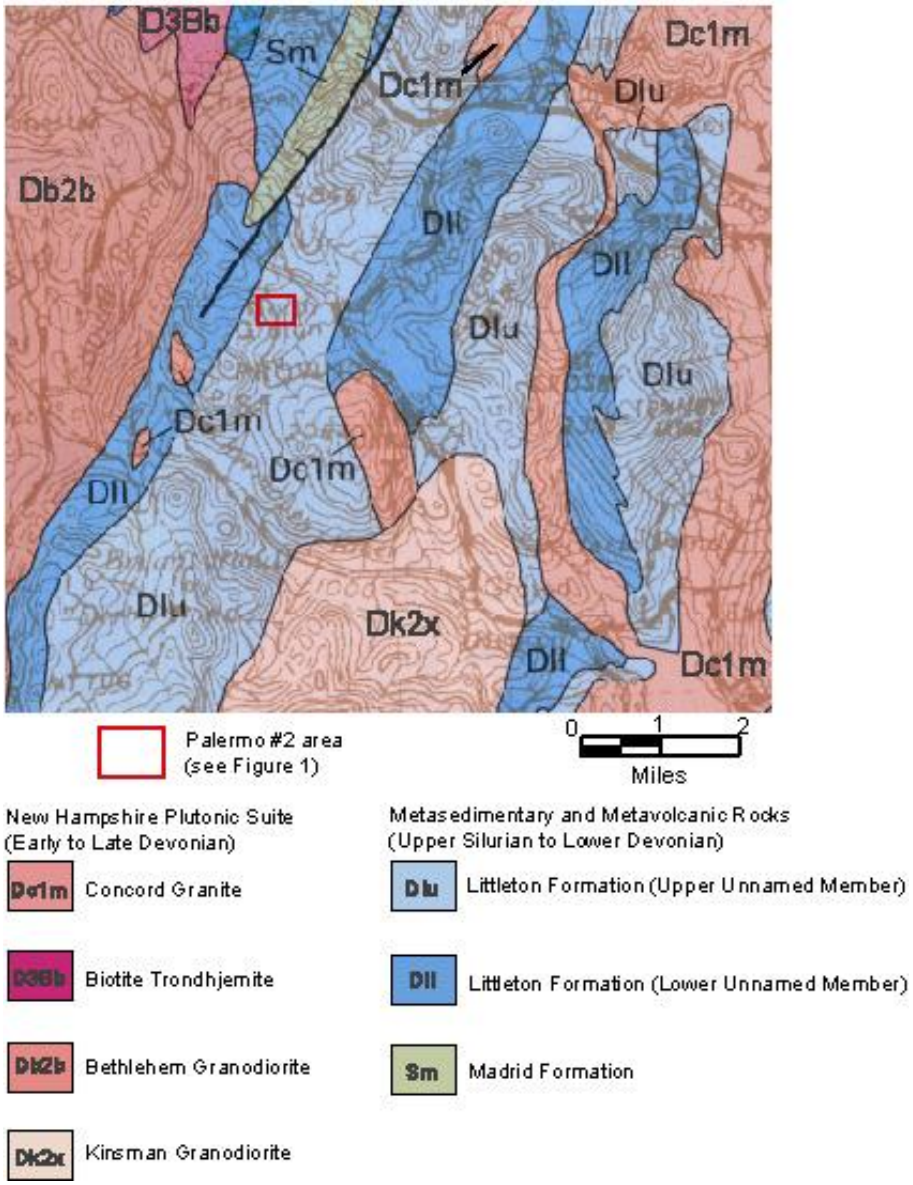

Figure 2: Bedrock geologic map of a portion of Grafton County, NH denoting the location of the Palermo #2 pegmatite (Modified from Lyons *et al*., 1997 and Malinconico, 1982).

The emplacement of the Palermo #2 pegmatite most likely occurred syn- or post-Acadian orogeny. The Acadian orogeny (from ~420 to 360 Ma) involved numerous events including the deposition of flysch and molasse, episodic volcanic activity, several installments of folding and faulting, and emplacement of syn-, late- and post-tectonic intrusives with corresponding episodes of metamorphism; all relating to the collision of the microcontinent Avalonia with Laurentia (Osberg *et al.* 1989).

The Palermo #2 pegmatite is hosted by the sillimanite-muscovite grade metamorphic rocks of the upper unit (Kearsarge) of the Devonian Littleton formation. The Kearsarge member of the Littleton is composed of alternating beds of mica quartzite and mica quartz sillimanite schist that typically display graded bedding features (Malinconico 1982). These units were deposited as flysch during the later stages of the closing of Iapetus ocean during the early Paleozoic (Malinconico 1982).

The timing of the metamorphic and deformative events in central New Hampshire is discussed by Spear *et al*. (2002); Eusden and Lyons (1993); and Eusden and Barreiro (1989). Malinconico (1982) reports three episodes of deformation and/or metamorphism in the southeastern Rumney quadrangle during the Acadian orogeny: 1) metamorphism (M1) producing a staurolite-andalusite/kyanite assemblage with associated folding (D1) (possibly synchronous with the emplacement of the Kinsman granodiorite and Bethlehem granodiorite); 2) minor deformation (D2) with introduction of mild folding about east-west axes; 3) a more intense deformation (D3) with tight folding about northeasterly plunging axes. This deformative episode was accompanied by high grade metamorphism (M2) to a sillimanite-muscovite assemblage.

Several possible granitic parent bodies belonging to the syn- to post-orogenic New Hampshire Plutonic Suite (NHPS) are located within an 11 km radius of the Palermo #2 and related pegmatites (Figure 2). Foliated, gneissic S-type peraluminous granitoids of the Cardigan and Rumney plutons of the syntectonic Kinsman intrusive suite (413 ± 5 Ma, Barreiro and Aleinikoff, 1985) are located approximately 3 km southeast and 11 km northeast respectively. The Mt. Clough granodiorite of the Bethlehem intrusive suite (410 ± 5 Ma, Lyons *et al*., 1997) is located approximately 2.5

km to the west (Clark and Lyons 1986). Like the Kinsman Intrusives, the Mt. Clough granodiorite exhibits a fairly distinctive foliation texture (foliation exhibited is likely a result of D3). A portion of the post-tectonic Concord two-mica granite intrusive suite outcrops approximately 3 km to the south in the Jewell Hill area (Cameron *et al*. 1954). Lyons *et al*. (1997) reports a U/Pb age of 373 Ma for the Newfound Lake pluton of the Concord suite. The Concord granite does not display evidence of deformation (i.e. foliation). Malinconico (1982) reports retrograde metamorphism in the Rumney area may be related to the Concord granite. Whole-rock geochemical analyses of the Concord granite, Bethlehem granodiorite and Kinsman granodiorite are reported in Appendix I.

The NHPS granitoids are thought to have been derived from a magma-mixing process involving the anatexis of crustal rocks from the Central Maine Terrane (CMT), the Bronson Hill Anticlinorium and the possible involvement of a separate (likely mantle-related) magma source (Dorais 2003, Spear *et al.* (2002) and Lathrop *et al*. 1996).

Cameron *et al.* (1954) suggested that the pegmatites in the Palermo area might be related to the Concord granite due to the lack of cross-cutting relationships and the absence of deformation-related textures. Field work by the author has shown evidence that a phosphate-bearing pegmatite crosscuts the Concord granite approximately 3 km from the Palermo group of pegmatites in the Jewell Hill area. The Esty pegmatite is clearly syn- or post-Concord granite as it crosscuts and displays sharp contacts with the granite. The Esty pegmatite contains large masses (up to 10 cm) of a primary arrojadite group mineral as well as other phosphate species, suggesting a common provenance

with the pegmatites of the Palermo area. These observations suggest that the Palermo #2 pegmatite was likely emplaced syn- to post-Concord granite.

Clearly, additional work is needed in order to better establish a petrogenetic link between the pegmatites of the Grafton pegmatite field and potential parental plutons or other rocks (host rocks, etc). Isotopic analysis (Sm-Nd) and U-Pb age-dating of pegmatitic wall zone rocks, proximal granitoids and pegmatite host rocks could help constrain a possible granite-pegmatite relationship.

Methods

Field work and sample collection

Samples examined during this study were collected beginning in May 1997. Periodic sampling trips were made subsequently to coincide with mining activity. In addition to the samples collected by the author, R.W. Whitmore provided numerous specimens for research.

Whole-rock samples were collected along a linear traverse of the open cut so as to obtain a representative sampling of each pegmatite zone. The whole-rock samples were collected at 15 sites along the traverse and at least 2 kg of material was obtained at each site. Approximately 200-300 grams of material from each traverse sample site was ground to a particle size of approximately 0.3 to 1 mm. A heavy liquid separation using lithium metatungstate was carried out and the corresponding heavy (> 2.80 g/ml) and light fractions (< 2.80 g/ml) examined under a binocular stereomicroscope. Mineral separates were hand picked from the whole-rock and heavy liquid separation samples under a binocular stereomicroscope. The picked grains were then examined under the scanning electron microscope. Selected grains were then prepared for electron microprobe analysis.

Scanning Electron Microscope

Energy dispersive spectral analysis and backscattered electron images of polished mounts and mineral samples affixed to conductive putty were collected using a digital AMRAY 1820 scanning electron microscope. Polished mounts were prepared in the same fashion as those for the electron microprobe. Loose mineral and rock samples were attached to an aluminum sample stub with conductive putty and sprayed

with a conductive coating. Operating conditions for energy dispersive spectral analysis and backscattered electron imagery included an acceleration potential of 15-25 kV, 400 micron final aperture, 18 mm working distance, 0 to 35 degrees sample tilt, and 3.0 spot size. Backscattered electron images were collected using a frame size of 512x512 pixels and X-ray maps collected at 256x256 pixels with a 20-50 ms dwell time per pixel. Data and images were acquired using Iridium/EDS2000 software by IXRF Systems, Inc.

Electron Microprobe

Samples analyzed by the electron microprobe were mounted in epoxy, ground down and polished to a flat, high finish using a Buehler polishing table. Polishing consisted of three steps: 1.0, 0.3 and 0.05 micron alumina grit. Samples were rinsed and placed in an ultrasonic cleaner to remove excess polishing compound. The samples were then rinsed with distilled water and allowed to dry. After drying the samples were coated with 250 ± 20 angstroms of carbon under a vacuum of 1×10^{-5} Torr. Coated samples were kept in a desiccator before being placed in the microprobe.

Quantitative chemical analyses were acquired by Alexander U. Falster using a fully automated ARL-SEMQ electron microprobe. Operating conditions for feldspars, micas, and phosphates included: 15 kV acceleration potential, 15 nA beam current and 60 seconds counting time. MAN was used for background determinations. A 1-2 micron beam diameter was used for feldspars, micas and phosphates. For beam sensitive phosphates the beam diameter was adjusted to 3-4 microns. Standards used for analyses of feldspars, micas and phosphates included: Clinopyroxene (Si K_α, Fe K_α, Ti K_α, Ca K_α, Mg K_α), Albite (Si K_α , Al K_α, Na K_α), Fibbia adularia (Si K_α, Al K_α, K K_α), Plagioclase An_{50} (Si K_α, Al K_α, Ca K_α), Cerro de Mercado apatite (P K_α, Ca K_α, F K_α),

Fayalite (Si K_α, Fe K_α), Rhodonite (Si K_α, Mn K_α), Andalusite (Si K_α, Al K_α), Fluortopaz (Al K_α, Si K_α, F K_α), Strontium sulfate (Sr L_α), Barium sulfate (Ba L_α), Pollucite (Cs L_α) and Rubidium Leucite (Rb L_α).

MAN standards for feldspars, micas, and phosphates included: Periclase, hematite, vanadium(V) oxide, zinc oxide, quartz, fluorite, as well as any of the above where applicable.

Operating conditions for Nb-Ta oxides and zircon included: 25 kV acceleration potential, 20 nA beam current and 60 seconds counting time. MAN was used for background determinations. A 2-3 micron beam diameter was used for analyses of Nb-Ta oxides and zircon. Standards used for analyses of Nb-Ta oxides and zircon included: Zirconium(IV) oxide (Zr L_α), manganotantalite (Ta M_α, Mn K_α), yttrium niobate (Nb L_α), Tin(IV) oxide (Sn L_α), Hematite (Fe K_α), rutile (Ti K_α), Bismuth germanate (Bi M_α) and stibiotantalite (Sb L_α).

MAN standards for Nb-Ta oxides and zircon included: Periclase, hematite, vanadium(V) oxide, quartz, fluorite, zinc oxide, Harding microlite, as well as any of the above where applicable.

Data were processed via Probe for Windows by MicroBeam, Inc.

X-Ray Diffractometer

X-ray diffraction patterns of powdered mineral samples were obtained using a SCINTAG XDS 2000 X-ray diffractometer (Cu $K\alpha$ radiation). Powder patterns were run over a range of 2-70° 2 theta using a step size of 0.04 to 0.1° 2 theta. X-ray powder diffraction data was acquired and processed by DMSNT (Diffraction Master Systems for Windows NT) by Scintag, Inc.

Single crystal X-ray diffraction patterns for mineral identification were obtained via a Gandolfi camera. Sample run times were dependent on sample size and Fe content and varied between 8 and 24 hours.

X-Ray Fluorescence Spectrometry

Analyses of whole rock samples using X-ray fluorescence spectrometry were performed at the Smithsonian Institution, Washington, D.C. and at the Coordinated Instrumentation Facilities at Tulane University. Samples were pulverized in tungsten carbide and ceramic (alumina) mills using a Spex shatterbox. Mills were decontaminated between samples using an expendable charge for each new sample. Sample run times ranged from ~ 10 to 20 minutes depending on the hardness of the material.

Samples analyzed at Tulane University included a suite pulverized in a tungsten carbide mill and a suite pulverized in a ceramic mill. For each sample approximately 4 g of sample was weighed out and mixed with ~ 0.9 g of Hoechst Wax C Micropowder using a Retsch Mixer at 20 rpm for 3 minutes. The mixed samples were then pressed into pellets. The finished pressed pellets were stored in a desiccator and analyzed with a Spectro EDXRF (EDS system). Standards included JR-2 (Japanese rhyolite), SRM 2704 (NIST Buffalo River sediment) and USGS BVHO-1(basalt).

Samples analyzed at the Smithsonian Institution were analyzed with a Philips PW1480 X-ray spectrometer. Major elements were analyzed using fused discs. Fused discs were prepared by mixing ~ 2 g of oven dried sample (also determined LOI) with 4.05 g of lithium tetraborate. Contents were then put into a Pt crucible and 5 drops of lithium iodide fluxing agent added. The Pt crucible was placed in a Philips PerlX3

Automatic Bead machine which produced the finished fused disc. Trace elements were analyzed using pressed pellets. Approximately 5 grams of powdered sample were pressed in an ARL press for 10 seconds at 3500 psi. Fused discs were analyzed using 40 Kv and 60 mA for SiO_2, Al_2O_3, Fe_2O_3, MgO, CaO, Na_2O, K_2O, TiO_2, P_2O_5, and MnO using USGS standards G2 and W2.

Neutron Activation

Neutron activation analyses of powdered whole rock samples (for pulverization procedure see preparation for XRF) were performed by the Phoenix Memorial Laboratories at the University of Michigan, Ann Arbor. Quartz tubes were cut into ~ 5 cm sections using a hydrogen-oxygen torch, individual sections were then sealed at one end. The tube sections were boiled in aqua regia and rinsed with distilled water with the process being repeated for five cycles. After cleaning, the tube sections were dried, weighed and loaded with ~ 200 mg of powdered sample. The open ends of the quartz tubes were then sealed with the hydrogen-oxygen torch and the tubes placed in the distilled water bath where they could be inspected for leakage.

The sealed samples were exposed to 20 H core-face irradiation at an average flux rate of 4.2×10^{12} $n/cm^2/s$. Following irradiation, two separate counts of gamma activity were done: a 5000-second (live time) count of each sample after a 1-week decay period; and a 10000-second count (live time) after a period of 4-5 weeks decay. Element concentrations were determined based on comparison with three replicates of the standard reference material NIST1633A (coal fly ash) with all data reductions based on NIST certified values. Samples of NIST688 (basalt) and NIST278 (obsidian) were included as check standards.

The Palermo #2 Pegmatite

The Palermo #2 pegmatite is one the larger pegmatites in the Grafton field, measuring approximately 400 m in length and ranging from 7 to 50 m in width (Figure 3). With the exception of an open cut at the widest portion of the dike and two small prospect pits, the pegmatite is obscured by vegetation and soil.

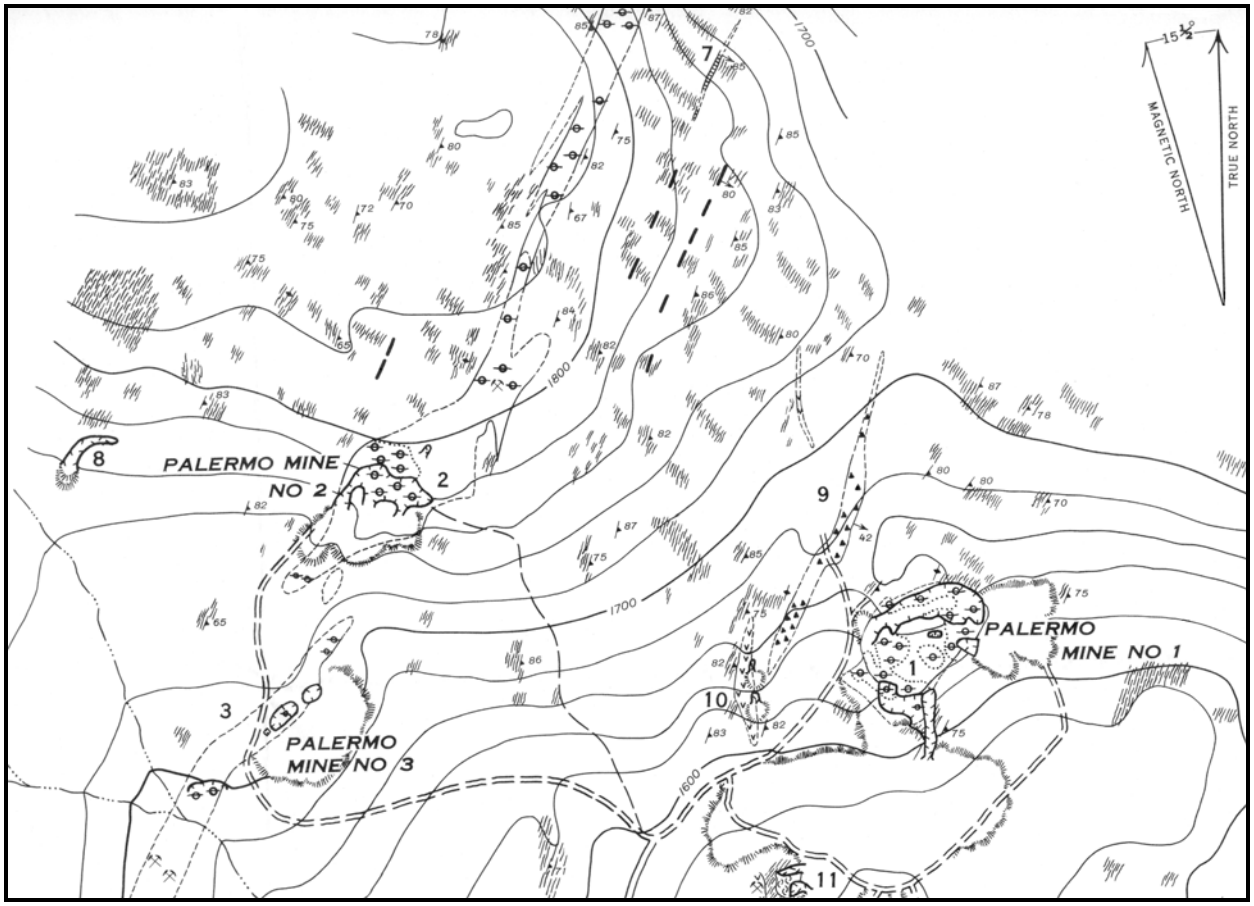

Figure 3: Topographic map showing the location of the Palermo #2 and adjacent pegmatites, North Groton, New Hampshire (from Cameron *et al*., 1954).

The pegmatite is concordant with the country rock (Lower member of the Littleton formation) and strikes N. 20º E. The dip in the vicinity of the open cut is variable from 85º E/SE to nearly vertical on the hanging wall and approximately 80-85º E/SE on the footwall. The hanging wall and footwall contacts are sharp and well-defined,

suggesting a significant temperature difference existed between the pegmatite melt and the host rock.

The pegmatite is zoned, with border, wall, intermediate, core margin and core zones that are typically weakly defined (gradational). The pegmatite appears to be asymmetrically zoned, with the hanging wall half of the pegmatite showing an increase in the thickness of the wall and intermediate zones in the vicinity of the open cuts and the core margin/core zones are located much closer to the footwall side of the pegmatite.

The border zone is approximately 1 to 4 cm in thickness and is discontinuous. The border zone is composed of quartz and muscovite, as well as small amounts of plagioclase, almandine and fluorapatite. The border zone is fairly fine-grained, exhibiting an average grain size of less than 0.5 cm.

The wall zone ranges from 1 to 5 meters in thickness and shows increased grain size in comparison to the border zone. The average grain size in the wall zone is approximately 2-3 cm. The wall zone is composed mainly of quartz, plagioclase, perthite, muscovite and biotite. Minor to trace amounts of fluorapatite, schorl, almandine and zircon also occur in the wall zone. Quartz forms coarse graphic intergrowths with plagioclase. Muscovite is present in books to 15 cm and may occur as an intergrowth with biotite. The accessory phases fluorapatite, schorl, almandine and zircon occur as subhedral to euhedral crystals to 3 mm in size.

The intermediate zone composes the bulk of the volume of pegmatite and varies from 5 to 25 meters in thickness. The transition from wall to intermediate zone is gradational, however the increasing grain size and presence of abundant book mica

typifies the intermediate zone. Quartz, plagioclase, perthite, muscovite, biotite are the major minerals composing the intermediate zone. The accessory mineralogy of the intermediate zone is more complex that that of the wall zone: fluorapatite, schorl, almandine, beryl, native bismuth, pyrite, sphalerite, galena, xenotime, monazite, magnetite, rutile and hematite occur in small amounts in the intermediate zone. The accessory phases are generally subhedral to euhedral and are typically less than 3 mm in size. Grain size in the intermediate zone is quite coarse, the majority of grains are greater than 4 cm in size. Blocky masses of perthite occur to 30 cm and book muscovite is abundant (5-30 cm in size). Quartz forms coarse graphic intergrowths with plagioclase and perthite. Secondary cavities (<1 cm) containing euhedral albite, apatite and muscovite occur rarely in large masses of plagioclase. However, the vast majority of minerals in the intermediate zone do not show evidence of significant replacement or alteration.

The core margin is generally between 2 to 3 meters in thickness and forms a rind on the outer surface of large pods of monomineralic quartz (core). Major minerals composing the core margin include: quartz, perthite, plagioclase, muscovite, schorl, beryl, triphylite, fluorapatite and hydroxylapatite. Major minerals occur as anhedral to subhedral masses or as euhedral crystals up to 2 meters in size. Large masses (up to 50 cm) of the primary phosphates triphylite and hydroxylapatite are fairly abundant and occur in contact with or proximal to the outer margin of the quartz core. Schorl is also concentrated in the core margin relative to the rest of the pegmatite and concentrations or nests of crystals to 10 cm are abundant. Euhedral crystals of beryl to 30 cm are frequently observed in the core margin. Book muscovite is sparse in the core margin

and consequently these areas were avoided during the mica mining periods. Accessory minerals occurring in the core margin include: ferrisickerlite, heterosite, siderite, montebrasite, graftonite, xenotime-(Y), monazite-(Ce), wolfeite, “arrojadite”, sarcopside, rockbridgeite, beraunite, laueite, strunzite, vivianite, ludlamite, kryzhanovskite, jahnsite-(CaMnFe), jahnsite-(CaMnMg), jahnsite-(CaMnMn), stewartite, ushkovite, whitmoreite, childrenite, eosphorite, messelite, fairfieldite, mitridatite, strengite, phosphosiderite, scorzalite, lazulite, paravauxite, gordonite, gormanite, souzalite, augelite, chlorapatite, whiteite-(MnFeMg), whiteite-(CaFeMg), whiteite-(CaMnMg), crandallite, goyazite, collinsite, autunite, torbernite, native bismuth, pyrite, sphalerite, galena, pyrrhotite, arsenopyrite, chalcopyrite, bornite, löllingite, uraninite, ferrocolumbite, rutile, almandine, zircon and bertrandite. The accessory minerals occur mainly as microscopic (< 3 mm) subhedral to euhedral crystals. Many of the phosphate-bearing accessory minerals are products of metasomatic alteration of primary phosphates by late-stage, carbonate-bearing aqueous fluids. This alteration process will be discussed in detail in the chapter regarding phosphate paragenesis.

The core of the Palermo #2 pegmatite consists mainly of large (up to 10 m), ellipsoidal masses of quartz. The pods are discontinuous and may be separated by several meters of core margin or intermediate zone. The quartz masses are essentially monomineralic, although occasionally large blocks of perthite or beryl crystals may be observed projecting into the quartz from the core margin. The pods of core quartz exposed in the open cut portion of the pegmatite display an unusual orientation in that they plunge approximately 25º toward the northwest. The plunging orientation and the small size of the pods relative to the overall dimensions of pegmatite suggest that larger

masses of quartz (core) may be present at depth. It is currently impossible to confirm the existence of a larger core as access to the lower portions of the two inclines is restricted to the uppermost areas due to the accumulation of debris as a consequence of more recent mining activity. Another large mass of monomineralic quartz is exposed in a prospect pit approximately 30 meters NE along strike from the main open cut. The lack of exposure in the vertical dimension at this location precludes any conclusion regarding the relationship between the prospect pit quartz mass exposure and the smaller masses of quartz core observed in the open cut.

A large xenolith of the country rock (schist) is present just to the right of the center of the open cut. The block is approximately 1.5 meters in length and does not show particularly strong evidence of reaction with the pegmatitic melt except for the presence of an outer rim that is strongly enriched in muscovite relative to typical Littleton schist.

Mineralogy

Rock-forming Minerals:

Feldspar group:

Albite – $NaAlSi_3O_8$

Microcline – $KAlSi_3O_8$

Both albite and microcline are present throughout the Palermo #2 pegmatite with albite occurring in higher proportions in the outer zones (border, wall, intermediate) whereas microcline occurs mainly in the inner zones (core margin, core). Albite forms blocky masses up to 10 cm and also occurs in lamellar streaks in microcline (perthite). Albite rarely occurs as translucent euhedral crystals in secondary cavities in masses of primary albite. Microcline typically occurs as perthite (exhibiting fine exsolution lamellae of albite) and crude single crystals in the core margin that may reach up to 1 m in size. Pegmatites of a peraluminous nature containing large quantities of phosphate minerals other than apatite may exhibit elevated phosphorus content in feldspars via a $Al^{3+} + P^{5+} = 2\ Si^{4+}$ substitution (London *et al*. 1990). The phosphorus (expressed as P_2O_5) content of alkali feldspar from Palermo #2 is shown in Figure 4. P_2O_5 content in alkali feldspar ranges from 0.03 (detection limit) to 0.47% and displays an increase from the wall zone to intermediate to core margin zone.

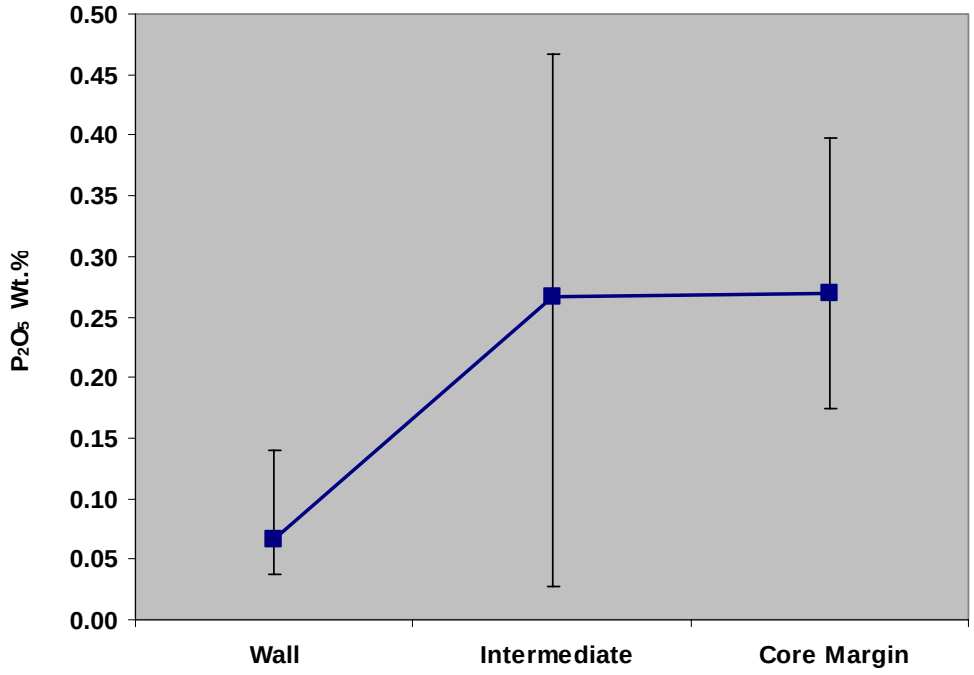

Figure 4: P_2O_5 content of alkali feldspar from the wall, intermediate and core margin zones of the Palermo #2 pegmatite. Bars signify variance in P_2O_5 content of data from each pegmatite zone.

Several researchers have reported that P is preferentially incorporated into the K-feldspar structure (Smith, 1974, 1983, Mason 1982). Feldspars from Palermo #2 appear to reflect this relationship as K-feldspars typically contain higher amounts of P_2O_5 than sodic plagioclase feldspars.

Mica group:

Biotite – $KFe^{2+}_3AlSi_3O_{10}(OH)_2$

Muscovite – $KAl_2\square AlSi_3O_{10}(OH)_2$

Muscovite and biotite are the dominant mica minerals present at Palermo #2. Biotite occurs more frequently in the outer zones of the pegmatite and is rarely encountered in the core margin zone. Muscovite is abundant throughout the pegmatite and was the primary commodity the pegmatite was mined for. Book muscovite is

common in the wall and intermediate zones and therefore mining activity prior to 1960 was concentrated in these zones. Large books of muscovite up to 20 cm occur in the core margin in association with quartz and large perthitic feldspars. Intergrowths of biotite and muscovite occur infrequently in the wall and intermediate zones.

Quartz – SiO_2

Quartz is abundant throughout the pegmatite and is a major component along with feldspars (albite and microcline) and micas (muscovite and biotite). The core zone of the pegmatite consists of large monomineralic masses of quartz up to 7 m across in the central portion of pegmatite. Euhedral crystals of quartz to 5 mm may occur in cavities created by the dissolution of primary minerals including beryl, feldspars, tourmaline, etc. Smoky quartz occurs sporadically in the core margin of the pegmatite and is related to the presence of small amounts of uraninite and/or U-bearing secondary phosphates (autunite, torbernite).

Minor/accessory/trace minerals:

Silicates:

Beryl – $Be_3Al_2Si_6O_{18}$

Beryl is present in moderate quantities in the core margin/core of Palermo #2. Beryl forms crude to sharp hexagonal prisms up to 30 cm in length that range in color from light green (Fe^{2+}/Fe^{3+}) to blue (Fe^{2+}) to yellow (Fe^{3+}) (Figure 5). Beryl crystals that project into the quartz core frequently contain transparent areas that make suitable gemstock (Figure 6). The majority of gem material from Palermo #2 is green to blue in color although the oxidized yellow variety heliodor may occur in the vicinity of radioactive minerals such as uraninite, autunite and torbernite. Cesium content (from

EDS) in beryl from Palermo #2 is low (< 1 %) as is typical of beryl-phosphate subtype granitic pegmatites (Trueman and Černý, 1982).

Figure 5: Large yellow beryl at the core margin-core interface. The yellow color (Fe^{3+}) is due to the presence of the nearby radioactive minerals uraninite and zircon.

Figure 6: Nearly transparent blue beryl (2 cm in length) from the core margin/core interface at Palermo #2.

Schorl – $NaFe^{3+}_3Al_6(BO_3)_3[Si_6O_{18}](OH)_4$

Schorl is the sole member of the tourmaline group that occurs at Palermo #2. Schorl occurs as lustrous black subhedral to euhedral prisms to 5 cm. Schorl is present in small amounts in the wall and intermediate zones, but is much more prevalent in the core margin zone. Schorl is associated with quartz, perthitic feldspar, albite, muscovite, and triphylite. In some cases schorl has undergone partial to complete dissolution in the vicinity of altered primary phosphates.

Almandine – $Fe^{2+}_3Al_2(SiO_4)_3$

Almandine is an uncommon mineral at Palermo #2 and typically occurs in the core margin in association with fluorapatite, quartz and feldspar. Almandine forms subhedral to anhedral reddish pink masses up to 2 mm and may be associated with green fluorapatite, altered muscovite, schorl and triphylite. In many cases almandine appears to be etched indicating that conditions favorable for dissolution of garnet existed in the late stages of crystallization or occurred during subsolidus alteration of phosphate species. Chemical compositions of garnet from Palermo #2 are given in Table 1. Compositionally, garnet from Palermo #2 falls in the almandine field with a fairly significant spessartine component (Figure 7 and 8). Pyrope (Mg) and grossular (Ca) components are quite low. FeO content ranges from ~ 25.7 to 28.9 wt.% whereas MnO content falls between 13.1 and 17.1 wt.%. Fe/Mn ratios occur within a range from ~ 1.50 (most geochemically evolved) to 2.20 (least evolved) (Figure 9). CaO content (0.15-0.21 wt.%) is quite constant between analyzed samples whereas MgO content (0.35-0.91 wt.%) displays more variability. Fe/Mn ratios have been employed by Hildreth (1979, 1981) and Mahood (1981) to show the variation of Fe/Mn with

fractionation of rhyolitic magmas. This relationship has been noted in granitic pegmatites by Černý *et al*. (1981, 1985). A decrease in Fe/Mn ratio from outer to inner zones with a single pegmatite has been noted by Foord (1976), Černý & Hawthorne (1982) and Baldwin & von Knorring (1983). A comparison of Fe/Mn versus Mn in garnet from Palermo #2 and other notable phosphate-bearing granitic pegmatites is shown in Figure 10.

Table 1: Representative electron microprobe analyses of garnet from the core margin of the Palermo #2 pegmatite.

	P2-CM-17	P2-CM-18	P2-CM-20
SiO_2	36.08	37.00	36.45
TiO_2	0.13	0.13	0.15
Al_2O_3	20.49	20.87	20.79
FeO	26.62	28.16	28.19
MnO	15.56	13.43	13.72
MgO	0.35	0.91	0.80
CaO	0.20	0.18	0.19
K_2O	0.00	0.00	0.01
Totals	99.42	100.68	100.31
	Cations based on 12 oxygen atoms		
Si	2.991	3.009	2.986
Ti	0.008	0.008	0.009
Σ	2.999	3.017	2.995
Al	2.002	2.000	2.007
Σ	2.002	2.000	2.007
Fe	1.845	1.915	1.931
Mn	1.092	0.925	0.952
Mg	0.043	0.110	0.098
Ca	0.018	0.016	0.016
K	0.000	0.000	0.001
Σ	2.998	2.966	2.999
Fe/Mn=	1.717	2.104	2.062

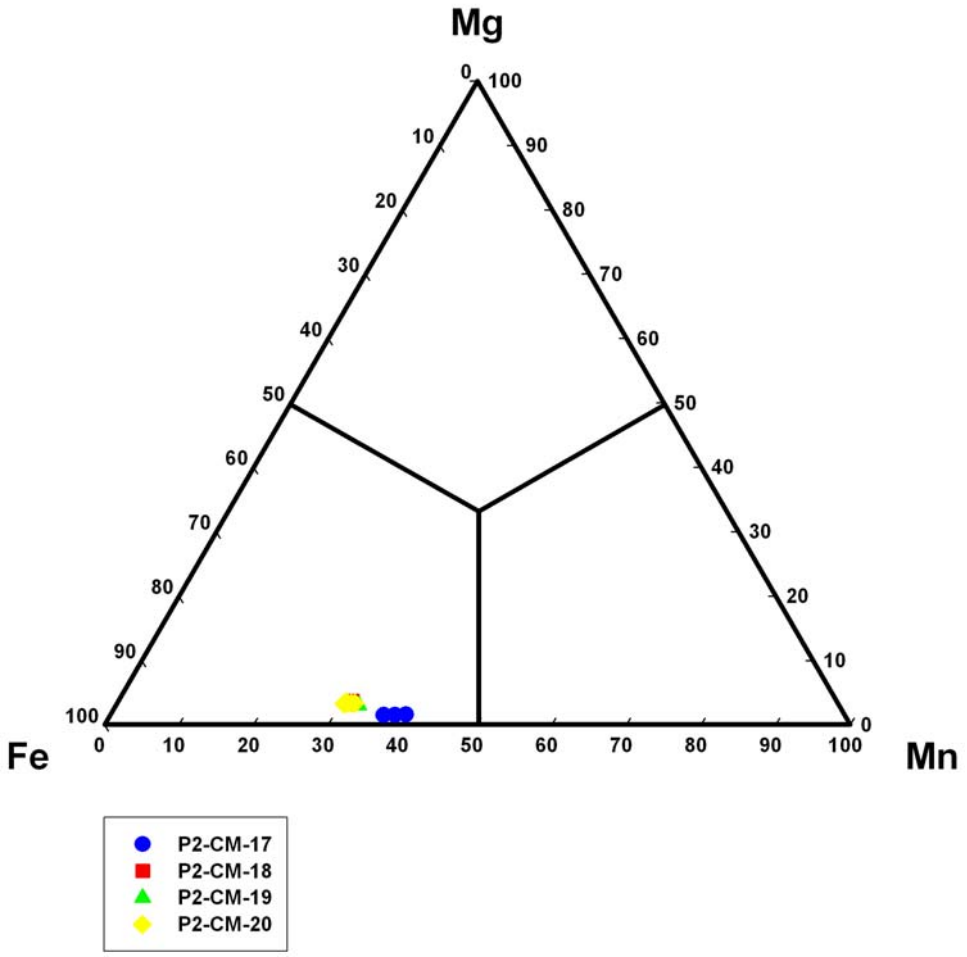

Figure 7: Ternary FeMnMg (atoms per formula unit - apfu) plot of almandine garnet from Palermo #2.

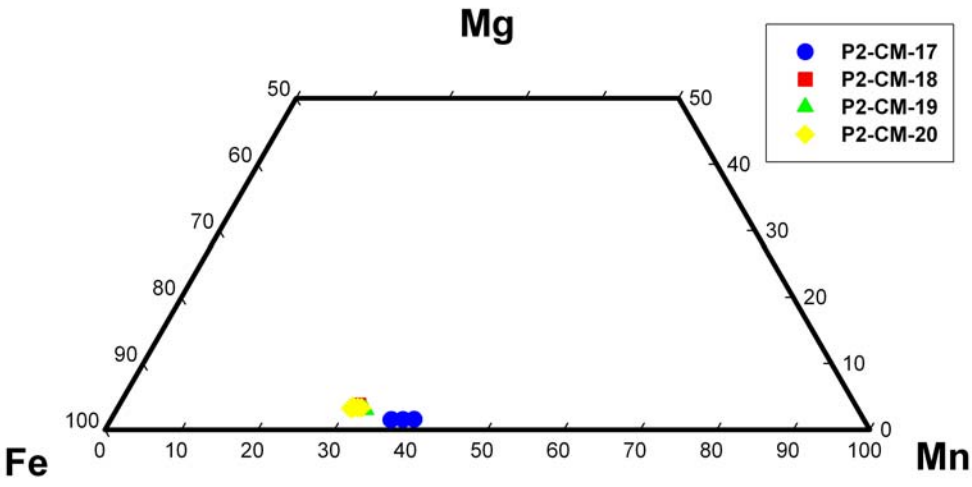

Figure 8: Ternary $FeMnMg_{50}$ (apfu) plot of almandine garnet from Palermo #2.

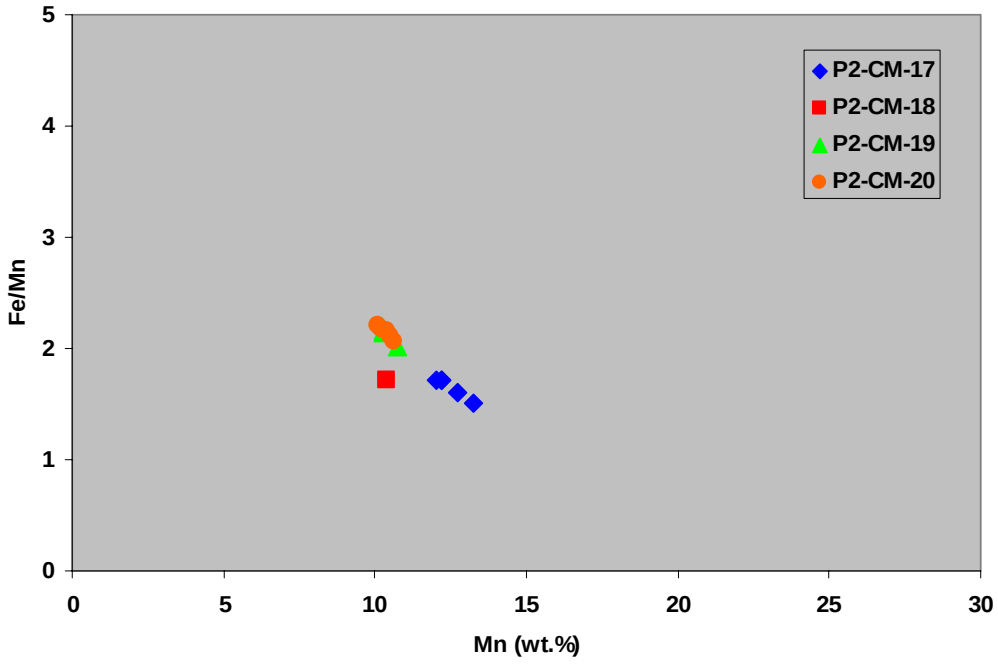

Figure 9: Fe/Mn versus Mn plot of almandine garnet from the core margin zone of the Palermo #2 pegmatite.

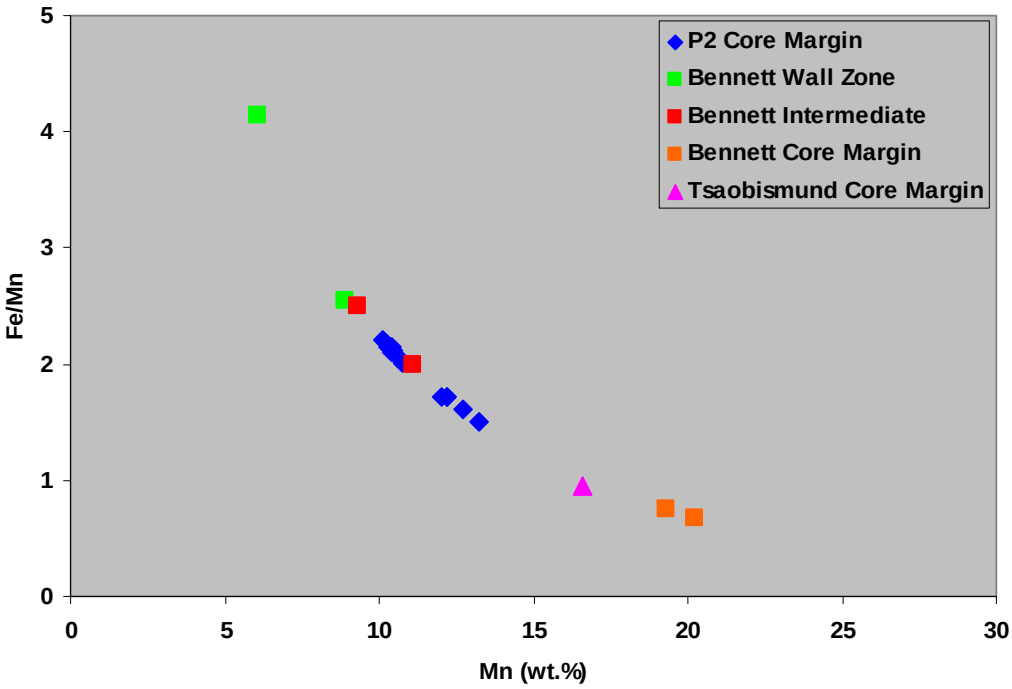

Figure 10: Fe/Mn versus Mn plot of garnet from the Palermo #2, Bennett (Oxford Co., Maine) and the Tsaobismund pegmatite (Namibia). Tsaobismund data from Fransolet *et al*., 1986. Bennett data from Wise and Rose, 2000.

Zircon – $ZrSiO_4$

Zircon occurs in small quantities in all zones of Palermo #2. Crystals are generally euhedral, are <1 mm to 3 mm in size and exhibit a brown to reddish brown color. Zircon distribution is as follows: zircon occurs sparingly in the wall and intermediate zones and is much more prevalent in the core margin/core zones where it is associated with triphylite, sulfides, almandine and uraninite. Zircon exhibits solid-solution with hafnon ($HfSiO_4$) and thorite ($ThSiO_4$), therefore some degree of substitution of Hf and Th for Zr is not uncommon in fractionated granites and pegmatites. The HfO_2 content of zircon from the wall zone ranges from ~1.0 to 3.3% whereas HfO_2 in the core margin ranges from ~ 4.5 to 7.5% (Table 2). Hafnium (Hf) content of zircon may be used as a monitor of fractionation in granitic pegmatites and, as has been noted in many other granitic pegmatites by Černý *et al*. (1985), Hf content in zircon from Palermo #2 steadily increases from the wall to core margin zones (Figure 11). Figure 12 illustrates a positive correlation between Hf substitution for Zr and the increasing degree of evolution within the pegmatite. Thorium oxide (ThO_2) content in zircon from Palermo #2 ranges from below detection limit to 0.30 wt.% in the wall zone to 0.15 to 0.54 wt.% in the core margin zone. Zircon also exhibits solid-solution with and is isostructural to xenotime-(Y) (YPO_4). In contrast to the substitution relationship between Hf and Zr, Figure 13 shows P substitution for Si in zircon from Palermo #2 is not correlatable with increasing fractionation within the pegmatite. This relationship suggests that P for Si substitution may be controlled by a different mechanism.

Table 2: Representative electron microprobe analyses of zircon from the Palermo #2 pegmatite.

	P2-TR-15 wall	P2-TR-4 intermediate	P2-CM-10 core margin
P_2O_5	0.41	0.48	0.54
SiO_2	31.55	31.72	30.85
TiO_2	0.16	0.12	0.10
ZrO_2	64.89	62.32	61.27
HfO_2	2.33	4.99	5.39
ThO_2	0.18	0.15	0.15
Al_2O_3	0.39	0.00	0.00
FeO	0.26	0.00	0.00
MnO	0.03	0.02	0.02
CaO	0.25	0.17	0.16
MgO	0.08	0.11	0.02
Na_2O	0.05	0.06	0.03
K_2O	0.07	0.03	0.02
Totals	100.64	100.17	98.55
	Cations based on 12 oxygen atoms		
Zr	0.971	0.944	0.947
Hf	0.020	0.044	0.049
Th	0.001	0.001	0.001
Fe	0.007	0.000	0.000
Mn	0.001	0.001	0.001
Ca	0.008	0.006	0.005
Mg	0.003	0.005	0.001
Na	0.003	0.004	0.002
K	0.003	0.001	0.001
Σ	1.018	1.005	1.007
Si	0.968	0.985	0.978
Ti	0.004	0.003	0.002
Al	0.014	0.000	0.000
P	0.011	0.013	0.015
Σ	0.997	1.001	0.995

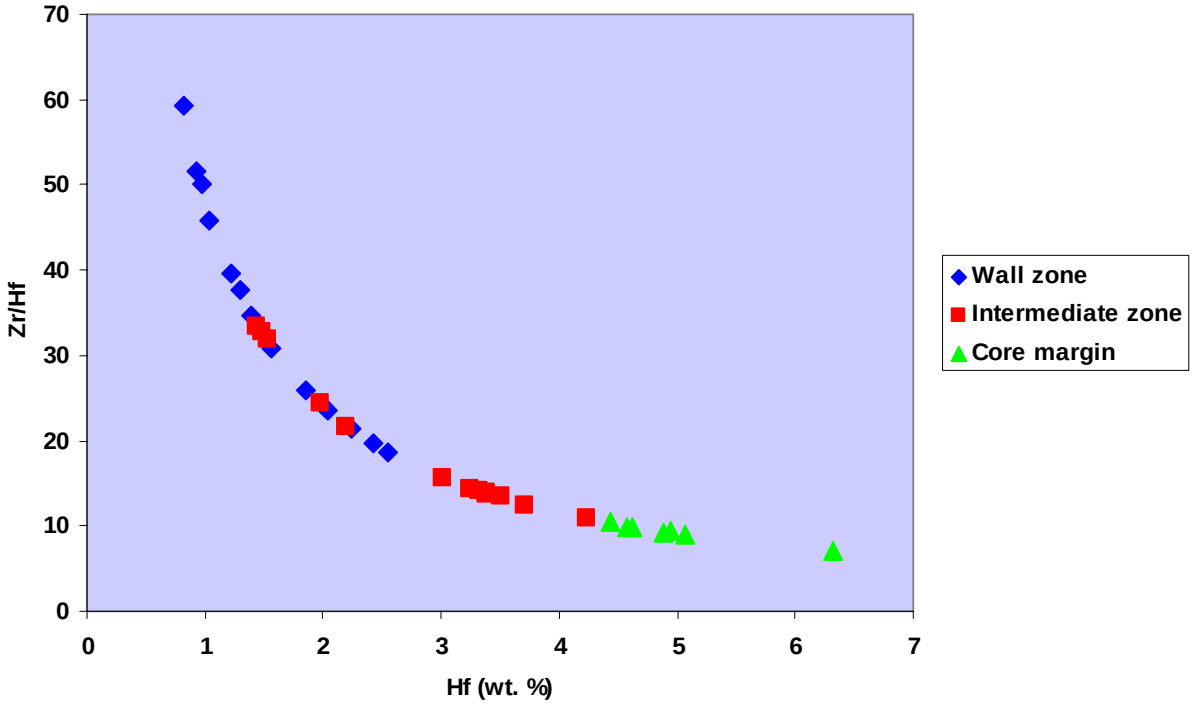

Figure 11: Zr/Hf versus Hf (wt.%) for zircon from the Palermo #2 pegmatite.

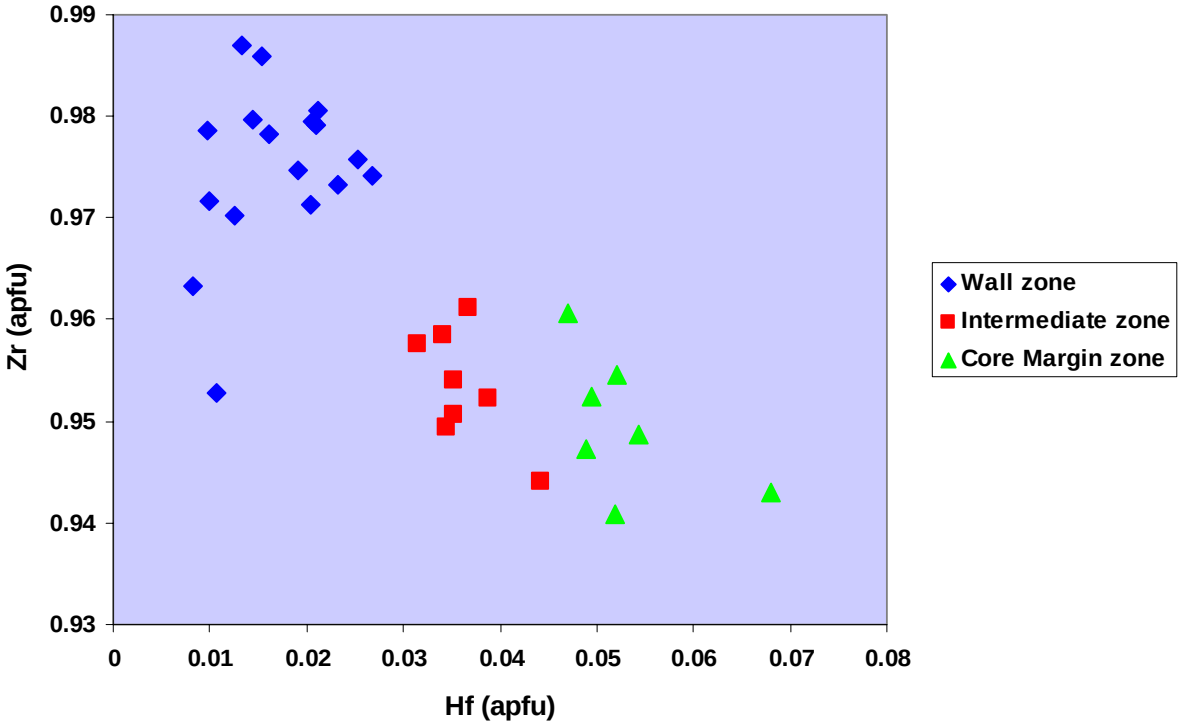

Figure 12: Hafnium (apfu) versus zirconium (Zr) content of zircon from the Palermo #2 pegmatite. Hafnium substitution for Zr increases with increasing degree of evolution in the pegmatite.

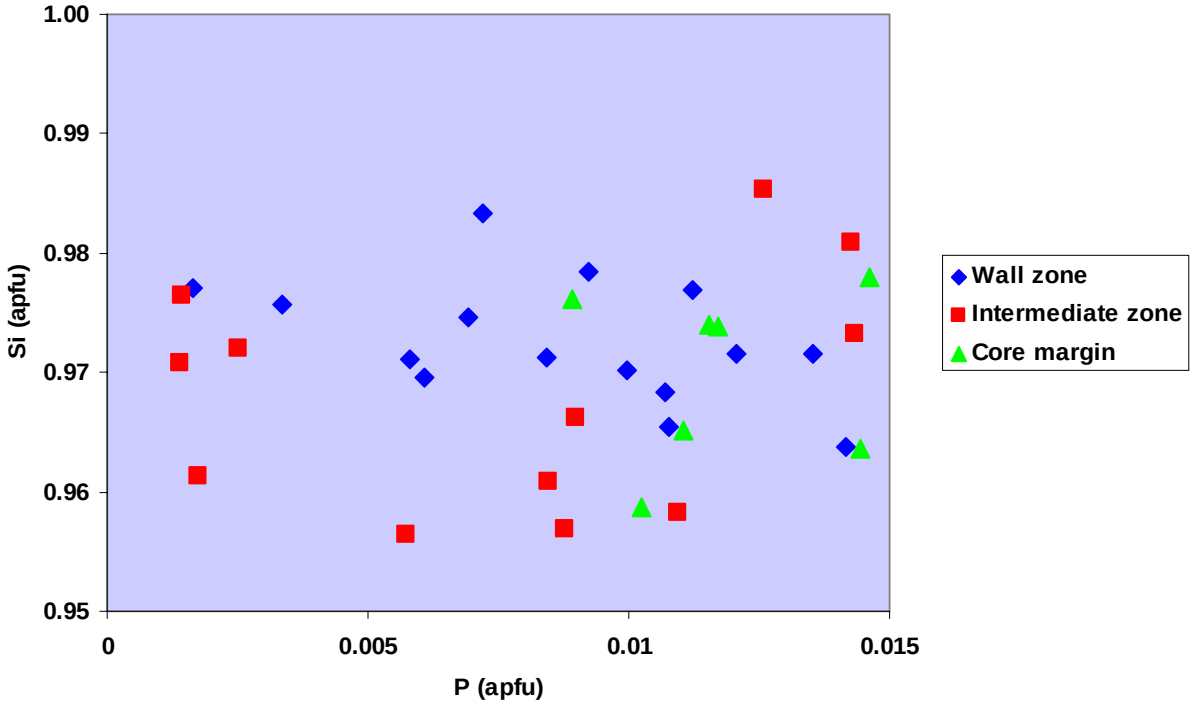

Figure 13: Si (apfu) versus phosphorus (P) in zircon from Palermo #2. P substitution for Si does not correlate with degree of evolution within the pegmatite.

Bertrandite – $Be_4Si_2O_7(OH)_2$

Bertrandite occurs as an alteration product of beryl and forms tabular colorless to white crystals to 1 mm (Figure 14). Bertrandite is found in the core margin/core of Palermo #2 in dissolution molds of beryl crystals and is associated with millimetric euhedral quartz crystals. The presence of bertrandite suggests that the fluids responsible for the dissolution of beryl were neutral to somewhat acidic in nature (Černý, 2002) (Figure 15).

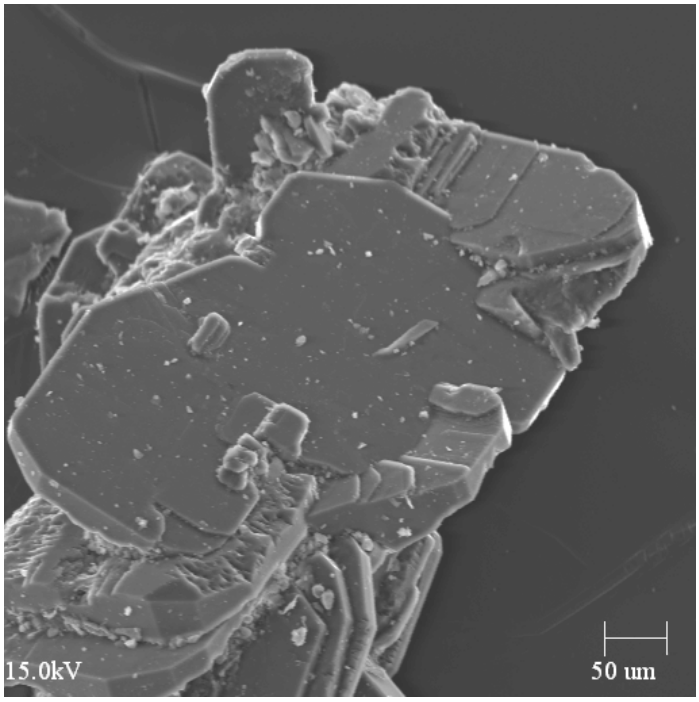

Figure 14: Secondary electron image of tabular bertrandite crystals from the core margin of the Palermo #2 pegmatite.

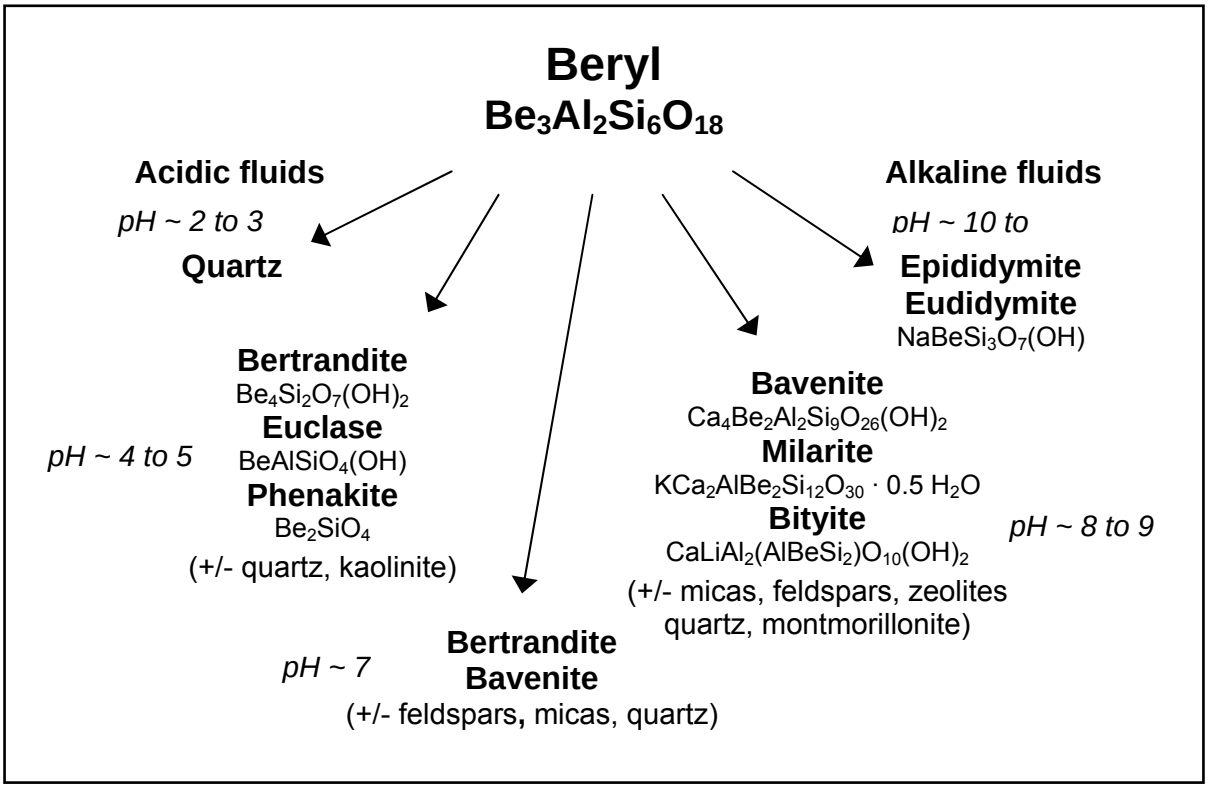

Figure 15: Typical silicate products resulting from the alteration of beryl in granitic pegmatites (Černý, 2002).

Native Elements:

Bismuth – Bi

Native bismuth occurs as very small, silvery metallic grains (< 1mm) in the intermediate and core margin zones. Native bismuth is associated with sulfides (pyrite, chalcopyrite), feldspars, quartz and muscovite.

Sulfides:

Pyrite – FeS_2

Pyrite mainly occurs in the core margin of the pegmatite where it exhibits cubic or octahedral forms. Pyrite forms euhedral crystals to 1 mm and is associated with pyrrhotite, quartz, chalcopyrite, perthitic feldspar and fine-grained muscovite.

Sphalerite -- ZnS

Sphalerite occurs in small quantities in the core margin of the Palermo #2 pegmatite. Sphalerite forms resinous brown masses up to 2 mm and is associated with pyrite, chalcopyrite, galena, siderite, zircon, uraninite and quartz.

Arsenopyrite – $FeAsS_2$

Arsenopyrite is present as a rare accessory mineral at Palermo #2. Arsenopyrite is found in the intermediate and core margin zones as small (< 1 mm), silvery pseudo-orthorhombic crystals associated with pyrite, zircon, quartz, siderite and perthitic feldspar.

Galena -- PbS

Galena is a rare accessory phase at Palermo #2. Galena occurs in the core margin as small, silvery metallic masses to 700 μm associated with pyrite, sphalerite, chalcopyrite, quartz and siderite.

Chalcopyrite – $CuFeS_2$

Chalcopyrite occurs sporadically in the core margin of Palermo #2 where it forms in brassy metallic masses to 800 μm in size. Chalcopyrite is typically associated with pyrite, sphalerite, siderite, bornite and quartz. Chalcopyrite and bornite are the only significant primary Cu-bearing phases at Palermo #2.

Bornite – Cu_5FeS_4

Bornite is a rare accessory phase that is restricted to the core margin. Bornite occurs in small grains to 200 μm in size and is typically associated with pyrite, chalcopyrite, quartz and perthitic feldspar.

Pyrrhotite – $Fe_{1-x}S$

Pyrrhotite occurs in small quantities as an alteration product of pyrite in the core margin of the Palermo #2 pegmatite. Pyrrhotite is associated with pyrite, chalcopyrite, quartz, muscovite and perthitic feldspar.

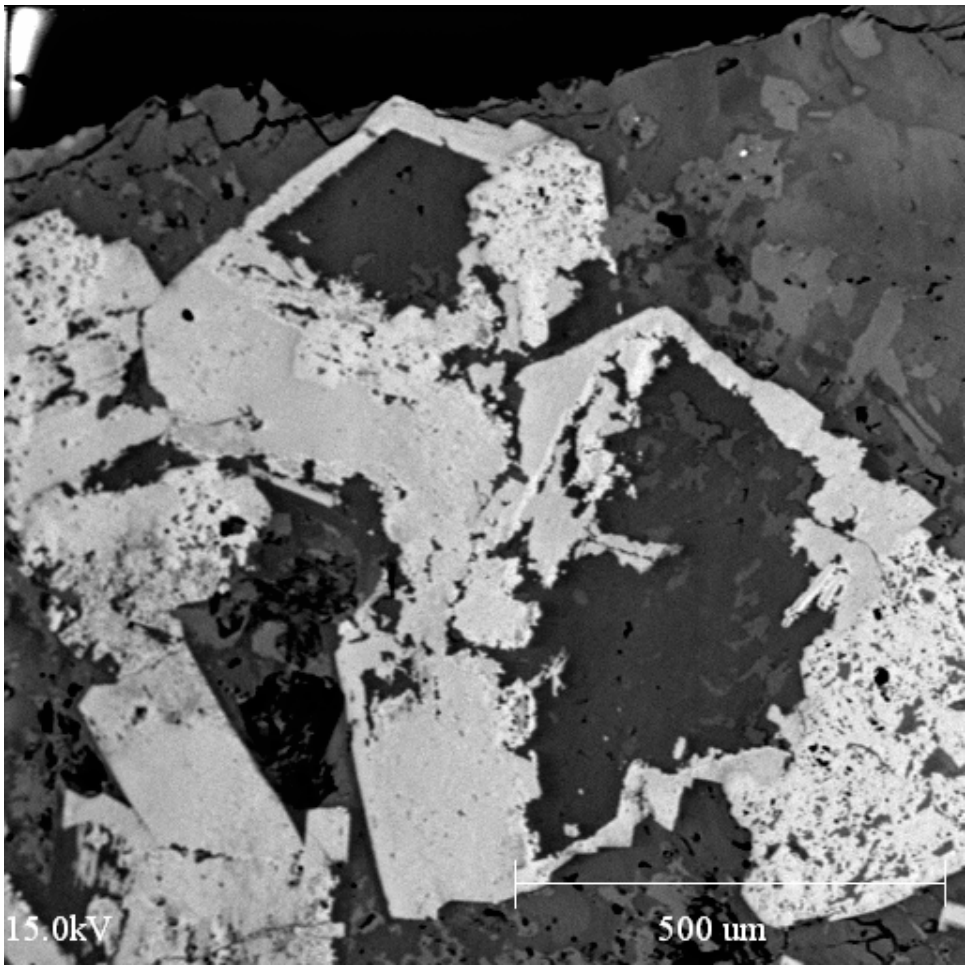

Figure 16: Backscattered electron image of skeletal pyrite crystals (light gray) exhibiting partial replacement by pyrrhotite (white).

Oxides:

Uraninite – UO_2

Uraninite occurs in small quantities in the core margin in association with zircon, sulfides and primary phosphates (triphylite, fluorapatite). Uraninite forms small (< 2 mm) masses and sometimes occurs as euhedral crystals (Figure 17). Alteration of uraninite results in the formation of autunite and torbernite in the presence of late stage phosphate-bearing fluids. Perthitic feldspars proximal to uraninite often display a distinctive brick red color.

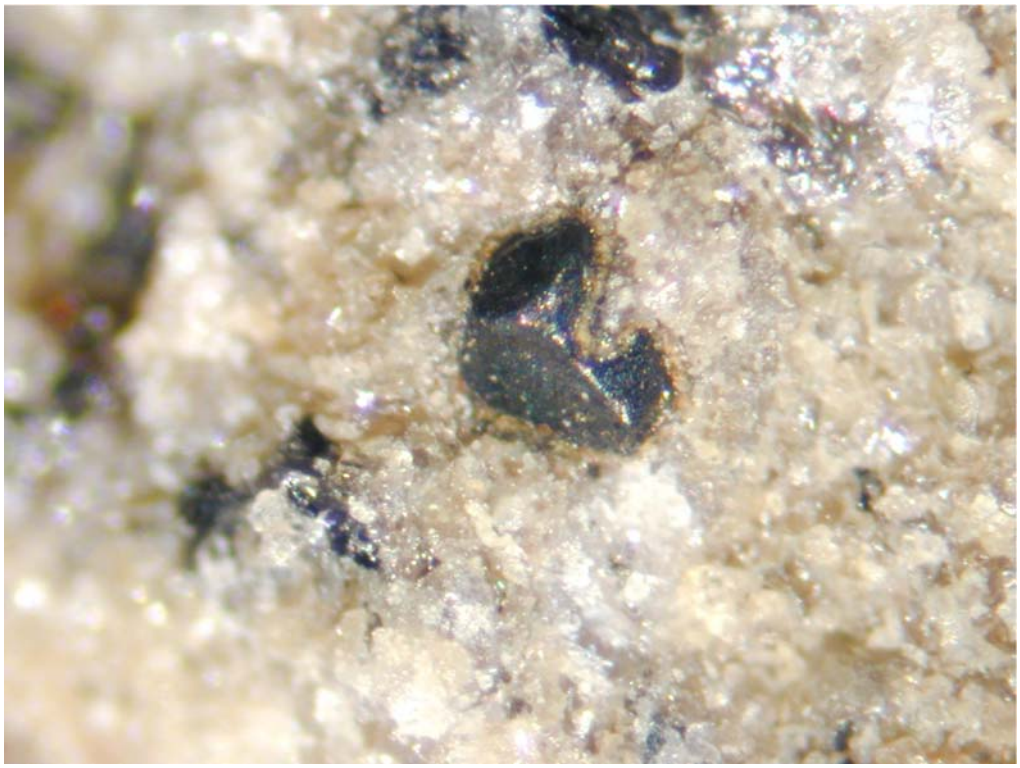

Figure 17: Euhedral uraninite crystal exhibiting cubic and octahedral forms from Palermo #2. Field of view is approximately 3 mm.

Ferrocolumbite – $Fe^{2+}Nb_2O_6$

Ferrocolumbite, an extremely rare phase at Palermo #2, is found exclusively in the core margin in association with siderite, zircon, uraninite and fluorapatite. Ferrocolumbite occurs as lustrous metallic black tablets to 1.5 mm in maximum dimension. Ferrocolumbite displays low Ta/(Ta+Nb) and Mn/(Mn+Fe) ratios (see Table 3) that fall in the ferrocolumbite field of Černý and Ercit (1989) (Figure 18). Compositionally, ferrocolumbite from Palermo #2 shows an increase in Ta and corresponding decrease in Nb from core to rim, indicating some fractionation of Nb and Ta occurred during crystallization. Ferrocolumbite from Palermo #2 exhibits slightly lower Nb/Ta and Fe/Mn ratios compared to those from two other pegmatites from the Grafton field (Palermo #1 and Eight Ball), indicating a slightly higher degree of

fractionation (Černý *et al*. 1986). Notably, Ti is the only minor component present in microprobe detectable quantities in ferrocolumbite from Palermo #2.

Table 3: Representative electron microprobe analyses of columbite group minerals from Palermo #2 and nearby pegmatites in the Grafton field.

	P2-CM-02	Palermo #1	Eight Ball
Nb_2O_5	58.03	60.86	63.43
Ta_2O_5	21.11	18.31	14.81
TiO_2	1.16	0.73	1.66
FeO	12.84	13.66	14.79
MnO	6.68	6.11	5.32
Totals	99.82	99.66	100.01
Cations based on 6 oxygen atoms			
Nb	1.605	1.669	1.701
Ta	0.351	0.302	0.239
Ti	0.053	0.033	0.074
Σ	2.010	2.004	2.014
Fe	0.657	0.693	0.734
Mn	0.346	0.314	0.267
Σ	1.003	1.007	1.001
Mn/(Mn+Fe)	0.34	0.31	0.27
Ta/(Ta+Nb)	0.18	0.15	0.12

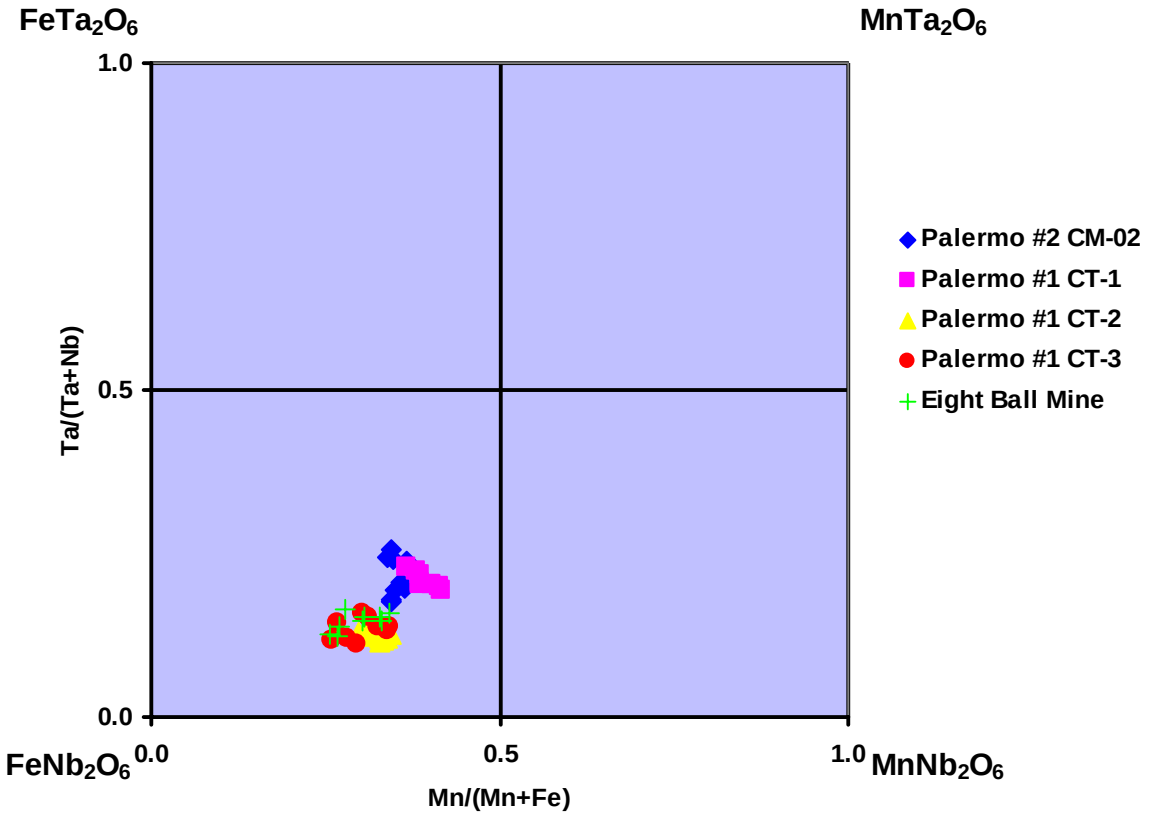

Figure 18: Compositions (atomic proportions) of columbite group minerals from Palermo #2 and two other pegmatites from the Grafton field, western New Hampshire.

Magnetite/Hematite – Fe_3O_4 / Fe_2O_3

Magnetite and hematite occur in very small quantities throughout the Palermo #2 pegmatite. Magnetite is generally massive, although well-formed octahedral crystals have been observed. Hematite forms platy aggregates of lustrous metallic crystals. Crystals/masses of magnetite and hematite are typically less than 1 mm in size.

Rutile – TiO_2

Rutile occurs as sub-millimeter brownish-black prisms in the wall, intermediate and core margin zones (Figure 19). Rutile is associated with Fe-oxides (magnetite, hematite), feldspars, quartz and muscovite.

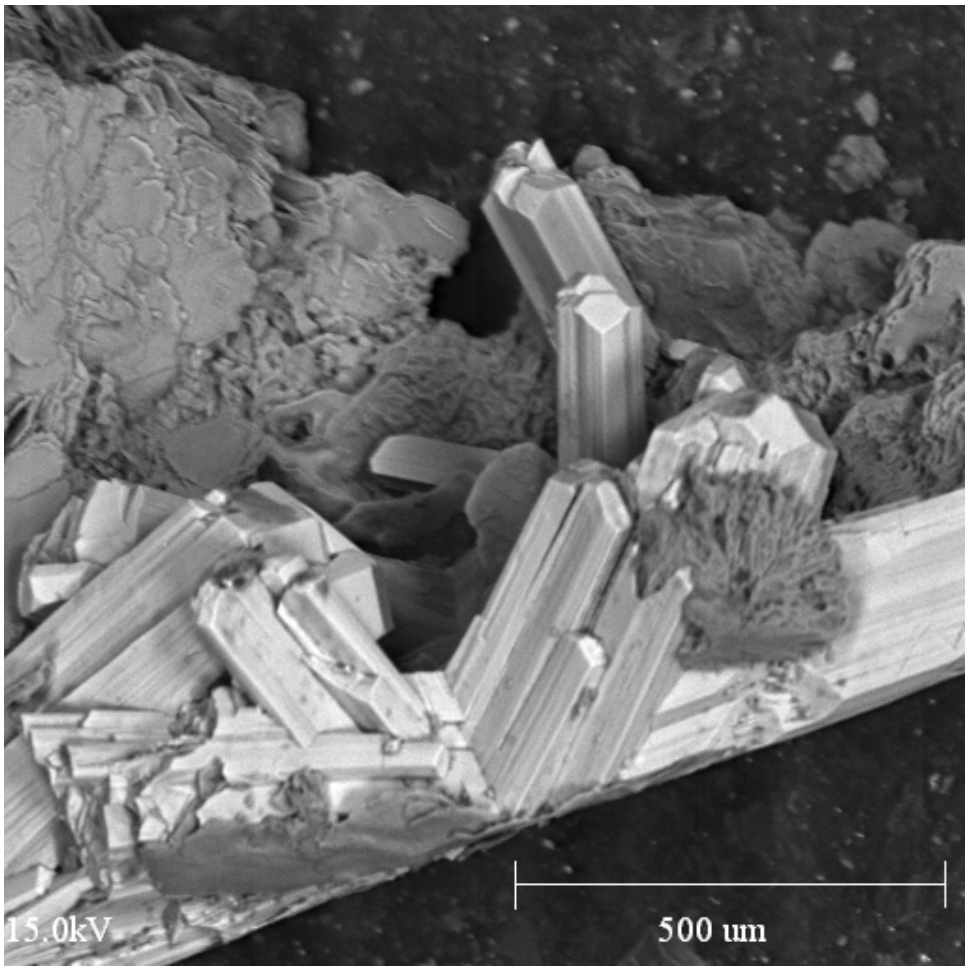

Figure 19: Backscattered electron image of twinned rutile crystals from the wall zone of the Palermo #2 pegmatite.

Carbonates:

Siderite – $FeCO_3$

Siderite is locally abundant in areas of the core margin that display alteration of primary phosphates. Siderite occurs as a partial to complete replacement of

hydroxylapatite, fluorapatite and triphylite. Siderite is typically present as saccharoidal masses that range from white to brownish in color. Euhedral crystals occur in cavities within massive siderite and display simple rhombohedral or scalenohedral forms (Figures 20 and 21). Siderite is often associated with a variety of secondary phosphates including but not restricted to: rockbridgeite, beraunite, fairfieldite group, plumbogummite group and strunzite. At least two distinct generations of siderite have been noted at Palermo #2 (Figure 22). The secondary generation of siderite displays an increasing Mn content illustrated by energy dispersive X-ray mapping in Figure 23. Siderite at Palermo #2 is most likely a product of late-stage, carbonate-bearing aqueous fluids.

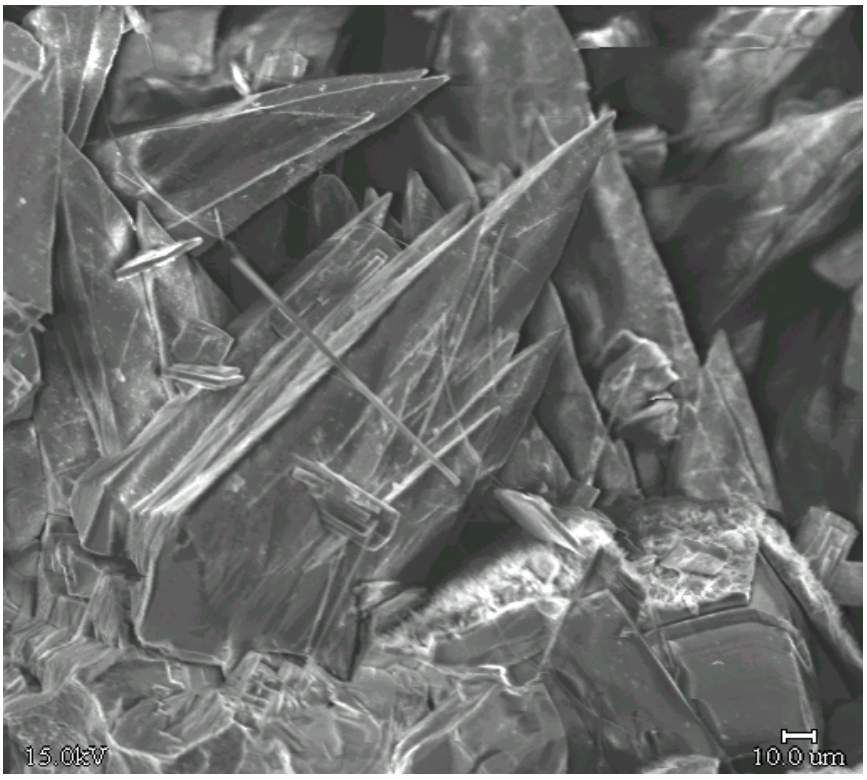

Figure 20: Backscattered electron image of scalenohedral siderite crystals with strunzite needles from Palermo #2.

Figure 21: Siderite crystals exhibiting rhombohedral forms from the Palermo #2 pegmatite. Field of view is approximately 4 mm.

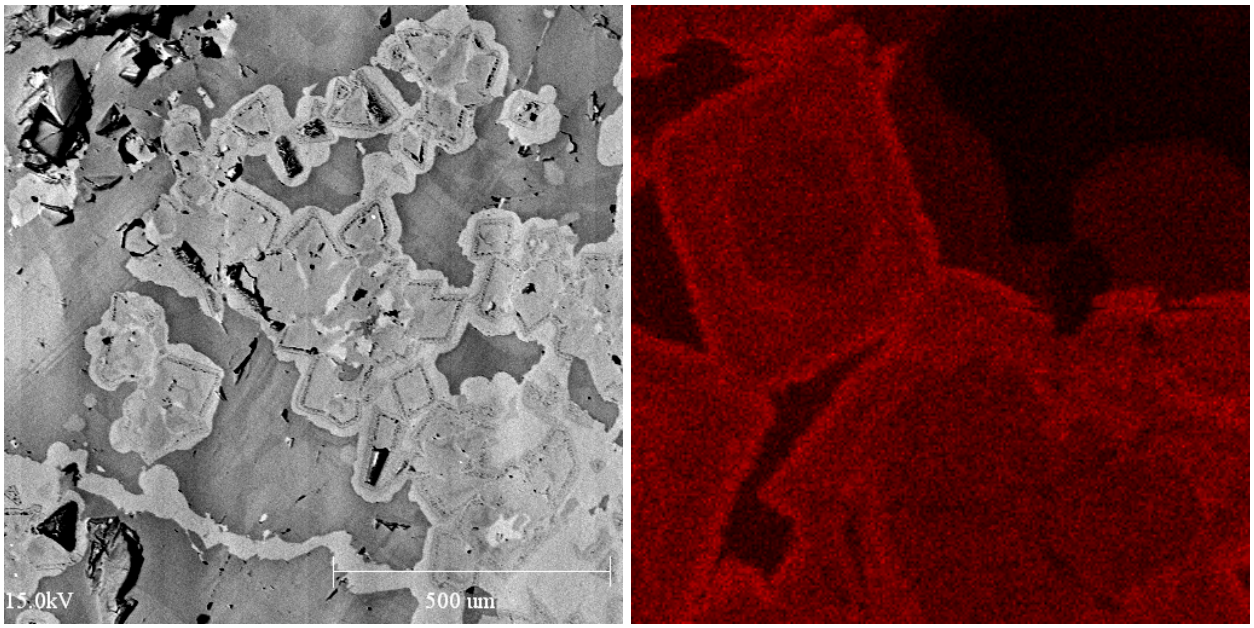

Figure 22 (left): Backscattered electron image of rhombic siderite crystals exhibiting a secondary overgrowth of Mn-rich siderite.
Figure 23 (right): Energy dispersive X-ray map of siderite showing an increase of Mn (red) from the core to rim of the crystals.

Sulfates:

Gypsum – $CaSO_4 \cdot 2\ H_2O$

Gypsum occurs as curved, colorless crystals to 1 mm on pyrite/pyrrhotite in association with rockbridgeite. Gypsum is most likely a product of the weathering environment.

Arsenides:

Löllingite – $FeAs_2$

Löllingite is present as lustrous silvery metallic crystals up to 2 mm in the core margin of Palermo #2. Löllingite is associated with secondary phosphates, quartz, pyrite, sphalerite and zircon.

Primary Phosphates:

Triphylite – $LiFePO_4$

Triphylite at Palermo #2 occurs almost exclusively in the core margin zone of the pegmatite. Triphylite is a primary phase and typically forms grayish blue masses up to 50 cm associated with coarse perthite, schorl, quartz and beryl (Figure 24). Euhedral crystals (to 20 cm) of triphylite are rare and frequently exhibit some degree of alteration to ferrisicklerite (Figure 25). Triphylite is perhaps the most important primary phosphate involved in the formation of secondary phosphate species. The majority of triphylite at Palermo #2 has undergone some degree of metasomatic alteration and exhibits a dark brown (ferrisicklerite) to purplish brown to dark purple rind (heterosite). Triphylite may be completely replaced by these and/or additional alteration products or may show alteration in only a small percentage of the overall volume of the mass or crystal. Triphylite masses may also display rinds of dark blue vivianite (a low temperature

secondary phosphate). Vivianite also commonly infiltrates triphylite masses as thin coatings along fractures and {100}, {010} and {011} cleavage planes. The presence of vivianite imparts a darker blue color to triphylite. Compositionally triphylite from Palermo #2 plots well into the triphylite field (Figure 26), evidenced by high Fe/(Fe+Mn) values (Table 4). FeO content ranges from 31.1 to 39.7 wt.% and MnO varies from 5.2 to 7.8 wt.%. In comparison with other worldwide phosphate-bearing pegmatites, triphylite from Palermo #2 contains relatively high amounts of MgO (1.5 to 4.0 wt.%). As with garnet and columbite group minerals, the ratio of Fe to Mn may be used to ascertain the degree of evolution of granitic pegmatites (decreasing Fe/Mn indicates increasing evolution/fractionation) (Černý *et al*., 1985). Ginsburg (1960) and Keller (1991) report that evaluation of the Fe/(Fe+Mn) ratio in triphylite-lithiophilite is a useful tool to estimate the degree of geochemical evolution of pegmatites. Figure 27 illustrates the ratio of Fe/Mn versus Mn in triphylite from Palermo #2 and several well-known New England phosphate-bearing pegmatites. In comparison with triphylite and lithiophilite from the Branchville, Emmons and Bennett pegmatites, triphylite from Palermo #2 displays a lesser degree of geochemical evolution. The role of triphylite in secondary phosphate paragenesis is discussed in detail in the section regarding phosphate paragenesis.

Figure 24: Masses of primary triphylite on the hanging wall side of the core margin of the Palermo #2 pegmatite.

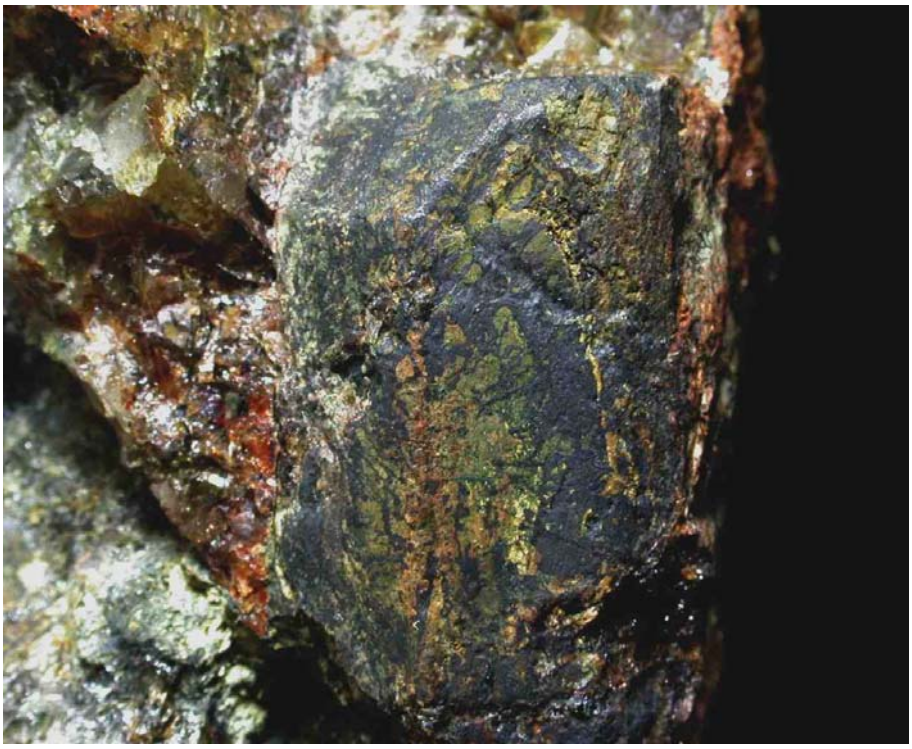

Figure 25: Euhedral triphylite crystal (2 cm in length), the dark color is due to alteration to ferrisicklerite.

Table 4: Representative electron microprobe analyses of triphylite from the core margin of the Palermo #2 pegmatite.

	P2-CM-23b	P2-CM-42	P2-CM-26	P2-CM-50
P_2O_5	45.89	46.33	46.41	45.69
SiO_2	0.39	0.39	0.62	0.77
TiO_2	0.08	0.00	0.00	0.00
Al_2O_3	0.68	0.17	0.06	0.04
FeO	31.38	33.09	34.68	33.22
MnO	7.61	6.98	5.39	7.43
MgO	3.76	3.69	3.61	3.34
SrO	0.01	0.00	0.00	0.00
CaO	0.18	0.00	0.00	0.00
Na_2O	0.01	0.00	0.00	0.00
Li_2O	9.57	9.52	9.51	9.52
Total	99.57	100.17	100.28	100.01
	Cations based on 4 oxygen atoms			
	Normalized to 1 P atom			
	Li calculated by difference			
P	1.000	1.000	1.000	1.000
Si	0.010	0.010	0.016	0.020
Σ	1.010	1.010	1.016	1.020
Fe	0.676	0.705	0.738	0.718
Mn	0.166	0.151	0.116	0.163
Mg	0.144	0.140	0.137	0.129
Sr	0.000	0.000	0.000	0.000
Ca	0.005	0.000	0.000	0.000
Al	0.021	0.005	0.002	0.001
Ti	0.002	0.000	0.000	0.000
Σ	1.014	1.001	0.993	1.011
Li	0.999	1.000	1.000	1.000
Na	0.001	0.000	0.000	0.000
Σ	1.000	1.000	1.000	1.000
Fe/(Fe+Mn) =	0.803	0.824	0.864	0.815

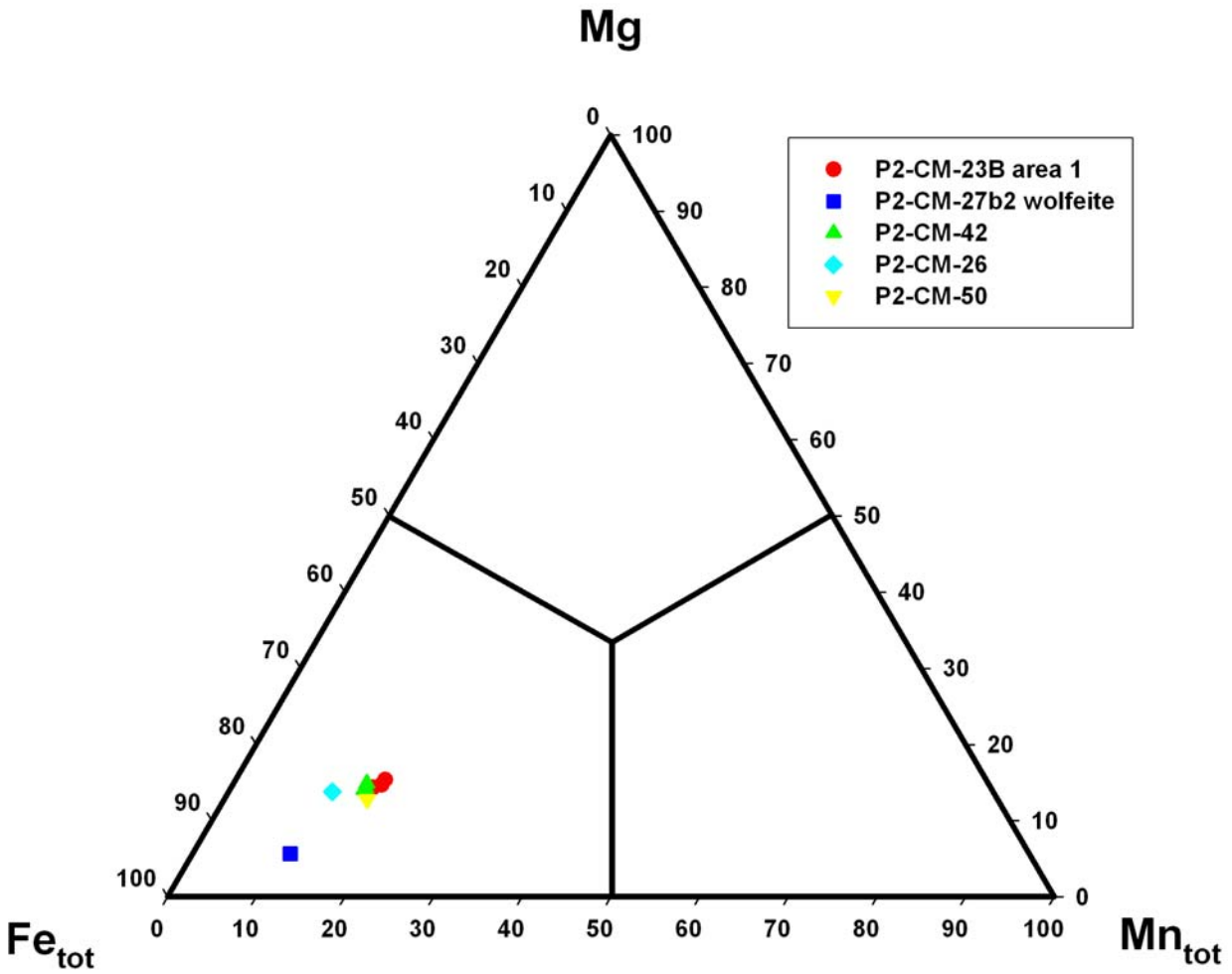

Figure 26: $Fe_{tot}Mn_{tot}Mg$ (apfu) ternary plot of triphylite from Palermo #2.

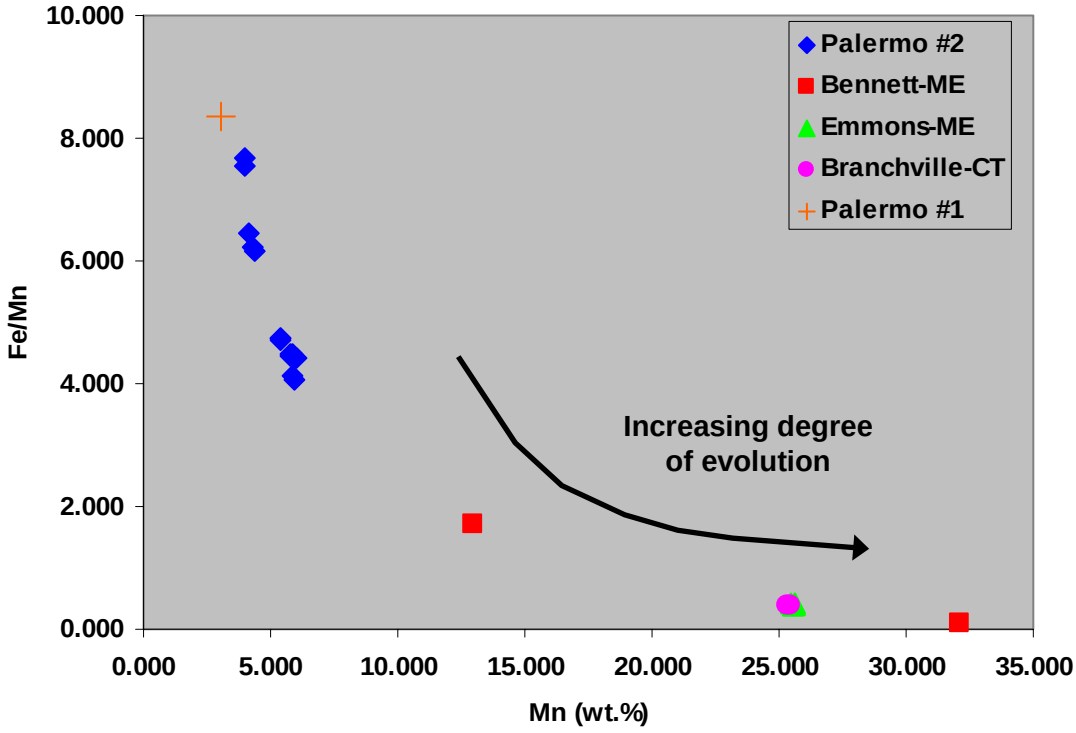

Figure 27: Fe/Mn versus Mn plot of triphylite and lithiophilite from the Palermo #2 and other noted New England phosphate-bearing pegmatites. Analyses of Bennett triphylite and lithiophilite from Wise and Rose, 2000. Analysis from Palermo #1 from unpublished data of M.A. Wise.

Apatite group:

Fluorapatite – $Ca_5(PO_4)_3F$

Hydroxylapatite - $Ca_5(PO_4)_3(OH)$

Chlorapatite - $Ca_5(PO_4)_3Cl$

Members of the apatite group are abundant throughout the Palermo #2 pegmatite. Fluorapatite and hydroxylapatite occur in the border through core margin zones, whereas chlorapatite is restricted to the core margin. Fluorapatite is quite variable in its occurrence and appearance. Fluorapatite in the border, wall and intermediate zones forms in masses or as crude prismatic green to white crystals that sometimes exhibit pinacoidal terminations. Crystals occurring in secondary cavities

may be green, white or colorless, display highly variable aspect ratios and may be more complex in morphology with the addition of pyramidal forms to the previously cited prisms and pinacoids (Figure 31). Fluorapatite masses and crystals may reach 1 cm in maximum dimension. Primary hydroxylapatite occurs throughout the pegmatite although it appears with much higher frequency in the core margin zone. Hydroxylapatite ranges from green to white to colorless to sky blue in color and occurs in masses to 30 cm (Figure 32). Euhedral crystals of secondary hydroxylapatite in cavities display simple prism and pinacoidal forms. Chlorapatite, a secondary or tertiary phase, typically occurs as small white masses related to the alteration of montebrasite (Figure 34). Chlorapatite may form very rare white prismatic crystals in voids created by subsolidus alteration of primary phosphates (montebrasite) (Figure 33). The presence of chlorapatite and/or hydroxylapatite as a consequence of the subsolidus alteration of montebrasite has been reported from pegmatites in the White Picacho district, AZ (London and Burt, 1982) as well as at the Daheim and Okatjimukuju Farm pegmatites in the Karibib-Usakos pegmatite field of Namibia (Baldwin *et al*., 2000). Chlorapatite has also been observed as a product derived from the alteration of alluaudite in the Angarf-Sud pegmatite, Anti-Atlas, Morocco (Fransolet *et al*., 1985).

Table 5 presents electron microprobe analyses of apatite group minerals from Palermo #2. Fluorine content varies considerably, however fluorapatite from the outer zones of the pegmatite exhibits higher concentrations of F^- than those in the core margin zone. The anionic composition of apatite from the wall zone of the Palermo #2 pegmatite is shown in Figure 28. Apatite from the wall zone is dominantly fluorapatite and hydroxylapatite. Composition of apatite from the intermediate zone is shown in

Figure 29. Here the average composition is closer to the fluorapatite-hydroxylapatite join. Figure 30 illustrates apatite compositions from the core margin of Palermo #2. Apatite compositions are highly variable in the core margin and appear to be dependent on the timing of crystallization (primary vs. secondary vs. tertiary). Considering Figures 28, 29 and 30, it appears that as crystallization proceeded from the wall zone to the various stages of apatite formation in the core margin, F^- displays a decreasing trend whilst OH^- and Cl^- exhibit an increasing trend. The Palermo #2 pegmatite is anomalous in that it contains relatively large amounts of hydroxylapatite and that hydroxylapatite distribution is not restricted to the core margin of the pegmatite. The decrease in F-content of apatite group minerals from wall zone to core margin may be a monitor of decreasing F-content in the pegmatite forming-melt. This trend is also illustrated by a corresponding increase in OH- and Cl-content in apatite group species.

Carbonate-hydroxylapatite has been reported from the proximal Palermo #1 pegmatite by Segeler *et al*. (1981) and Francis *et al*. (1993). Members of the apatite group from Palermo #2 do not exhibit significant carbonate content. Site occupancy of the PO_4^{3-}-site is quite high (see Table 5), leaving the site only 0.00 to 0.03 apfu that could possibly be attributed to CO_2^{3-}.

Table 5: Representative electron microprobe analyses of apatite group minerals from the Palermo #2 pegmatite.

	Fluorapatite P2-TR-14 wall	Fluorapatite P2-TR-11 intermediate	Hydroxylapatite P2-CM-06 core margin	Hydroxylapatite P2-CM-11 core margin	Chlorapatite P2-CM-36 core margin
P_2O_5	41.88	41.88	41.30	41.95	42.08
SiO_2	0.00	0.00	0.00	0.00	0.00
TiO_2	0.00	0.00	0.00	0.00	0.17
Al_2O_3	0.08	0.08	0.00	0.01	0.01
CaO	53.83	54.03	53.05	55.36	49.08
MnO	1.75	1.57	0.71	0.19	5.25
FeO	0.15	0.11	0.03	0.02	1.82
MgO	0.00	0.00	0.00	0.00	0.04
SrO	0.00	0.08	1.65	0.00	0.00
Na_2O	0.08	0.13	0.00	0.00	0.10
F	2.01	2.23	1.66	1.49	0.60
Cl	0.00	0.00	0.28	0.66	3.21
H_2O	0.83	0.73	0.89	0.90	0.69
$O=(F,Cl)_2$	-0.85	-0.94	-0.76	-0.78	-0.98
Total	99.76	99.90	98.80	99.79	102.07
	Normalized to 12 oxygen atoms + 1(OH^-, F^-, Cl^-)				
	OH^- calculated by difference				
P	2.983	2.968	2.999	2.996	2.981
Si	0.000	0.000	0.000	0.000	0.000
Ti	0.000	0.000	0.000	0.000	0.011
Al	0.008	0.008	0.000	0.001	0.001
Σ	2.991	2.976	2.999	2.997	2.993
Ca	4.853	4.845	4.876	5.003	4.400
Mn	0.125	0.112	0.052	0.013	0.372
Fe	0.011	0.007	0.002	0.001	0.127
Mg	0.000	0.000	0.000	0.000	0.005
Sr	0.000	0.004	0.082	0.000	0.000
Na	0.013	0.020	0.000	0.000	0.016
Σ	5.002	4.988	5.012	5.017	4.920
F^-	0.535	0.591	0.449	0.397	0.159
Cl^-	0.000	0.000	0.040	0.094	0.455
OH^-	0.465	0.409	0.511	0.509	0.386
Σ	1.000	1.000	1.000	1.000	1.000

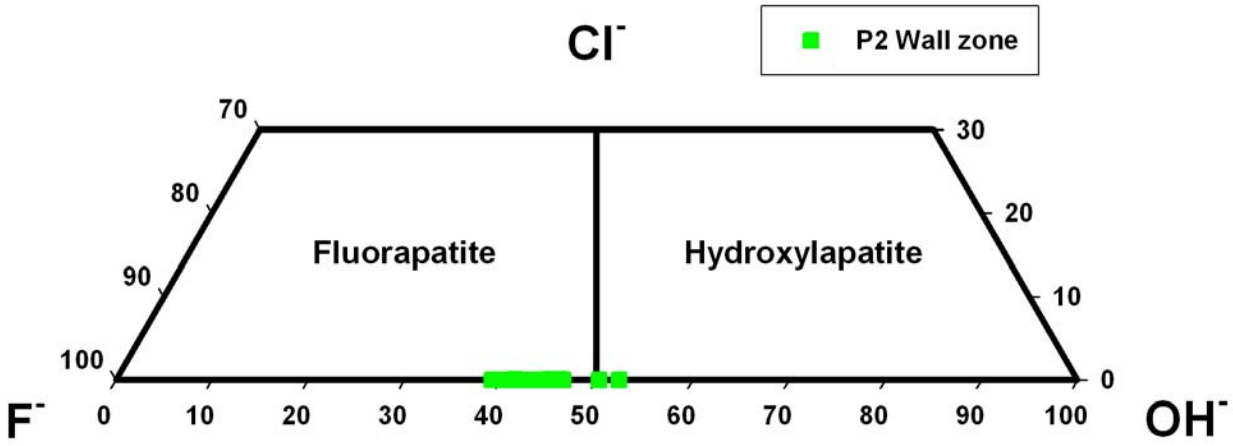

Figure 28: Ternary plot of the anionic content (apfu) of apatite group minerals from the wall zone of the Palermo #2 pegmatite.

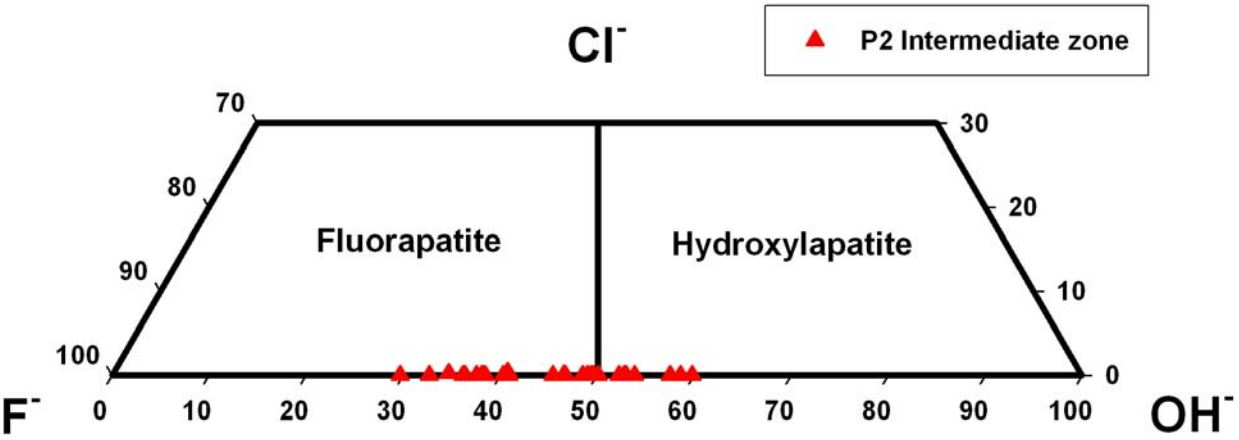

Figure 29: Ternary plot of apatite group anions (apfu) from the intermediate zone of the Palermo #2 pegmatite.

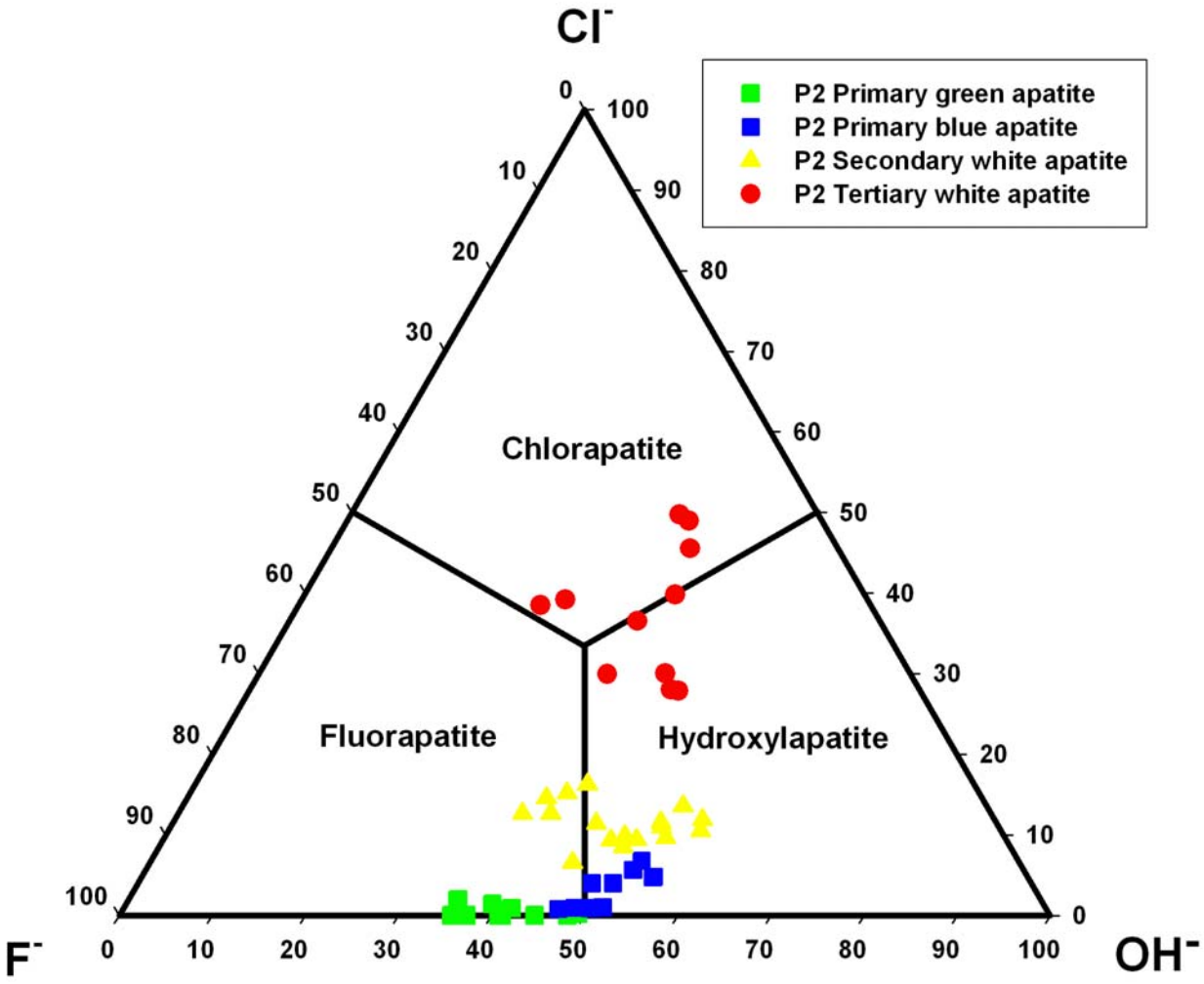

Figure 30: Ternary plot of anionic content (apfu) of apatite group members from the core margin zone of the Palermo #2 pegmatite.

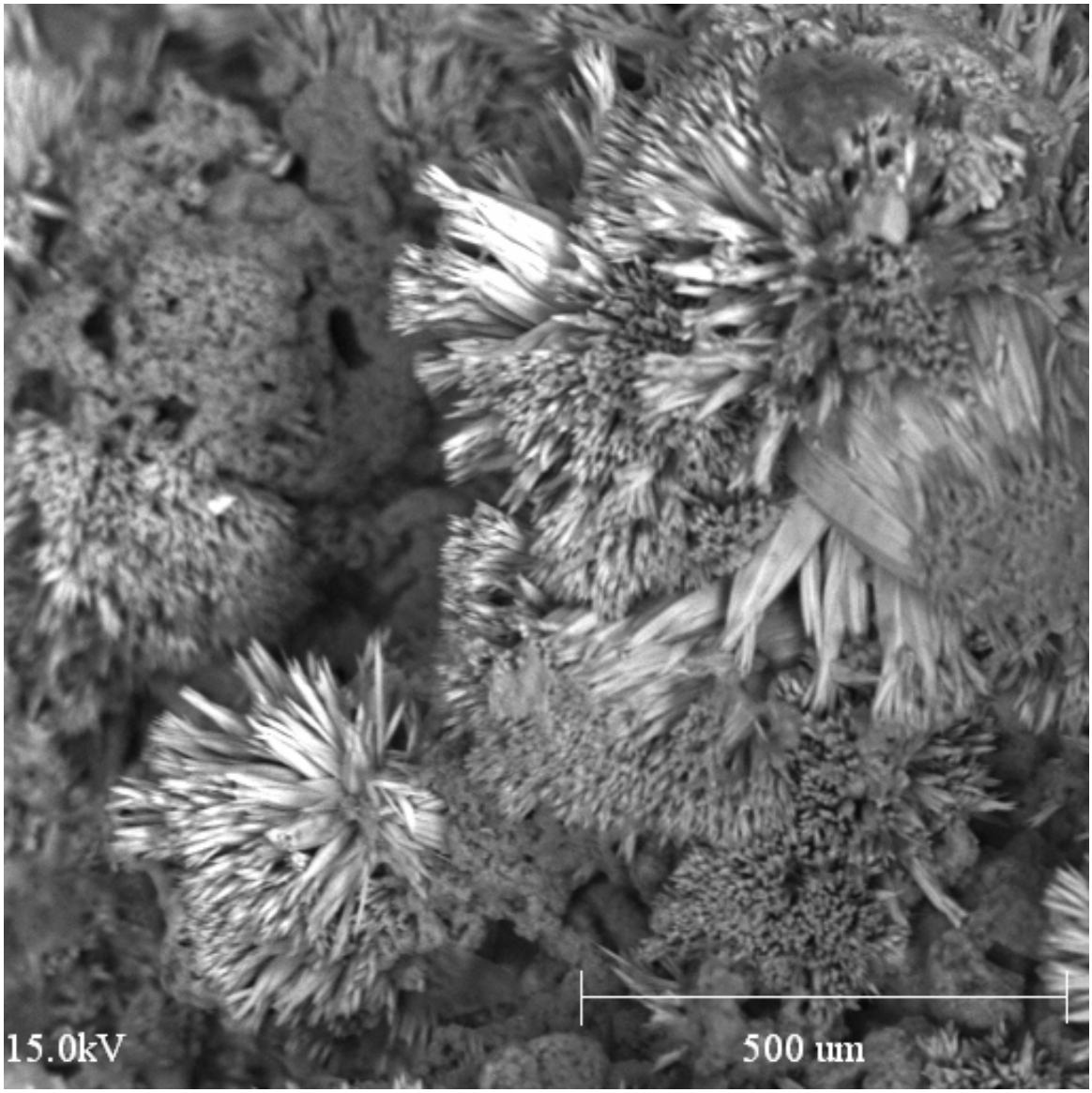

Figure 31: Backscattered electron image of nearly acicular secondary fluorapatite hosted within a cavity in siderite from the core margin of Palermo #2.

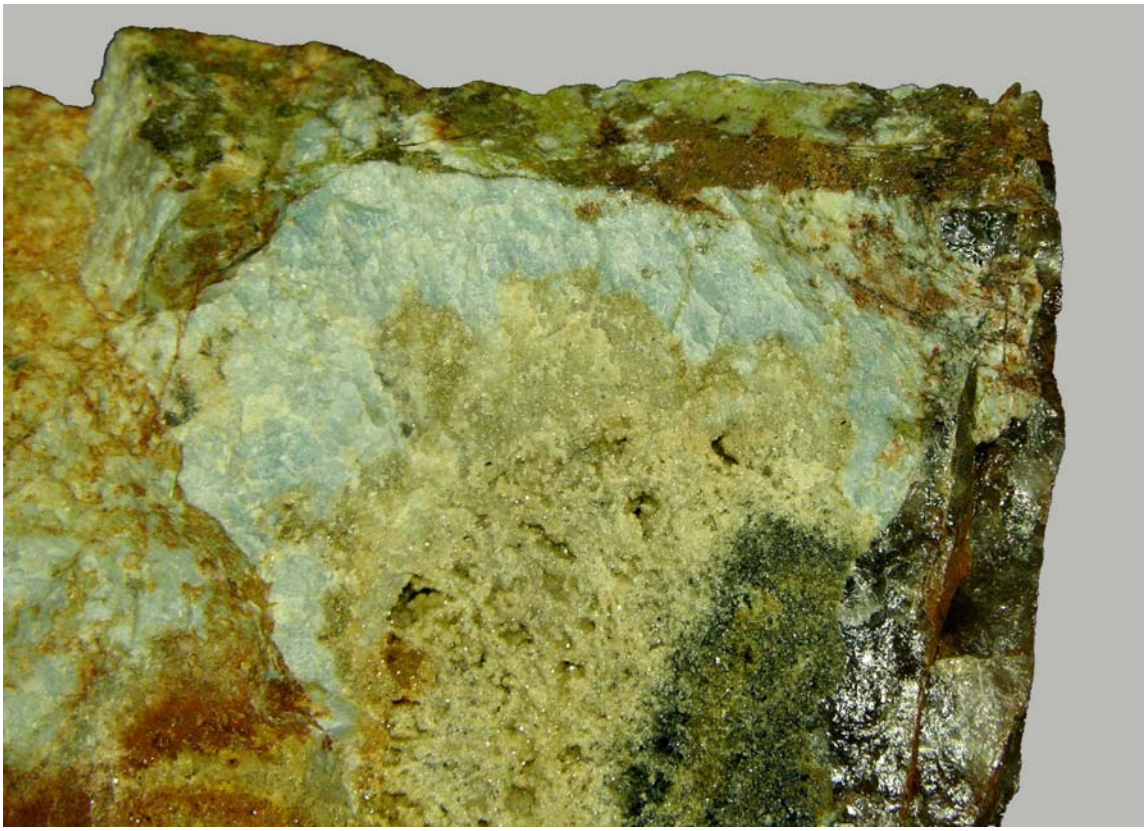

Figure 32: Primary hydroxylapatite (light blue) pod exhibiting partial replacement by siderite (tan) from the Palermo #2 pegmatite. Field of view is approximately 10 cm.

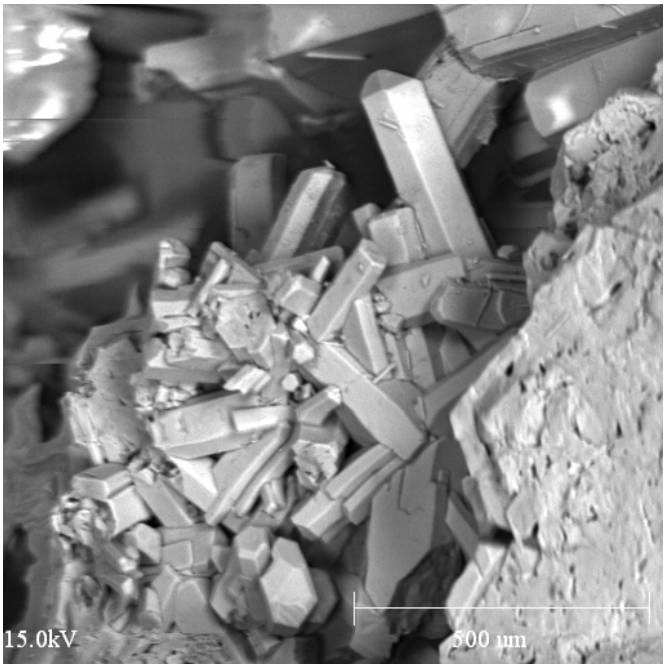

Figure 33: Backscattered electron image of euhedral chlorapatite crystals related to the alteration of montebrasite from the Palermo #2 pegmatite.

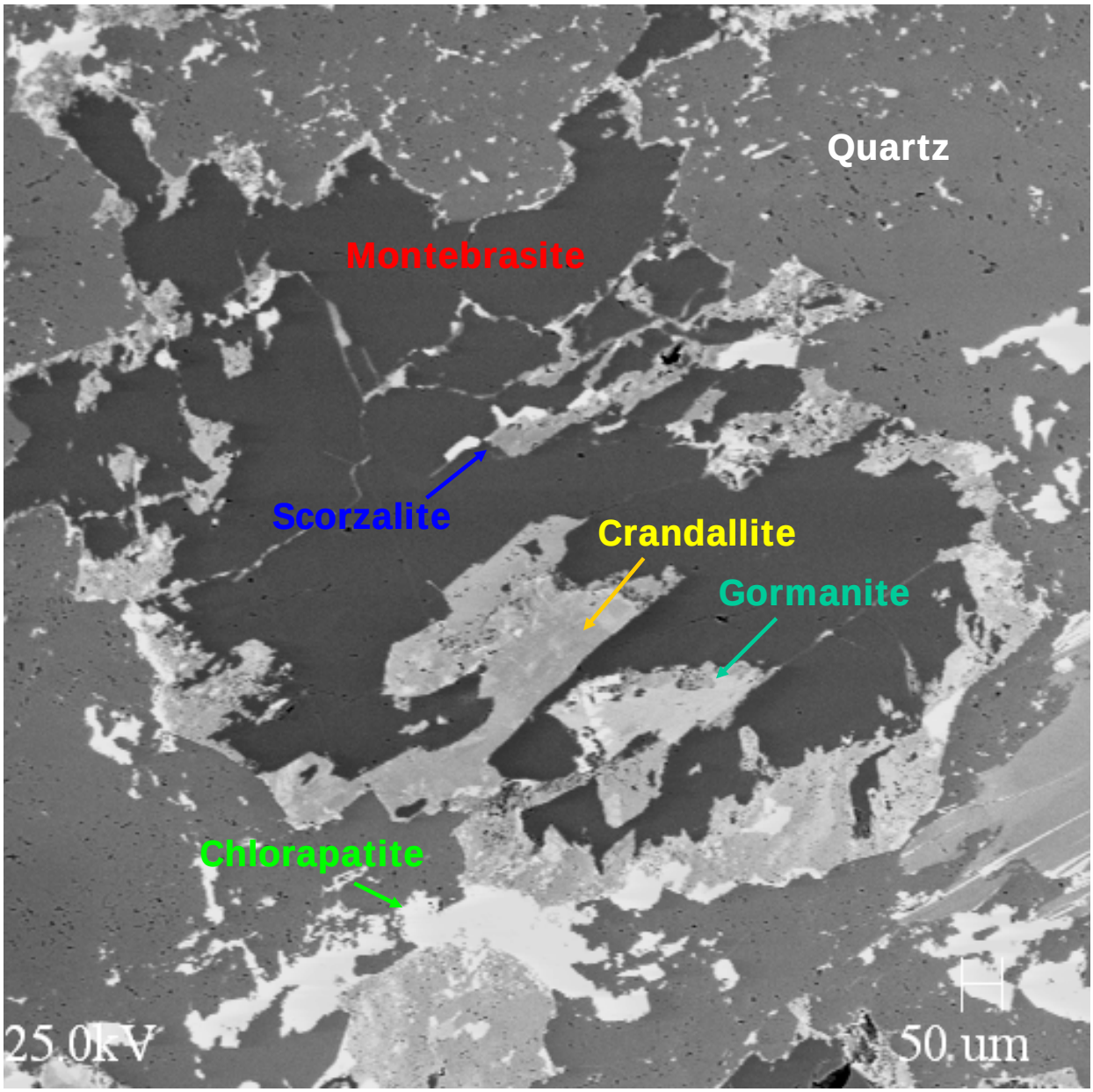

Figure 34: Backscattered electron image of chlorapatite as one of several alteration products of montebrasite from the Palermo #2 pegmatite (Nizamoff *et al.* 2003).

Montebrasite – (Li,Na)AlPO$_4$(OH,F)

Montebrasite occurs as a primary phase and is restricted to the core margin of Palermo #2. Montebrasite is present as white masses up to 2 cm in association with muscovite, scorzalite-lazulite, quartz and triphylite (Figure 35). Nearly all montebrasite at Palermo #2 displays some alteration to scorzalite-lazulite, augelite, gormanite-souzalite, crandallite-goyazite or apatite group (hydroxylapatite and chlorapatite) secondary phosphates (Figure 37). F^- content is quite low and ranges from 1.04 to 2.48% (Table 6). London and Burt (1982) and Černá *et al*. (1972) report similar F content (1.5 to 3.5%) is indicative of secondary montebrasite from pegmatites of the White Picacho district, AZ and the Tanco pegmatite, Manitoba, Canada respectively. Examination of montebrasite from Palermo #2 in polished and thin section reveals it to be a primary phase (Figure 36). In contrast to the Palermo #1 pegmatite, montebrasite from the Palermo #2 pegmatite does not exhibit any evidence of alteration via Na-bearing fluids (lack of Na-bearing secondary phosphates: brazilianite and wardite).

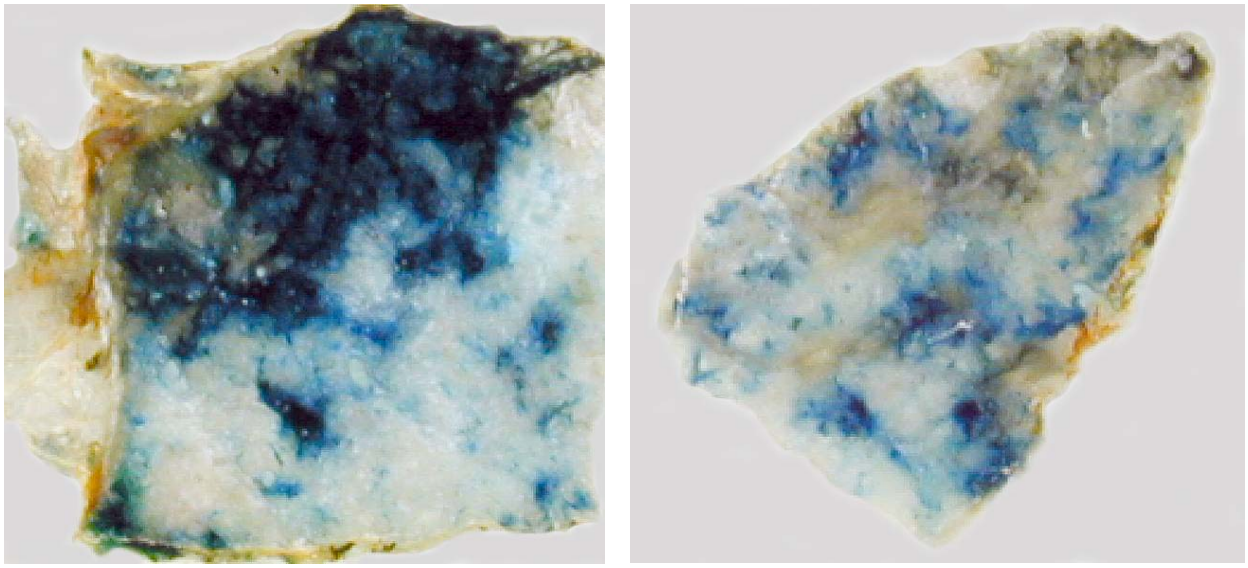

Figure 35: Primary montebrasite (white) exhibiting alteration to scorzalite-lazulite (blue) from the Palermo #2 pegmatite. Field of view is approximately 1.5 cm.

Table 6: Representative electron microprobe analyses of montebrasite from the Palermo #2 pegmatite.

	P2-CM-24	P2-CM-27	P2-CM-08
P_2O_5	47.87	46.25	46.90
SiO_2	0.01	0.18	0.07
TiO_2	0.03	0.00	0.19
Al_2O_3	33.90	33.54	34.59
FeO	0.17	0.15	0.04
CaO	0.01	0.00	0.09
MnO	0.07	0.00	0.01
MgO	0.00	0.00	0.08
Na_2O	0.43	0.08	0.01
Li_2O	10.32	10.19	10.33
H_2O	5.24	5.15	5.37
F	2.34	2.15	1.88
O=F	0.99	0.91	0.79
Total	99.41	96.79	98.76
Cations based on 4 oxygen atoms			
Normalized to 1 P atom			
Li^+ and OH^- calculated by difference			
Li	0.978	0.996	0.994
Na	0.021	0.004	0.001
Ca	0.000	0.000	0.002
Σ	0.999	1.000	0.997
Al	0.986	1.010	1.027
Fe	0.004	0.003	0.001
Ti	0.001	0.000	0.004
Mn	0.002	0.000	0.000
Mg	0.000	0.000	0.003
Σ	0.993	1.013	1.035
P	1.000	1.000	1.000
Si	0.000	0.005	0.002
Σ	1.000	1.005	1.002
OH^-	0.817	0.826	0.850
F	0.183	0.174	0.150
Σ	1.000	1.000	1.000

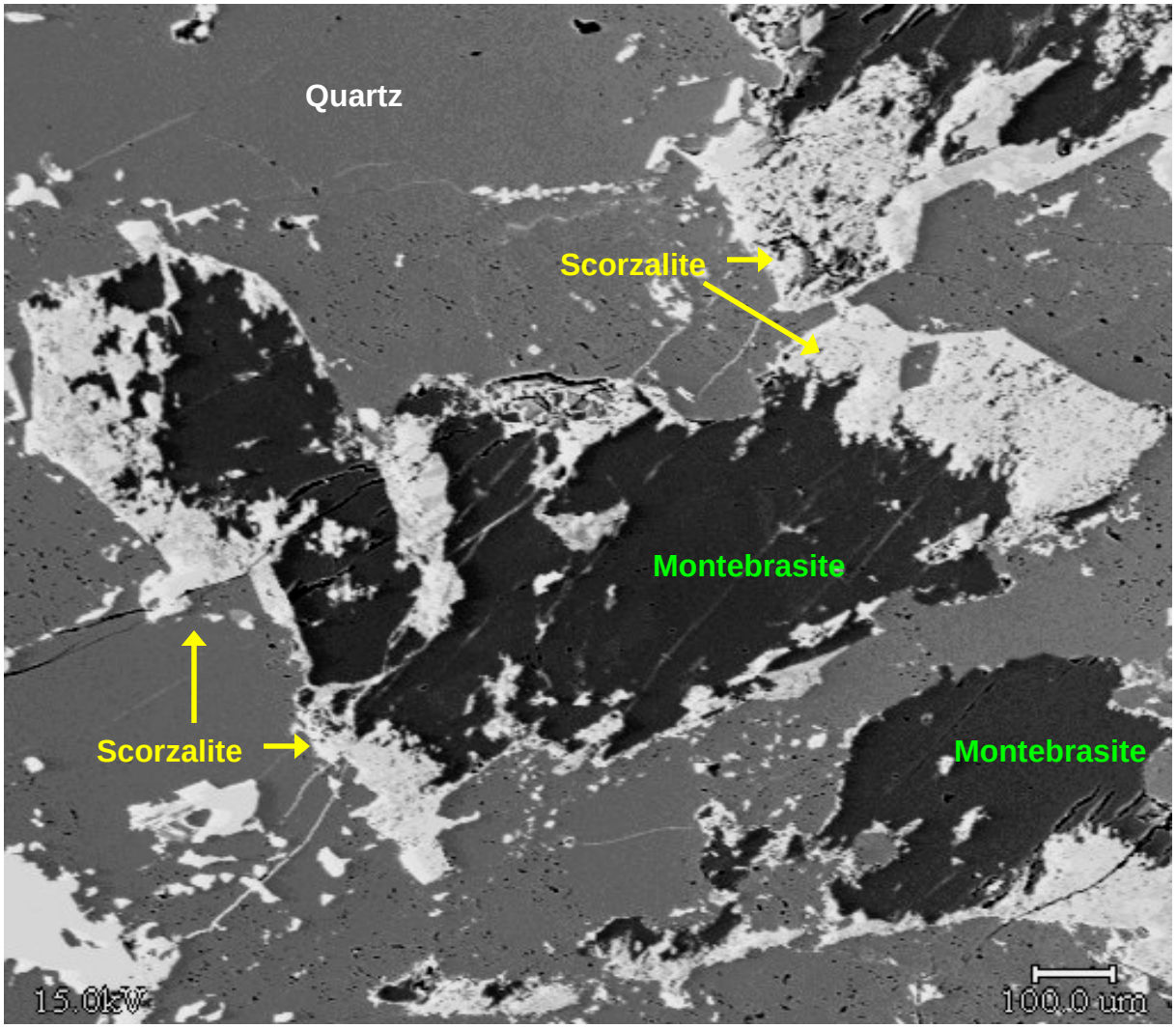

Figure 36: Backscattered electron image showing incipient alteration of montebrasite (black) to scorzalite (white) (Nizamoff *et al.* 2003).

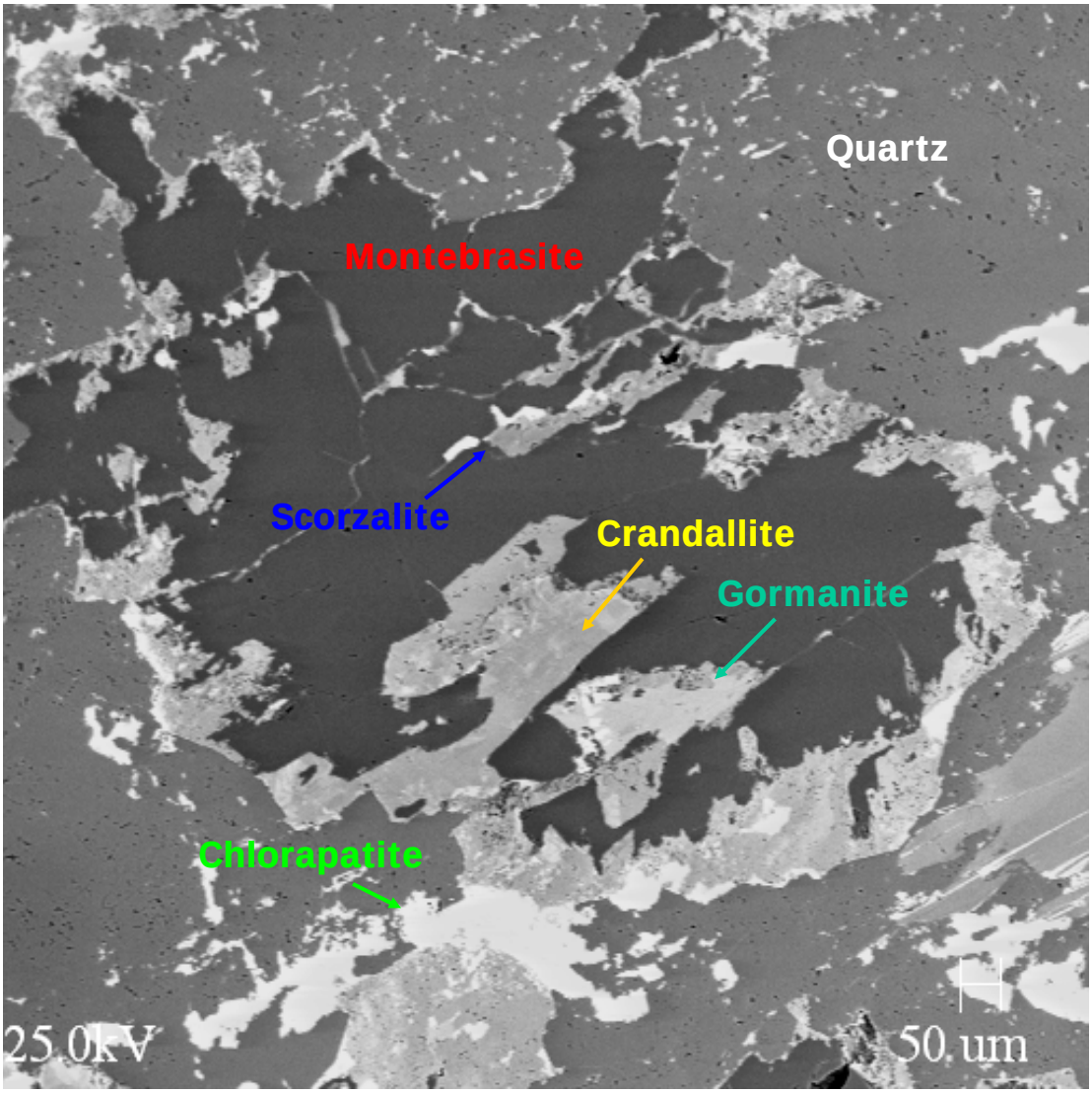

Figure 37: Backscattered electron image depicting primary montebrasite (black) and associated alteration products (scorzalite-medium gray, gormanite-medium gray, crandallite-light gray, hydroxyl-/chlorapatite-white) from Palermo #2.

Graftonite – $(Fe^{2+},Mn^{2+},Ca)_3(PO_4)_2$

Graftonite is a rare primary phosphate at Palermo #2, forming crudely crystallized dark reddish brown masses up to 10 cm in maximum dimension (Figure 38). Sarcopside is present as a lamellar intergrowth with graftonite. Graftonite and sarcopside occur in alternating layers that are approximately 1 mm in thickness. Several authors have suggested that the lamellar intergrowth of graftonite and

sarcopside is a result of an exsolution process (Peacor & Garske, 1964; Hurlbut, 1965; Hurlbut & Aristarain, 1968; Moore, 1972; Smeds *et al*. 1998). Wise and Černý (1990) report the lamellar intergrowth observed as being an exsolution product of a high temperature, (Li,Ca)-rich precursor of graftonite. FeO content in graftonite from Palermo #2 ranges from 37.6 to 38.3 wt.% and MnO ranges from 12.4 to 12.6 wt.% (Table 7 and Figure 39). CaO content remains nearly constant at 7.1 wt.%. The lack of compositional variability may be a result of the few analyses of graftonite from Palermo #2. In contrast with graftonite from Palermo #2, graftonite from the nearby Palermo #1 and Rice Mine pegmatites contains greater amounts of CaO (10.1 and 11.9 wt.%, respectively) and MnO (13.5 and 17.1 wt.%, respectively) with correspondingly lower amounts of FeO (32.5 and 28.2 wt.%, respectively) (Figure 40).

Figure 38: Graftonite-sarcopside intergrowth from the Palermo #2 pegmatite. Field of view is approximately 3 cm.

Table 7: Representative electron microprobe analyses of graftonite and sarcopside from the Palermo #2 pegmatite.

	Graftonite P2-CM-45	Sarcopside P2-CM-45
P_2O_5	40.76	40.62
SiO_2	0.00	0.00
Al_2O_3	0.00	0.00
FeO	37.59	44.40
MnO	12.51	12.68
MgO	1.72	1.79
ZnO	0.03	0.00
CaO	7.10	0.12
Na_2O	0.00	0.00
Total	99.71	99.60
Cations based on 8 oxygen atoms		
P	1.993	2.014
Si	0.000	0.000
Σ	1.993	2.014
Fe	1.816	2.174
Na	0.000	0.000
Mn	0.612	0.629
Mg	0.148	0.156
Zn	0.001	0.000
Ca	0.439	0.007
Al	0.000	0.000
Σ	3.016	2.966
Fe/(Fe+Mn) =	0.75	0.78

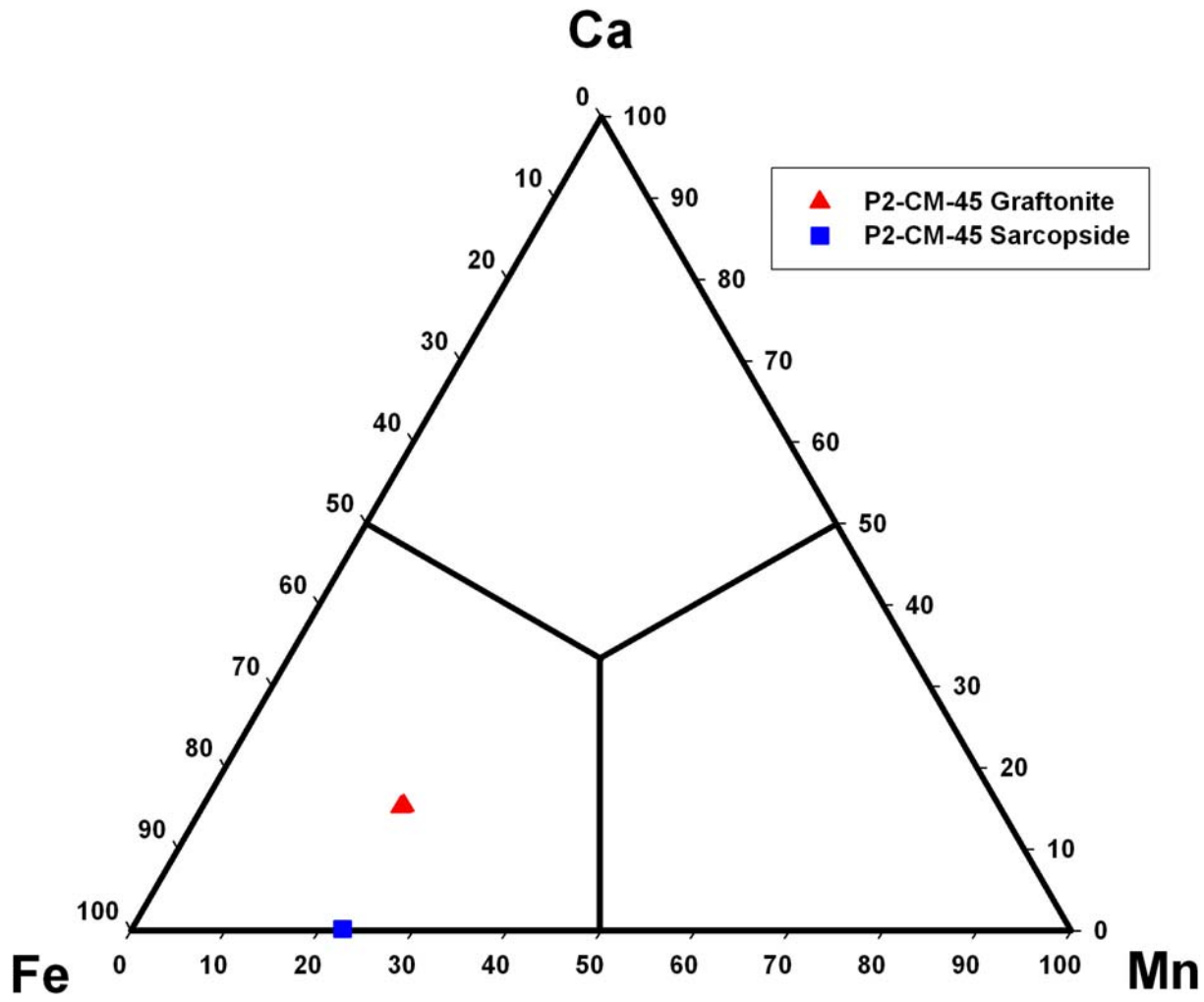

Figure 39: Ternary plot of Fe, Mn and Ca for graftonite and sarcopside from the Palermo #2 pegmatite.

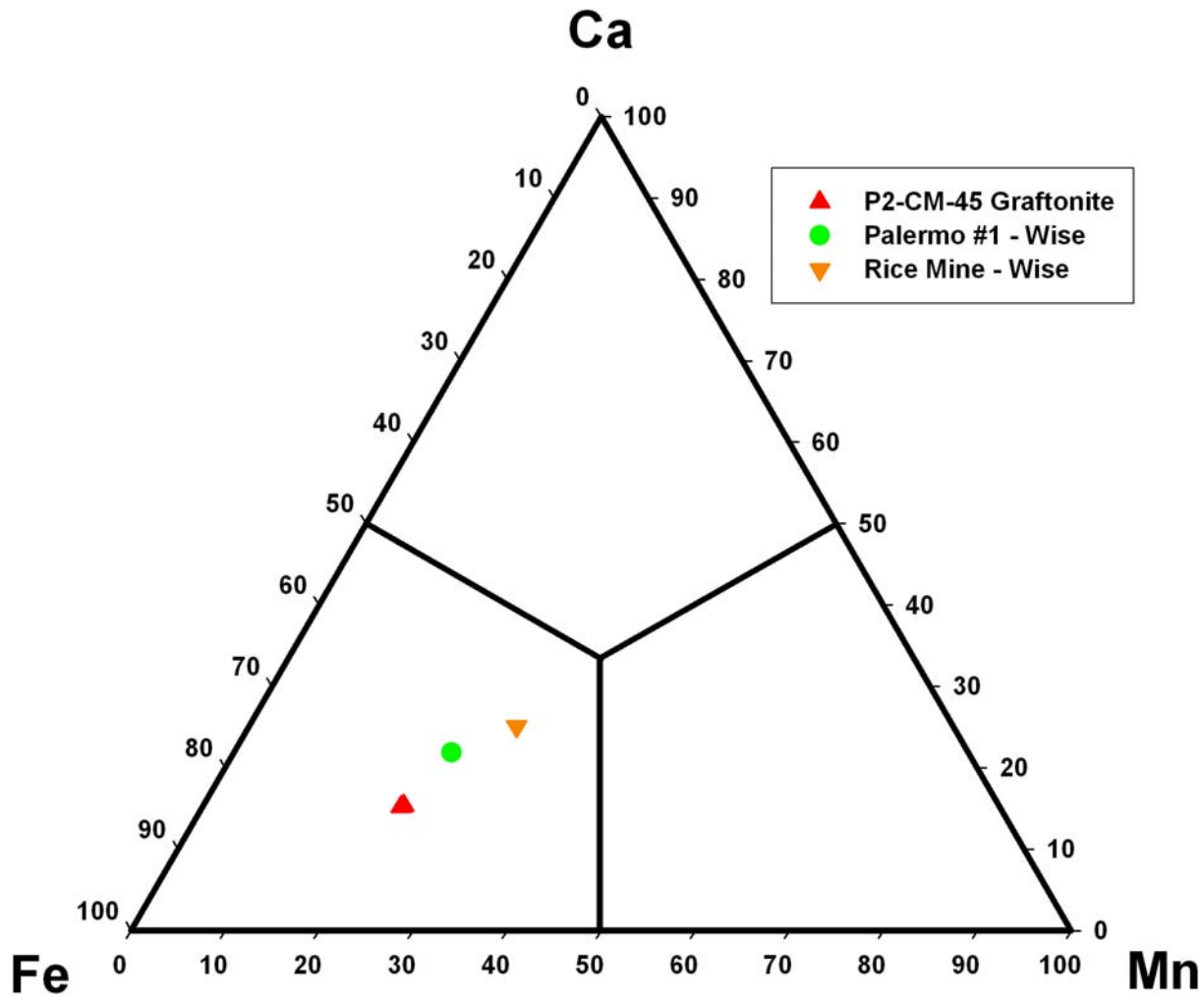

Figure 40: Ternary plot of Fe, Mn and Ca for graftonite from the Palermo #2 pegmatite and proximal Palermo #1 and Rice Mine pegmatites. Palermo #1 and Rice Mine data provided by M.A. Wise.

Sarcopside – $Fe_3(PO_4)_2$

Sarcopside is a rare primary phase at Palermo #2 and only occurs as an intergrowth with graftonite. Light reddish brown (graftonite) and brownish gray (sarcopside) alternating ~1 mm thick layers are thought to represent exsolution from a high temperature, (Li,Ca)-rich precursor of graftonite (Wise and Černý, 1990) (Figure 38). Compositionally, sarcopside differs from graftonite in that it contains less CaO with

a corresponding increase in FeO (Table 7 and Figure 39). MnO and MgO contents are nearly identical between the two species.

Monazite- (Ce) – (Ce, La, Nd)PO_4

Monazite-(Ce) is very rare at Palermo #2 and occurs at the intermediate zone/core margin zone interface. Monazite-(Ce) forms small (< 1 mm) grains hosted by quartz and feldspars (Figure 41). Microprobe analyses of monazite confirmed that Ce is the dominant REE present (Table 8). Nd_2O_3 and La_2O_3 contents range from 16.5 to 17.0 wt.% and 8.1 to 8.8 wt.% respectively.

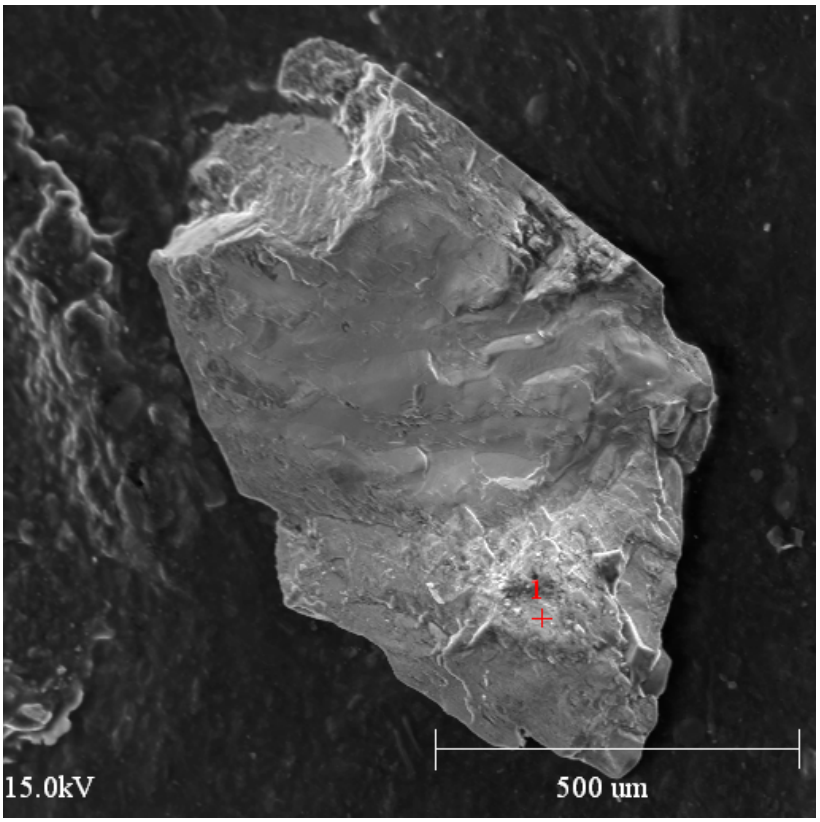

Figure 41: Backscattered electron image of monazite-(Ce) from the Palermo #2 pegmatite.

Xenotime – (Y) – YPO_4

Xenotime-(Y) is a rare phase at Palermo #2 and was identified through heavy mineral separation. Xenotime-(Y) occurs as subhedral grains to 500 μm in size and is typically hosted by quartz and feldspars near the intermediate and core margin zone interface (Figure 42). Compositionally xenotime-(Y) from Palermo #2 is interesting due to its relatively high content of mid-weight rare-earth elements (MREE) (Table 8). Dysprosium (Dy), gadolinium (Gd), erbium (Er) and ytterbium (Yb) oxide contents are moderately elevated and range from ~2 to 4.5%. Roda *et al*. (2004) reports that xenotime-(Y) from the Cañada pegmatite, a phosphate-bearing pegmatite in Salamanca, Spain contains a similar moderate enrichment of Yb_2O_3 (avg. 2.7 wt.%), Dy_2O_3 (6.4 wt.%) and Gd_2O_3 (to 4.3 wt.%).

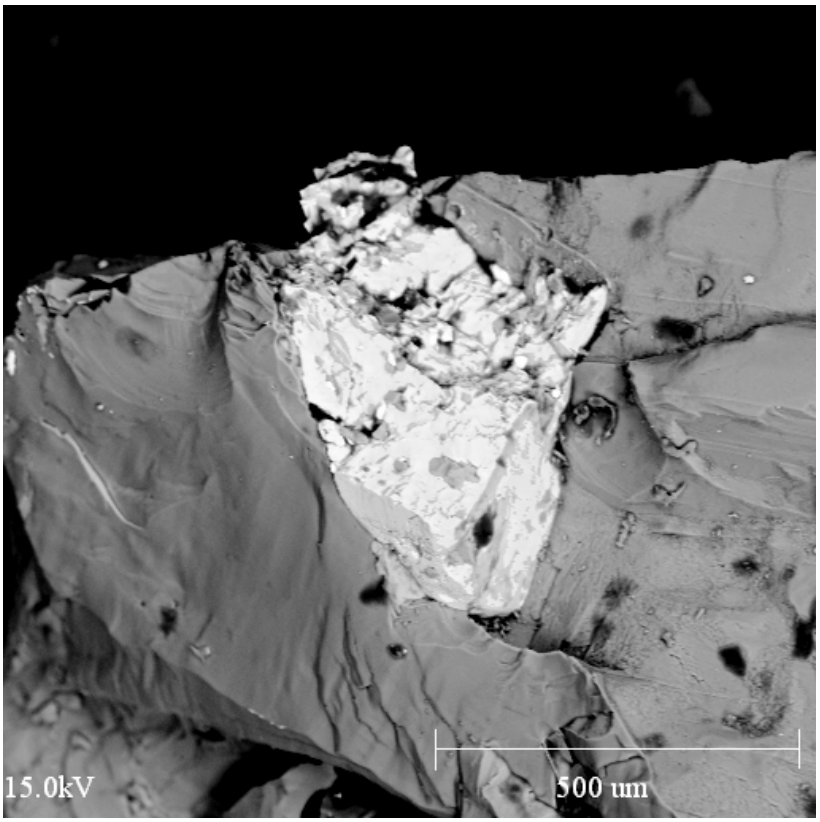

Figure 42: Backscattered electron image of a grain of xenotime-(Y) (white) hosted by quartz from the core margin of the Palermo #2 pegmatite.

Table 8: Representative electron microprobe analyses of xenotime-(Y) and monazite-(Ce) from the Palermo #2 pegmatite.

	Xenotime	Monazite
P_2O_5	35.01	31.87
SiO_2	0.03	2.09
ThO_2	0.02	1.98
UO_2	0.02	0.56
Y_2O_3	49.23	0.00
La_2O_3	0.00	8.78
Ce_2O_3	0.00	26.52
Pr_2O_3	0.00	2.12
Nd_2O_3	0.02	16.99
Sm_2O_3	0.26	2.90
Eu_2O_3	0.00	0.56
Gd_2O_3	2.68	2.45
Tb_2O_3	0.94	0.09
Dy_2O_3	4.55	0.57
Ho_2O_3	0.54	0.00
Er_2O_3	2.05	0.00
Tm_2O_3	0.12	0.00
Yb_2O_3	3.78	0.00
Lu_2O_3	0.03	0.00
Al_2O_3	0.05	0.03
CaO	0.06	1.23
FeO	0.38	0.34
MnO	0.01	0.03
PbO	0.00	0.21
Total	99.77	99.32

	Xenotime	Monazite
Cations based on 4 oxygen atoms		
P	0.979	1.004
Si	0.001	0.078
Σ	0.980	1.082
Th	0.000	0.017
U	0.000	0.005
Y	0.865	0.000
La	0.000	0.120
Ce	0.000	0.361
Pr	0.000	0.029
Nd	0.000	0.226
Sm	0.003	0.037
Eu	0.000	0.007
Gd	0.029	0.030
Tb	0.010	0.001
Dy	0.048	0.007
Ho	0.006	0.000
Er	0.021	0.000
Tm	0.001	0.000
Yb	0.038	0.000
Lu	0.000	0.000
Al	0.002	0.001
Ca	0.002	0.049
Fe	0.010	0.011
Mn	0.000	0.001
Pb	0.000	0.002
Σ	1.038	0.904

Arrojadite group member – $KNa_4Ca(Fe^{2+}Mn^{2+})_{14}Al(PO_4)_{12}(OH,F)_2$

X-ray diffraction analyses have confirmed that a member of the arrojadite group occurs in small quantities at Palermo #2. "Arrojadite" forms masses of platy crystals up to 3 mm across that are typically intergrown with vivianite. Backscattered electron

images reveal that the “arrojadite” appears to be a primary phase that has undergone alteration to secondary products (Figure 43). Vivianite and goyazite(?) occur as alteration products of “arrojadite” from Palermo #2. Microprobe analyses are necessary to properly speciate the “arrojadite” from Palermo #2.

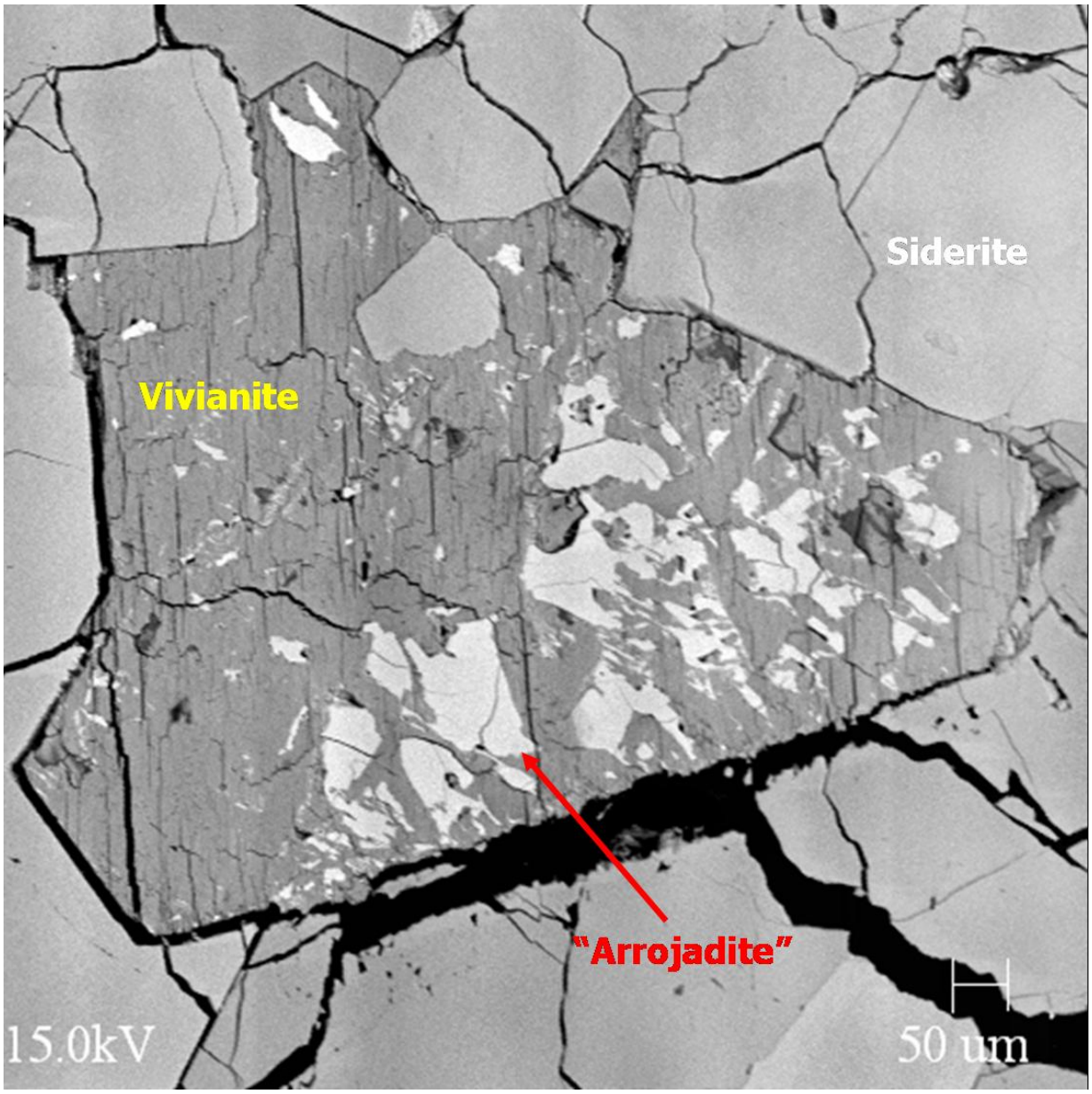

Figure 43: Backscattered electron image of vivianite associated with relict fragments of “arrojadite” from sample P2-CM-07 from the Palermo #2 pegmatite, North Groton, NH. The vivianite and “arrojadite” are hosted by granular crystals of siderite.

Wolfeite – $Fe^{2+}_2(PO_4)(OH)$

Wolfeite occurs exclusively as reddish brown inclusions (up to 1.5 cm) in triphylite (Figure 44). Most researchers consider wolfeite to be a primary phase (Plimer and Bucher, 1979; Moore, 1982), however work by Frondel (1949) and Masau *et al*. (2000) suggested that wolfeite can result from metasomatic alteration of arrojadite group minerals. Wolfeite from Palermo #2 does not exhibit strong textural evidence suggesting that it is an alteration product of triphylite. Compositionally wolfeite from Palermo #2 displays little variation in FeO, MnO and MgO content (Table 9).

Figure 44: Reddish grains of wolfeite hosted by gray-blue triphylite from the Palermo #2 pegmatite. Field of view is approximately 2 cm.

Table 9: Representative electron microprobe analyses of wolfeite from the Palermo #2 pegmatite.

	P2-CM-27a	P2-CM-27b
P_2O_5	32.80	32.68
SiO_2	0.04	0.12
Al_2O_3	0.02	0.04
FeO	43.10	44.23
MgO	3.97	3.23
CaO	0.05	0.05
MnO	16.02	15.99
Na_2O	0.06	0.10
H_2O	4.17	4.16
Total	100.23	100.60
Cations based on 4 oxygen atoms		
OH^- calculated by stoichiometry		
P	0.998	0.996
Si	0.001	0.004
Al	0.001	0.002
Σ	1.000	1.002
Fe	1.296	1.332
Mg	0.213	0.174
Ca	0.002	0.002
Mn	0.488	0.488
Na	0.004	0.007
Σ	2.003	2.003
OH	1.000	1.000
Σ	1.000	1.000

High Temperature Secondary Phosphates:

Ferrisicklerite – $Li(Fe^{3+}, Mn^{2+})PO_4$

Ferrisicklerite typically occurs as a dark brown rind on triphylite masses (Figure 45). Ferrisicklerite is a common alteration product of primary triphylite at Palermo #2 and may completely replace masses or crystals of triphylite. Ferrisicklerite is formed via high temperature metasomatic alteration of triphylite causing divalent Fe to be oxidized to trivalent Fe. A representative electron microprobe analysis of ferrisicklerite is shown Table 10.

Figure 45: Ferrisicklerite rind (dark brown) on the outer margin of a triphylite mass from the Palermo #2 pegmatite, North Groton, NH. View is 5 cm across.

Table 10: Representative electron microprobe analysis of ferrisicklerite from Palermo #2.

	P2-CM-23b
P_2O_5	46.96
SiO_2	0.97
Fe_2O_3	35.37
Al_2O_3	0.03
MnO	6.87
MgO	3.89
CaO	0.07
Na_2O	0.03
Total	98.11

Cations based on 4 oxygen atoms

Normalized to 1 P atom

Li by difference

Li	0.998
Na	0.002
Σ	1.000
Fe^{3+}	0.744
Mn^{2+}	0.146
Mg	0.146
Ca	0.002
Al	0.001
Σ	1.039
P	1.000
Si	0.024
Σ	1.024

Heterosite – $Fe^{3+}PO_4$

Heterosite occurs as light to dark purple masses and coatings on ferrisicklerite and triphylite (Figure 46). Heterosite is quite common in material collected from the mine tailings dump. Like ferrisicklerite, heterosite is formed via high temperature

metasomatic alteration of triphylite causing divalent Fe to be oxidized to trivalent Fe. Additionally Li^+ is concomitantly leached from the structure of ferrisicklerite resulting in the formation of heterosite. A representative electron microprobe analysis of heterosite is shown Table 11.

Table 11: Representative electron microprobe analysis of heterosite from the Palermo #2 pegmatite.

	P2-CM-23a
P_2O_5	47.27
SiO_2	0.28
TiO_2	0.12
Fe_2O_3	35.70
Al_2O_3	0.10
MnO	7.83
MgO	3.72
Na_2O	0.03
Total	95.93
Cations based on 4 oxygen atoms	
Normalized to 1 P atom	
Fe^{3+}	0.671
Al	0.003
Mn^{2+}	0.166
Mg	0.139
Na	0.002
Σ	0.981
P	1.000
Si	0.007
Ti	0.002
Σ	1.009

Figure 46: Heterosite (10 cm) from the Palermo #2 pegmatite, North Groton, NH. Note development of yellow strunzite and black rockbridgeite along the outer margin.

Lazulite group:

Scorzalite – $(Fe^{2+},Mg)Al_2(PO_4)_2(OH)_2$

Lazulite – $MgAl_2(PO_4)_2(OH)_2$

Scorzalite-lazulite occurs infrequently at Palermo #2 as a high temperature metasomatic alteration product of montebrasite and/or triphylite + muscovite. Scorzalite-lazulite occurs as blue masses to 3 cm surrounding montebrasite and other Al-bearing secondary phosphates (Figure 47 and 48). Scorzalite-lazulite is also found as small blue patches (< 1 cm) in the vicinity of triphylite that may be intermixed with muscovite. FeO content in scorzalite-lazulite ranges from 4.0 to 16.0 wt.% whereas MgO content varies from 2.6 to 10.6 wt.% (Table 12). Fransolet (1975) reports that scorzalite from the Angarf-Sud pegmatite, Anti-Atlas, Morocco is an alteration product of

triphylite with Al^{3+} introduced from the decomposition of muscovite. Fransolet (1975) also proposed that scorzalite formed in temperature range of ~600 to 500ºC under conditions of low fO_2 at Angarf-Sud.

Table 12: Representative electron microprobe analyses of scorzalite-lazulite from Palermo #2.

	Lazulite	Scorzalite
P_2O_5	45.18	42.23
SiO_2	0.00	0.00
TiO_2	0.05	0.19
Al_2O_3	32.88	31.88
FeO	8.01	15.89
MgO	8.10	2.58
MnO	0.01	0.12
CaO	0.00	0.11
Na_2O	0.07	0.00
F	0.02	0.00
H_2O	5.75	5.45
Total	100.07	98.45
Cations based on 9 oxygen atoms		
OH^- calculated by difference		
Fe	0.349	0.732
Mg	0.629	0.211
Mn	0.001	0.006
Ca	0.000	0.006
Na	0.007	0.000
Σ	0.986	0.955
Al	2.019	2.069
Σ	2.019	2.069
P	1.993	1.969
Si	0.000	0.000
Ti	0.002	0.008
Σ	1.995	1.977
F	0.003	0.000
OH	1.997	2.002
Σ	2.000	2.002

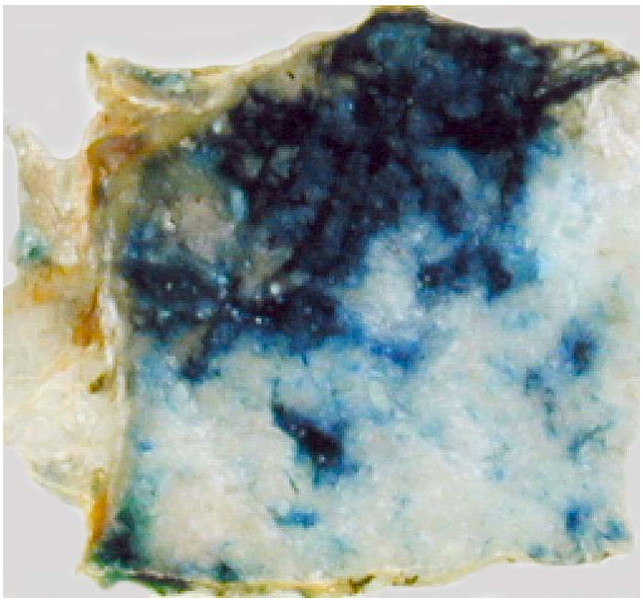

Figure 47: Scorzalite-lazulite (blue), an alteration product of montebrasite (white) from the Palermo #2 pegmatite. Field of view is approximately 1.5 cm

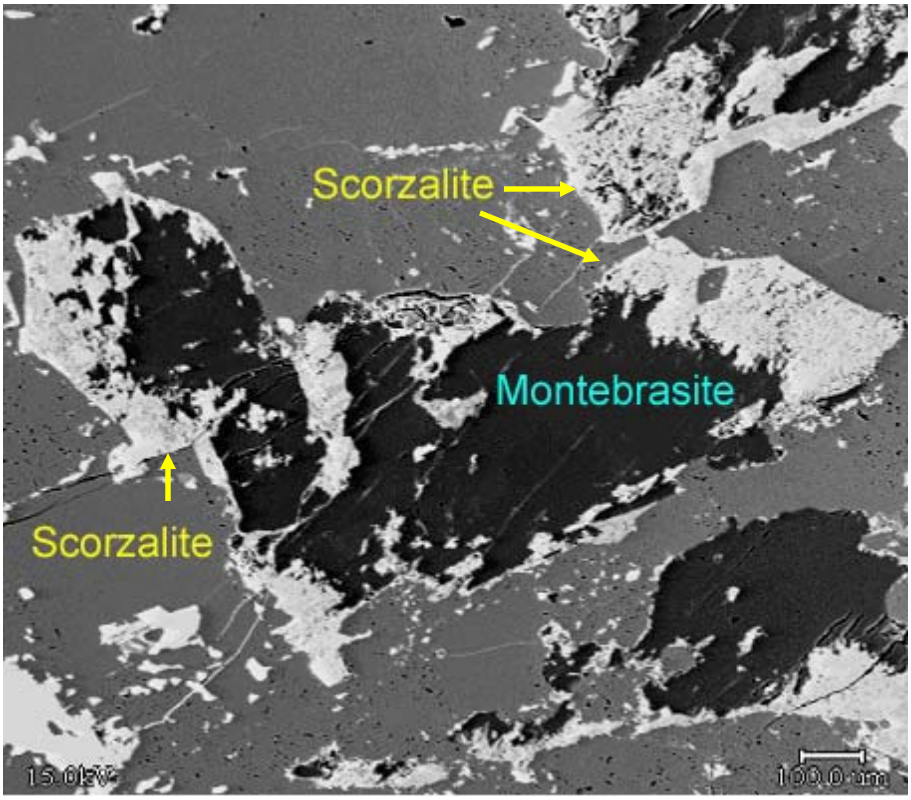

Figure 48: Backscattered electron image showing scorzalite (white) as an alteration product of montebrasite (black) from Nizamoff *et al.* (2003).

Augelite – $Al_2(PO_4)(OH)_3$

Augelite occurs as a high temperature alteration product of montebrasite at Palermo #2. Augelite forms small white to colorless masses (to 700μm) that occur sporadically in gormanite-souzalite (Figure 49). Augelite is a fairly rare phase at Palermo #2 and is associated with gormanite-souzalite, montebrasite, chlorapatite and goyazite-crandallite. A representative electron microprobe analysis of augelite is shown in Table 13.

Table 13: Representative electron microprobe analysis of augelite from the Palermo #2 pegmatite. Low analytical totals are due to the presence of OH^-.

	P2-CM-08
P_2O_5	35.32
TiO_2	0.17
Al_2O_3	48.68
MgO	0.73
FeO	1.32
MnO	0.32
Total	86.54
Cations based on 5.5 oxygen atoms	
Al	1.929
Mg	0.037
Fe^{2+}	0.037
Mn^{2+}	0.009
Σ	2.012
P	1.006
Ti	0.004
Σ	1.010

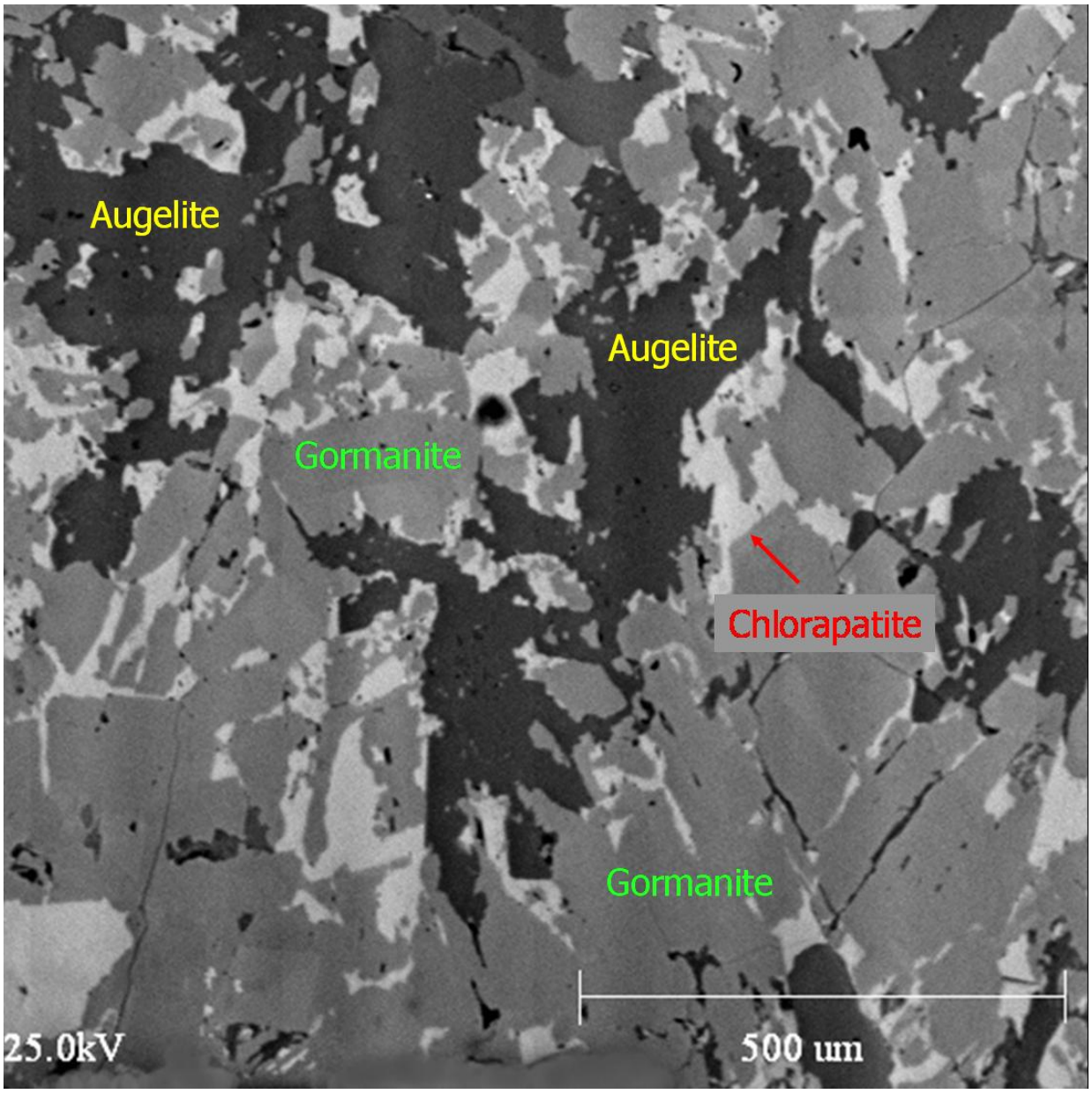

Figure 49: Backscattered electron image of augelite, gormanite and chlorapatite from sample P2-CM-08, Palermo #2 pegmatite.

Low Temperature Secondary Phosphates:

Rockbridgeite – $Fe^{2+}Fe^{3+}_4(PO_4)_3(OH)_5$

Frondelite – $Mn^{2+}Fe^{3+}_4(PO_4)_3(OH)_5$

Rockbridgeite-frondelite is a common low temperature alteration product of triphylite at Palermo #2. Rockbridgeite-frondelite occurs as black to green bladed crystals (< 1.5 mm) that often form mats or hemispherical aggregates (Figures 50 and 51). Rockbridgeite-frondelite typically forms in an oxidizing environment and may be associated with strunzite, laueite, stewartite, ushkovite, beraunite, jahnsite-(CaMnFe), jahnsite-(CaMnMn), jahnsite-(CaMnMg) and whitmoreite. A representative electron microprobe analysis of rockbridgeite is shown in Table 14. Whereas semi-quantitative EDS analyses indicate that frondelite is likely present at Palermo #2, electron microprobe analysis of said samples is necessary to confirm this finding.

Figure 50: Rockbridgeite (black) with beraunite (green), mitridatite (yellow green), jahnsite (brown) lining an alteration cavity in triphylite (blue-gray). Field of view is approximately 3 cm.

Table 14: Representative electron microprobe analysis of rockbridgeite from Palermo #2. Low analytical totals are due to the presence of OH^-.

	P2-CM-16
P_2O_5	32.22
SiO_2	0.02
TiO_2	0.00
Fe_2O_3	48.32
Al_2O_3	0.06
FeO	5.40
MnO	4.73
MgO	0.02
CaO	0.46
Na_2O	0.05
Total	91.29

Cations based on 14.5 oxygen atoms Fe^{2+} calculated by stoichiometry	
Fe^{2+}	0.496
Mn^{2+}	0.441
Mg	0.004
Ca	0.055
Na	0.010
Σ	1.006
Fe^{3+}	3.995
Al	0.007
Σ	4.002
P	2.997
Si	0.002
Σ	2.999

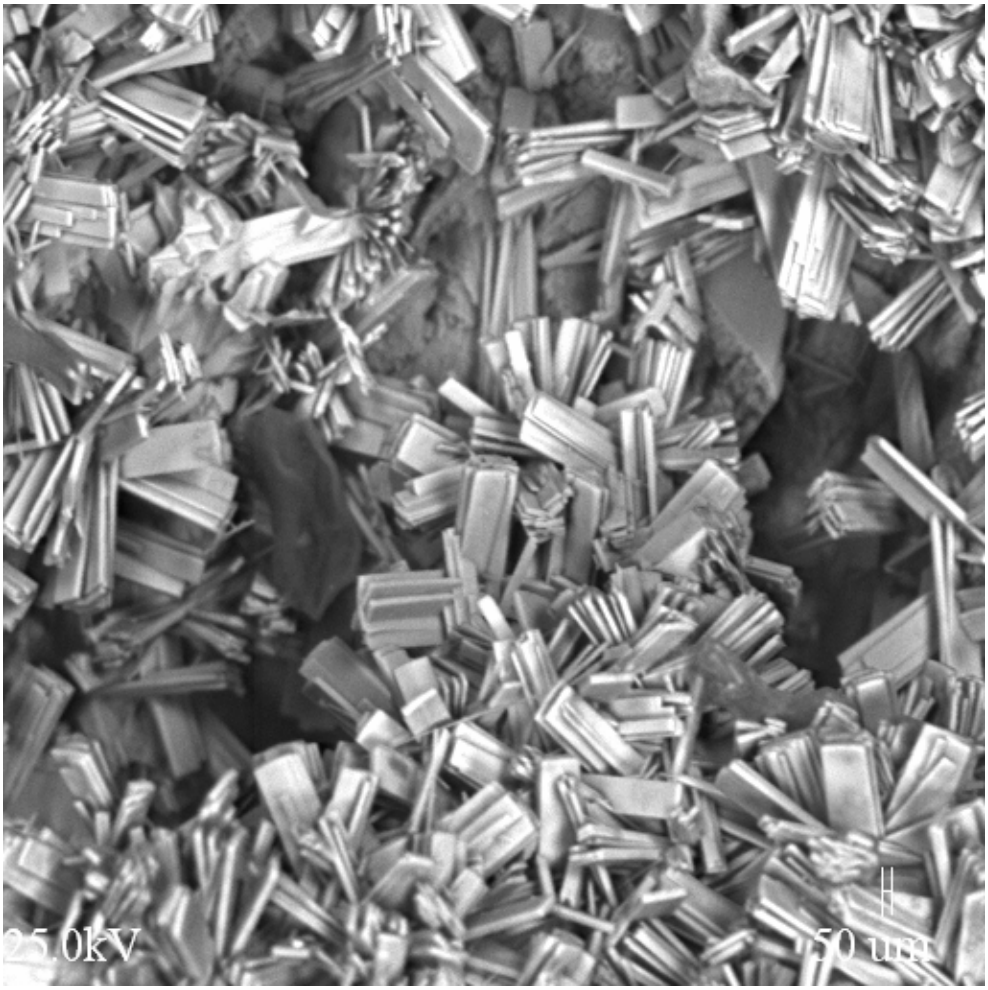

Figure 51: Backscattered electron image of rockbridgeite crystals in a secondary cavity in altered triphylite from the Palermo #2 pegmatite.

Beraunite – $Fe^{2+}Fe^{3+}_5(PO_4)_4(OH)_5 \cdot 4\ H_2O$

Beraunite occurs as greenish acicular crystals to 1.5 mm that often form spherical aggregates or as radiating sprays of crystals (Figure 52 and 53). In highly oxidized environments, beraunite may possess an orange color and form as botryoidal crusts. Beraunite typically forms in an oxidizing environment and may be associated with strunzite, laueite, stewartite, rockbridgeite-frondelite, jahnsite-(CaMnFe), jahnsite-

(CaMnMg), jahnsite-(CaMnMn) and whitmoreite. A representative electron microprobe analysis of beraunite is shown in Table 15.

Table 15: Representative electron microprobe analysis of beraunite from the Palermo #2 pegmatite. Low analytical totals are due to the presence of OH^- and H_2O.

	P2-CM-34
P_2O_5	31.45
SiO_2	0.03
Fe_2O_3	44.60
Al_2O_3	0.07
FeO	2.34
MnO	4.83
MgO	0.10
CaO	0.48
Na_2O	0.01
Total	83.91

Cations based on 18.5 oxygen atoms Fe^{2+} calculated by stoichiometry	
Fe^{2+}	0.292
Mn^{2+}	0.611
Mg	0.023
Ca	0.077
Na	0.004
Σ	1.007
Fe^{3+}	5.015
Al	0.012
Σ	5.027
P	3.978
Si	0.005
Σ	3.983

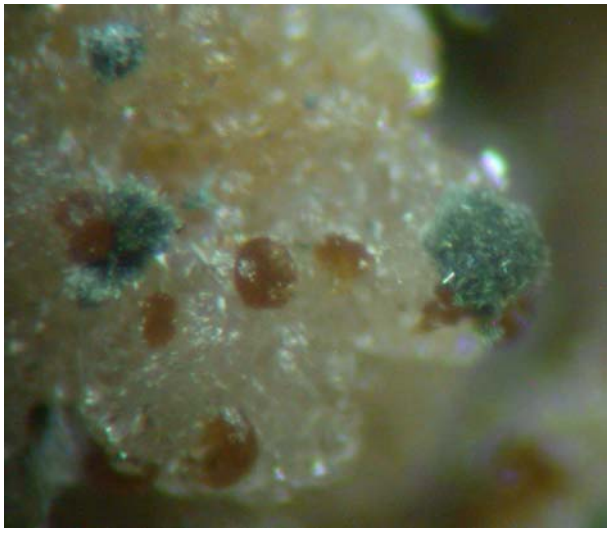

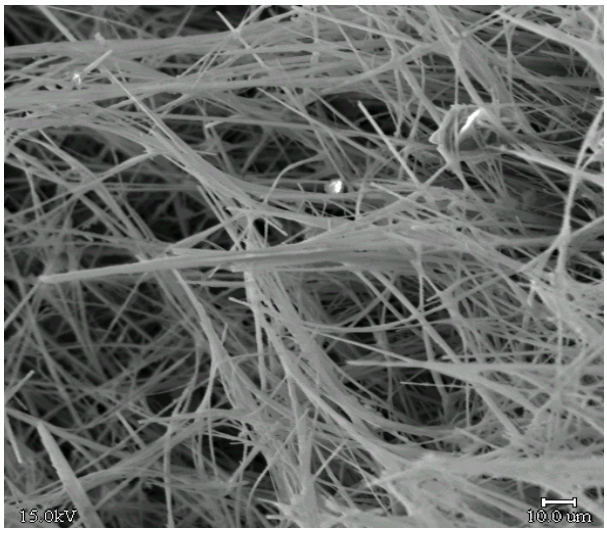

Figure 52 (left): Green beraunite with orange whitmoreite on siderite, field of view is approximately 3 mm.
Figure 53 (right): Backscattered electron image of beraunite from the Palermo #2 pegmatite.

Kryzhanovskite – $(Fe^{3+}, Mn)Fe^{3+}_2(PO_4)_2(OH)_3$

Kryzhanovskite is present as reddish brown to brown masses to 2 cm that often appear to show signs of being partially etched (Figure 54 and 55). Although Fe in kryzhanovskite is trivalent, these minerals typically occur in a non-oxidizing environment in association with vivianite, ludlamite and fairfieldite-messelite. Moore (1971) and Moore *et al*., (1980) suggested that kryzhanovskite may form from the oxidation of phosphoferrite - $Fe^{2+}Fe^{2+}_2(PO_4)_2 \cdot 3\ H_2O$. Based on Moore's supposition, it appears that at Palermo #2 phosphoferrite crystallized in the non-oxidizing assemblage with vivianite, ludlamite and fairfieldite group minerals and was subsequently oxidized to kryzhanovskite. Consequently in the observed assemblage at Palermo #2, kryzhanovskite has a pseudomorphic relationship with phosphoferrite. A representative electron microprobe analysis of kryzhanovskite is shown in Table 16.

Table 16: Representative electron microprobe analysis of kryzhanovskite from Palermo #2. Low analytical totals are due to the presence of OH^-.

	P2-CM-21
P_2O_5	37.09
SiO_2	0.12
TiO_2	0.05
Fe_2O_3	37.13
Al_2O_3	0.13
MnO	7.82
MgO	6.19
Na_2O	0.14
Total	88.67

Cations based on 8.5 oxygen atoms	
Mg	0.573
Mn^{2+}	0.411
Na	0.016
Σ	1.000
Fe^{3+}	1.734
Al	0.009
Σ	1.743
P	1.949
Si	0.008
Ti	0.002
Σ	1.959

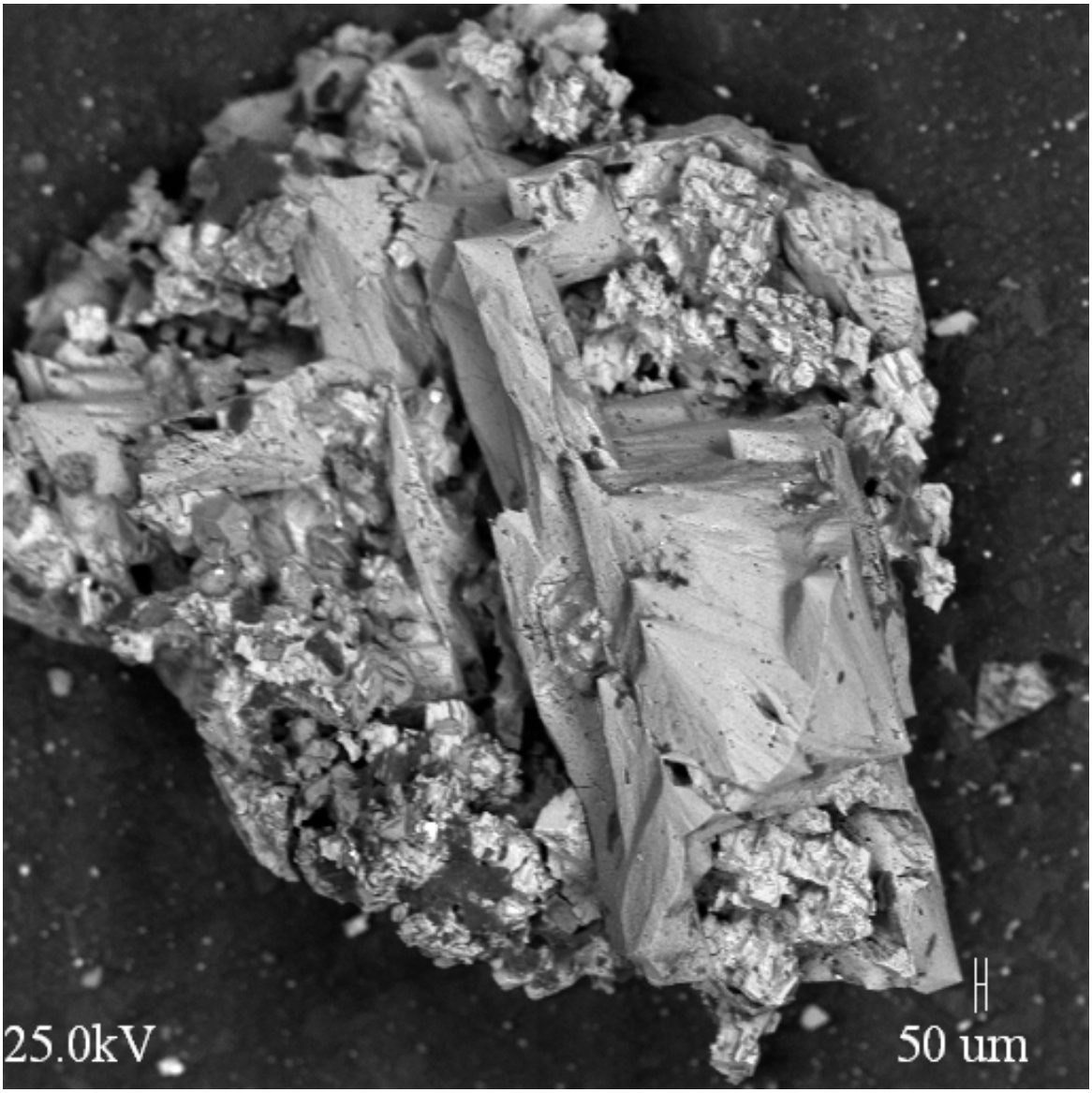

Figure 54: Backscattered electron image of kryzhanovskite crystals from sample P2-CM-21 from the Palermo #2 pegmatite.

Figure 55: Kryzhanovskite (brown) with vivianite (blue), ludlamite (light green) and laueite (orange in cavity). Field of view is approximately 3 cm.

Strunzite – $Mn^{2+}Fe^{3+}_2(PO_4)_2(OH)_2 \cdot 6\ H_2O$

Strunzite is present at Palermo #2 as straw-yellow acicular crystals to 1 cm in length (Figure 56). Strunzite forms in an oxidizing environment and may be associated with laueite, stewartite, rockbridgeite-frondelite, jahnsite-(CaMnFe), jahnsite-(CaMnMg), jahnsite-(CaMnMn), beraunite and whitmoreite. A representative electron microprobe analysis of strunzite is shown in Table 17.

Figure 56: Strunzite with whitmoreite (orange) on siderite (white) from the Palermo #2 pegmatite. Field of view is approximately 1 cm.

Table 17: Representative electron microprobe analysis of strunzite from the Palermo #2 pegmatite. Low analytical totals are due to the presence of OH^- and H_2O.

	P2-CM-09
P_2O_5	32.90
SiO_2	0.07
TiO_2	0.04
Fe_2O_3	35.89
Al_2O_3	0.00
FeO	1.90
MnO	6.79
MgO	2.24
CaO	0.52
Na_2O	0.13
Total	80.47

Cations based on 9 oxygens

Fe^{2+} calculated by stoichiometry

Normalized to 2 P ions

Mn^{2+}	0.413
Mg	0.240
Fe^{2+}	0.114
Ca	0.040
Na	0.018
Σ	0.825
Fe^{3+}	1.939
Al	0.000
Σ	1.939
P	2.000
Si	0.005
Ti	0.002
Σ	2.007

Whitmoreite – $Fe^{2+}Fe^{3+}_2(PO_4)_2(OH)_2 \cdot 4\ H_2O$

Whitmoreite occurs as orange to yellow-brown crystals to 1 mm that exhibit a variety of habits at Palermo #2. Whitmoreite typically forms central spheres from which acicular crystals protrude outward giving the appearance of a “naval mine” (Figure 57). Other forms observed at Palermo #2 include groupings of orange prismatic crystals (Figure 58) and smooth spherical masses of crystals. Whitmoreite forms under oxidizing conditions and may be associated with laueite, rockbridgeite-frondelite, beraunite and strunzite. A representative electron microprobe analysis of whitmoreite from sample P2-CM-08 is shown in Table 18.

Table 18: Representative electron microprobe analysis of whitmoreite from Palermo #2. Low analytical totals are due to the presence of OH^- and H_2O.

	P2-CM-08
P_2O_5	29.86
Fe_2O_3	32.83
Al_2O_3	0.12
FeO	11.90
MnO	1.75
MgO	0.16
CaO	0.10
Total	76.72

Cations based on 9 oxygen atoms

Fe^{2+} calculated by stoichiometry

Normalized to 2 P atoms

Fe^{2+}	0.787
Mn^{2+}	0.117
Mg	0.019
Ca	0.008
Σ	0.931
Fe^{3+}	1.955
Al	0.011
Σ	1.966
P	2.000
Σ	2.000

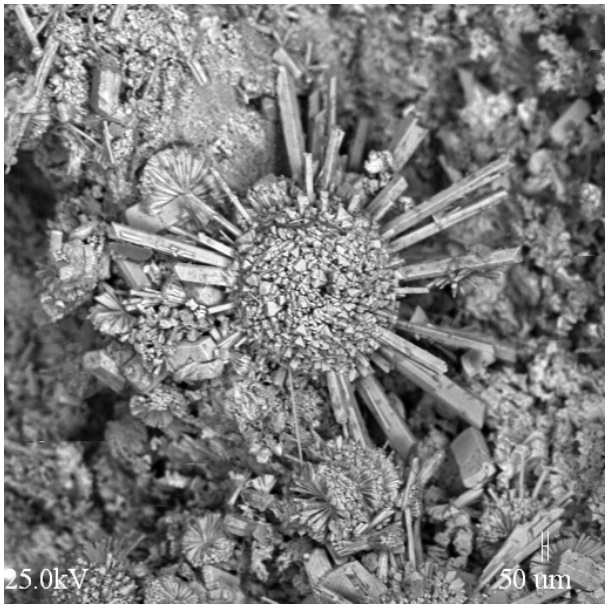

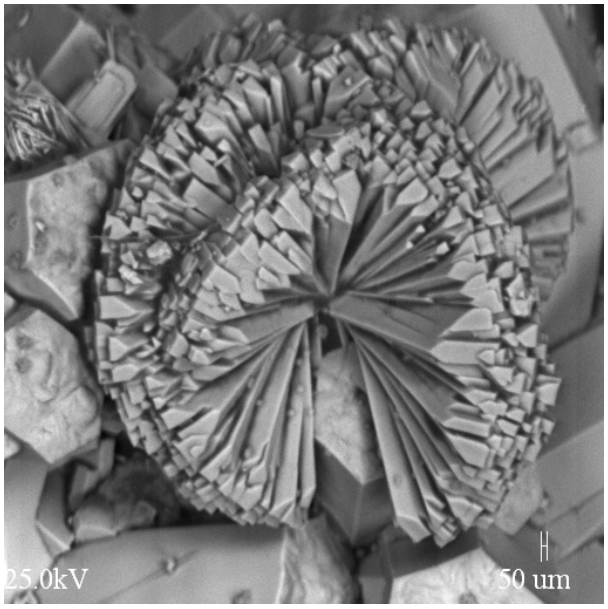

Figure 57 (left): Backscattered electron image of whitmoreite from sample P2-CM-35.
Figure 58 (right): Backscattered electron image of whitmoreite from sample P2-CM-42.

Vivianite – $Fe^{2+}_3(PO_4)_2 \cdot 8\ H_2O$

Vivianite is abundant in the vicinity of triphylite masses in the core margin of Palermo #2 where it may occur as thin bluish coatings along fractures and cleavage planes of other minerals such as triphylite. The presence of vivianite imparts a darker blue color to triphylite. Vivianite also forms bladed to blocky transparent blue crystals up to 3 mm in cavities resulting from the alteration of primary phosphates (Figure 59). Vivianite forms in a non-oxidizing environment and may be associated with ludlamite, kryzhanovskite, fairfieldite-messelite and hydroxylapatite. A representative electron microprobe analysis of vivianite is shown in Table 19.

Table 19: Representative electron microprobe analysis of vivianite from the Palermo #2 pegmatite. Low analytical totals are due to the presence of H_2O.

	P2-CM-23b
P_2O_5	28.26
SiO_2	0.46
TiO_2	0.02
FeO	30.83
MnO	6.99
MgO	3.80
CaO	0.18
Total	70.54

Cations based on 8 oxygen atoms	
Fe	2.098
Mn	0.482
Mg	0.461
Ca	0.016
Na	0.000
Σ	3.057
P	1.947
Si	0.037
Ti	0.001
Σ	1.985

Figure 59: Backscattered electron image of vivianite from the Palermo #2 pegmatite.

Ludlamite – $Fe_3(PO_4)_2 \cdot 4\ H_2O$

Ludlamite forms nearly colorless to apple green tablets and masses to 1 cm in size (Figure 61). Ludlamite often exhibits a slightly etched appearance crystal surfaces (Figure 60). Ludlamite forms in a non-oxidizing environment and may be associated with vivianite, kryzhanovskite, fairfieldite-messelite and hydroxylapatite. A representative electron microprobe analysis of ludlamite is shown in Table 20.

Table 20: Representative electron microprobe analysis of ludlamite from the Palermo #2 pegmatite. Low analytical totals are due to the presence of H_2O.

	P2-CM-27
P_2O_5	33.73
SiO_2	0.01
FeO	43.77
MnO	2.88
MgO	2.87
Total	83.26
Cations based on 8 oxygen atoms	
Fe	2.552
Mn	0.170
Mg	0.298
Σ	3.020
P	1.991
Si	0.001
Σ	1.992

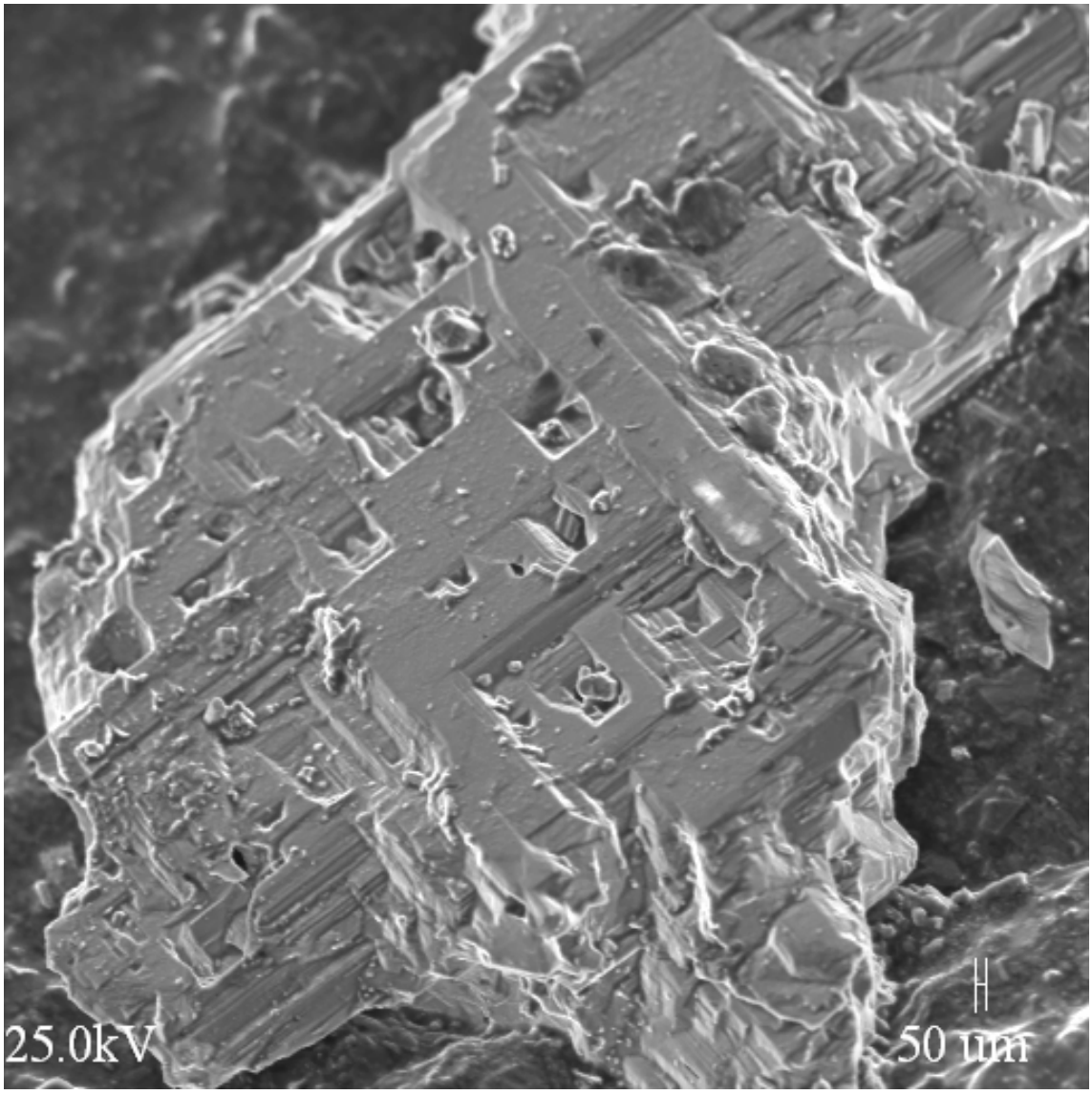

Figure 60: Backscattered electron image of ludlamite exhibiting hoppered and/or etched surfaces from Palermo #2.

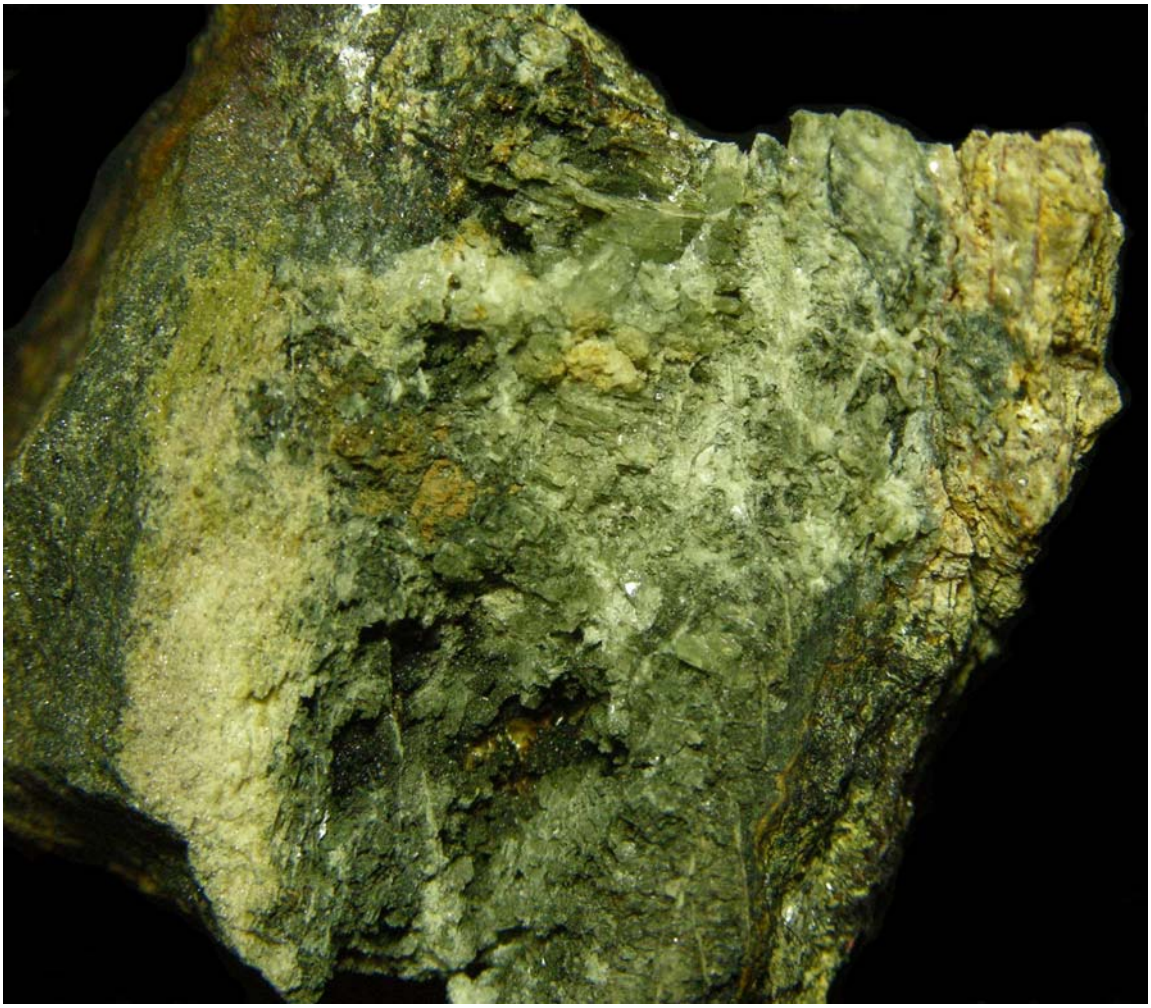

Figure 61: Light green to colorless ludlamite with siderite (light tan) and mitridatite (olive green) in sample P2-CM-25 from Palermo #2. Field of view is approximately 5 cm.

Mitridatite – $Ca_2Fe^{3+}{}_3(PO_4)_3O_2 \cdot 3\ H_2O$

Mitridatite occurs as a distinctive yellowish green to light olive green coating in secondary cavities produced by metasomatic alteration of primary phosphates (triphylite and apatite group). Mitridatite also occurs on fracture surfaces of minerals and may occur up to several meters away from its primary phosphate precursory minerals. Mitridatite typically forms fairly late in the paragenetic sequence under oxidizing conditions and may be associated with rockbridgeite-frondelite, strunzite, laueite, beraunite, jahnsite-(CaMnFe), jahnsite-(CaMnMn) and whitmoreite.

Childrenite – $Fe^{2+}Al(PO_4)(OH)_2 \cdot H_2O$

Eosphorite – $Mn^{2+}Al(PO_4)(OH)_2 \cdot H_2O$

Childrenite crystallizes in the orthorhombic system, with some crystals appearing to be monoclinic. Eosphorite crystallizes in the monoclinic system, with some crystals appearing to be pseudo-orthorhombic. Childrenite-eosphorite generally forms tan to orange-pink prismatic crystals up to 2 cm at Palermo #2 (Figure 62). Childrenite-eosphorite may display compositional zoning within crystals and typically forms in a non-oxidizing environment. Childrenite-eosphorite is normally associated with vivianite, fairfieldite-messelite, ludlamite, hydroxylapatite and siderite. Representative electron microprobe analyses of childrenite and eosphorite are shown in Table 21.

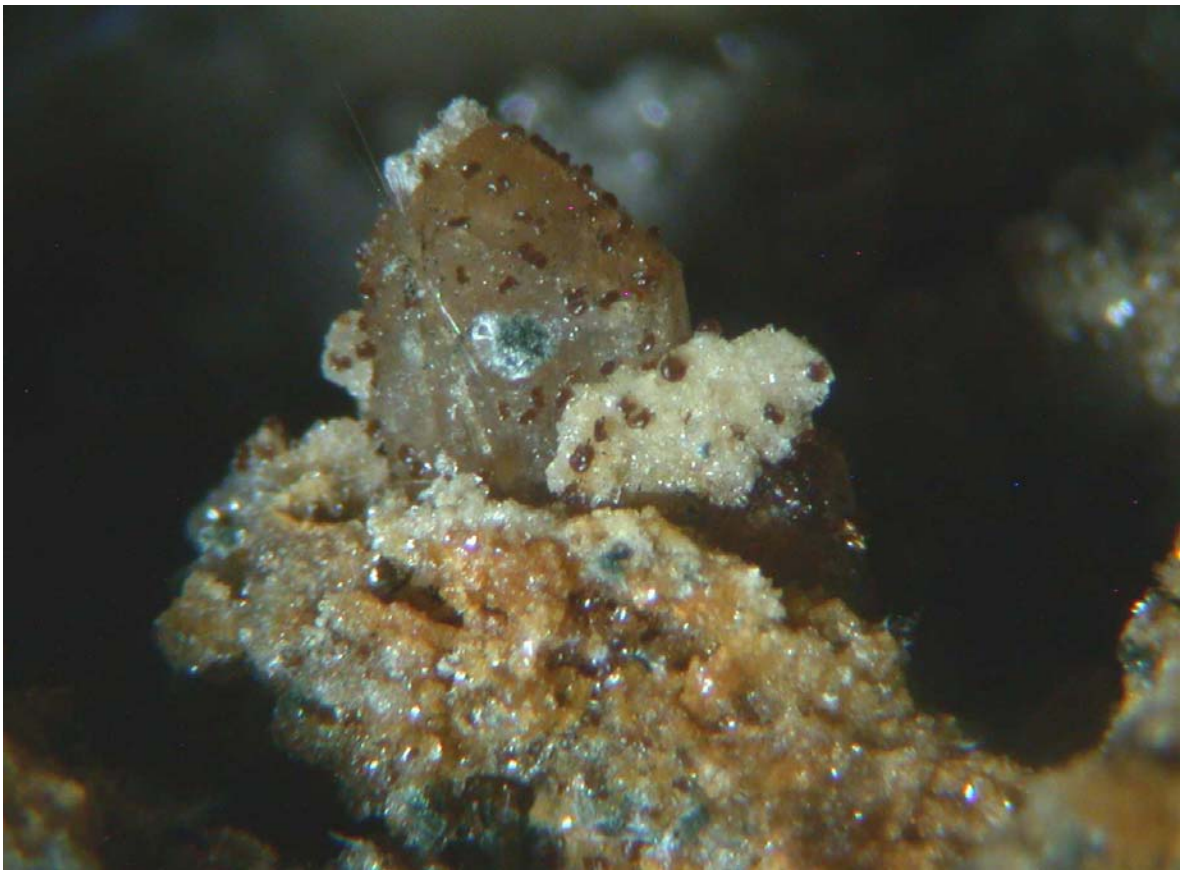

Figure 62: Childrenite-eosphorite (pinkish tan prismatic) with whitmoreite (orange spheres), beraunite (green mats), strunzite (straw needles) and siderite (brownish white). Field of view is approximately 1 cm.

Table 21: Representative electron microprobe analyses of childrenite-eosphorite from Palermo #2. Low analytical totals are due to the presence of OH^- and H_2O.

	Childrenite P2-CM-27	Eosphorite P2-CM-27A1
P_2O_5	31.43	31.46
Al_2O_3	22.22	22.54
FeO	19.77	13.37
MnO	10.35	16.95
CaO	0.59	0.38
MgO	0.40	0.27
Na_2O	0.10	0.19
SiO_2	0.00	0.04
TiO_2	0.20	0.12
Total	85.05	85.31
Cations based on 5 oxygen atoms		
P	1.003	1.000
Si	0.000	0.002
Ti	0.006	0.003
Σ	1.009	1.005
Al	0.987	0.997
Σ	0.987	0.997
Fe	0.623	0.420
Mn	0.330	0.539
Ca	0.024	0.015
Mg	0.022	0.015
Na	0.007	0.014
Σ	1.006	1.003

Gormanite – $Fe^{2+}_3Al_4(PO_4)_4(OH)_6 \cdot 2\ H_2O$

Souzalite – $Mg_3Al_4(PO_4)_4(OH)_6 \cdot 2\ H_2O$

Gormanite is found as greenish-blue acicular crystals that form nodular masses to 10 cm associated with montebrasite, scorzalite-lazulite, augelite, goyazite-crandallite and chlorapatite (Figure 63). Gormanite nodules and masses from Palermo #2 are likely the

largest reported from the United States. Souzalite occurs in greenish-blue patches to 0.5 cm in association with montebrasite, scorzalite-lazulite, gormanite, vivianite, kryzhanovskite, fairfieldite and whiteite group minerals and represents a localized concentration of Mg. Gormanite and souzalite are low temperature alteration products of montebrasite and possibly scorzalite-lazulite and generally form in non-oxidizing conditions. In some cases it appears that gormanite may be an alteration product of triphylite + muscovite. Representative electron microprobe analyses of gormanite and souzalite are shown in Table 22.

Figure 63: Gormanite-souzalite (bluish green) and associated minerals montebrasite (white) and scorzalite-lazulite (blue) from the Palermo #2 pegmatite. Field of view is approximately 2 cm.

Table 22: Representative electron microprobe analyses of gormanite-souzalite from sample P2-CM-21 from Palermo #2. Low analytical totals are due to the presence of OH^- and H_2O.

	Souzalite	Gormanite
P_2O_5	37.96	37.44
SiO_2	0.10	0.02
TiO_2	0.09	0.10
Al_2O_3	26.09	26.77
FeO	11.43	15.43
MnO	0.92	1.46
CaO	0.10	0.00
MgO	8.77	6.46
Na_2O	0.00	0.00
Total	85.46	87.68
Cations based on 19 oxygen atoms		
P	4.062	4.001
Si	0.013	0.003
Ti	0.008	0.009
Σ	4.083	4.013
Al	3.887	3.982
Σ	3.887	3.982
Fe	1.208	1.629
Mn	0.099	0.156
Ca	0.014	0.000
Mg	1.652	1.214
Na	0.000	0.001
Σ	2.973	3.000

Whiteite group:

Whiteite-(MnFeMg) – $Mn^{2+}Fe^{2+}Mg_2Al_2(PO_4)_4(OH)_2 \cdot 8\ H_2O$

Whiteite-(CaMnMg) – $CaMn^{2+}Mg_2Al_2(PO_4)_4(OH)_2 \cdot 8\ H_2O$

Whiteite-(CaFeMg) – $CaFe^{2+}Mg_2Al_2(PO_4)_4(OH)_2 \cdot 8\ H_2O$

Jahnsite-(CaMnFe) – $CaMn^{2+}Fe^{2+}{}_2Fe^{3+}{}_2(PO_4)_4(OH)_2 \cdot 8\ H_2O$

Jahnsite-(CaMnMg) – $CaMn^{2+}Fe^{2+}{}_2Fe^{3+}{}_2(PO_4)_4(OH)_2 \cdot 8\ H_2O$

Jahnsite-(CaMnMn) – $CaMn^{2+}Mn^{2+}{}_2Fe^{3+}{}_2(PO_4)_4(OH)_2 \cdot 8\ H_2O$

Six members of the whiteite group exist at Palermo #2: whiteite-(MnFeMg), whiteite-(CaMnMg), whiteite-(CaFeMg), jahnsite-(CaMnFe), jahnsite-(CaMnMg) and jahnsite-(CaMnMn). Jahnsite-(CaMnFe), jahnsite-(CaMnMg) and jahnsite-(CaMnMn) occur as yellow to orange to brown prismatic monoclinic crystals of less than 2 mm (Figure 64 and 65). Crystals of jahnsite may show striations parallel to the prism elongation. Jahnsite typically forms in an oxidizing environment and may be associated with laueite, rockbridgeite-frondelite, strunzite, beraunite, mitridatite and whitmoreite. Whiteite-(MnFeMg), whiteite-(CaFeMg) and whiteite-(CaMnMg) form brown to light tan to nearly colorless radiating sprays and aggregates of prismatic monoclinic crystals to 1.5 mm in size (Figure 66). Whiteite crystallizes in non-oxidizing to slightly oxidizing conditions and is often associated with paravauxite-gordonite, scorzalite-lazulite, fairfieldite-messelite and gormanite-souzalite. Whiteite group minerals occasionally exhibit compositional zoning within single crystals. Jahnsite-(CaMnFe) overgrowths on whiteite-(MnFeMg) have been observed. Additionally whiteite-(CaFeMg) has been observed as an overgrowth on jahnsite-(CaMnMn) (see Figure 67). Representative electron microprobe analyses of whiteite group species are shown in Table 23 and 24.

Table 23: Representative electron microprobe analyses of whiteite group minerals (jahnsite) from Palermo #2. Low analytical totals are due to the presence of OH^- and H_2O.

	Jahnsite-(CaMnMn) P2-CM-27	Jahnsite-(CaMnMg) P2-CM-09	Jahnsite-(CaMnFe) P2-RW-04
P_2O_5	34.46	35.76	34.09
SiO_2	0.07	0.06	0.02
TiO_2	0.15	0.14	0.08
Al_2O_3	0.97	1.45	2.10
Fe_2O_3	17.68	17.85	16.19
FeO	5.30	6.29	14.30
MnO	17.45	13.27	8.76
CaO	4.54	5.58	3.16
MgO	2.54	4.90	4.35
Na_2O	0.00	0.25	0.26
Total	83.16	85.55	83.30
	Cations based on 17 oxygen atoms		
	Fe^{3+} calculated by stoichiometry		
Ca	0.674	0.789	0.465
Mg	0.183	0.144	0.455
Mn	0.000	0.000	0.000
Na	0.000	0.063	0.070
Σ	0.857	0.996	0.990
Fe^{2+}	0.000	0.000	0.000
Mn	1.000	1.000	1.019
Σ	1.000	1.000	1.019
Mg	0.341	0.821	0.435
Fe^{2+}	0.613	0.695	1.642
Mn	1.046	0.484	0.000
Σ	2.000	2.000	2.077
Al	0.158	0.225	0.341
Fe^{3+}	1.841	1.774	1.673
Σ	1.999	1.999	2.014
P	4.037	3.998	3.963
Si	0.009	0.008	0.003
Ti	0.016	0.014	0.008
Σ	4.062	4.020	3.974

Table 24: Representative electron microprobe analyses of whiteite group minerals (whiteite) from the Palermo #2 pegmatite. Low analytical totals are due to the presence of OH^- and H_2O.

	Whiteite-(CaFeMg) P2-CM-27	Whiteite-(CaMnMg) P2-CM-30	Whiteite-(MnFeMg) P2-RW-04
P_2O_5	37.46	36.23	36.84
SiO_2	0.07	0.04	0.02
TiO_2	0.05	0.18	0.05
Al_2O_3	11.87	11.62	11.99
Fe_2O_3	2.25	2.00	1.65
FeO	4.75	6.93	6.33
MnO	6.89	11.48	8.97
CaO	2.77	6.93	2.84
MgO	11.90	4.23	8.56
Na_2O	0.10	0.10	0.76
Total	78.10	79.73	78.01
	Cations based on 17 oxygen atoms		
	Fe^{3+} calculated by stoichiometry		
Ca	0.378	0.977	0.397
Mg	0.248	0.025	0.000
Mn	0.000	0.000	0.412
Na	0.024	0.000	0.191
Σ	0.650	1.002	1.000
Fe^{2+}	0.505	0.000	0.689
Mn	0.495	1.000	0.238
Σ	1.000	1.000	0.927
Mg	2.000	0.830	1.661
Fe^{2+}	0.000	0.762	0.000
Mn	0.000	0.279	0.339
Σ	2.000	1.871	2.000
Al	1.780	1.803	1.839
Fe^{3+}	0.215	0.198	0.162
Σ	1.995	2.001	2.001
P	4.034	4.037	4.061
Si	0.008	0.005	0.003
Ti	0.005	0.018	0.005
Σ	4.047	4.060	4.069

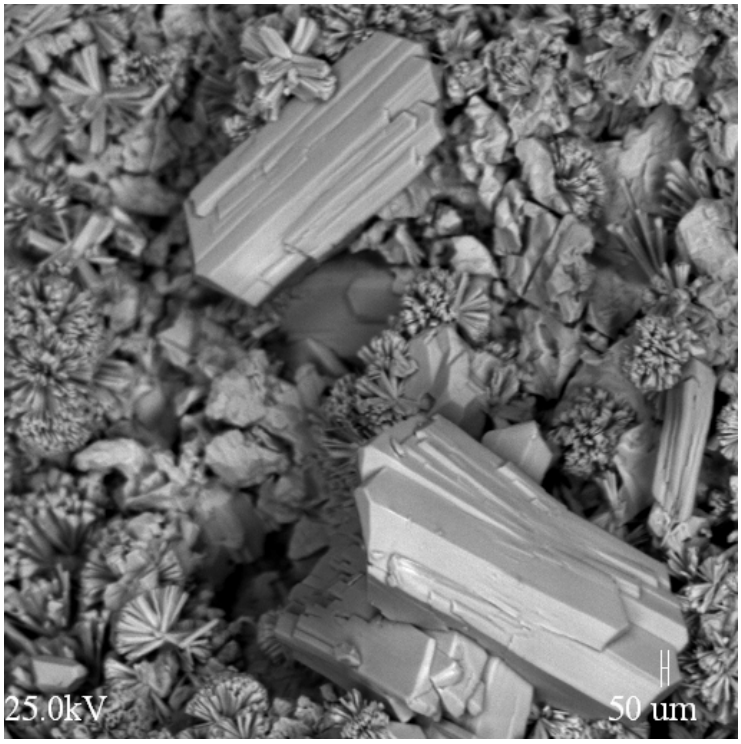

Figure 64: Backscattered electron image of jahnsite-(CaMnMn) on rockbridgeite from sample P2-CM-09 from Palermo #2.

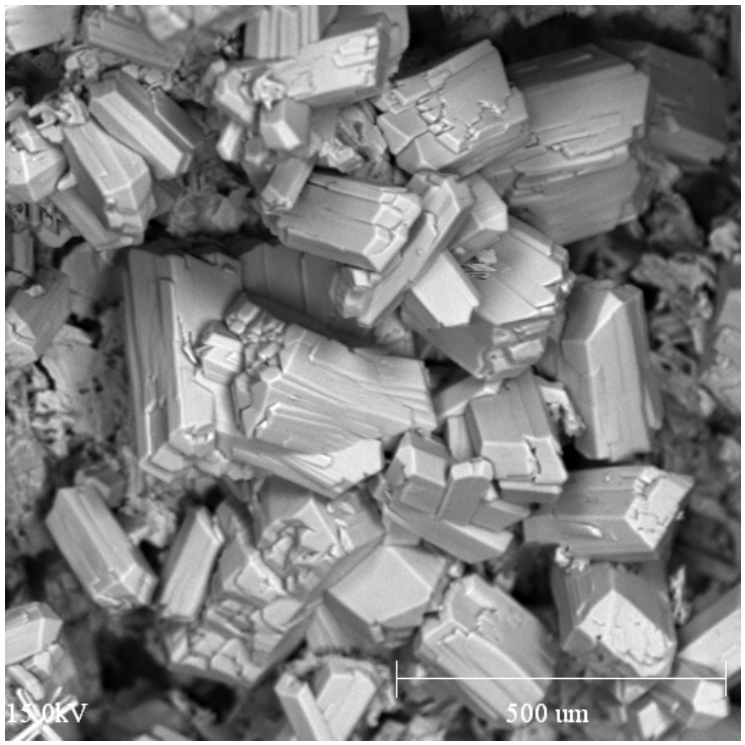

Figure 65: Backscattered electron image of jahnsite-(CaMnMn) crystals from sample P2-CM-09 from Palermo #2.

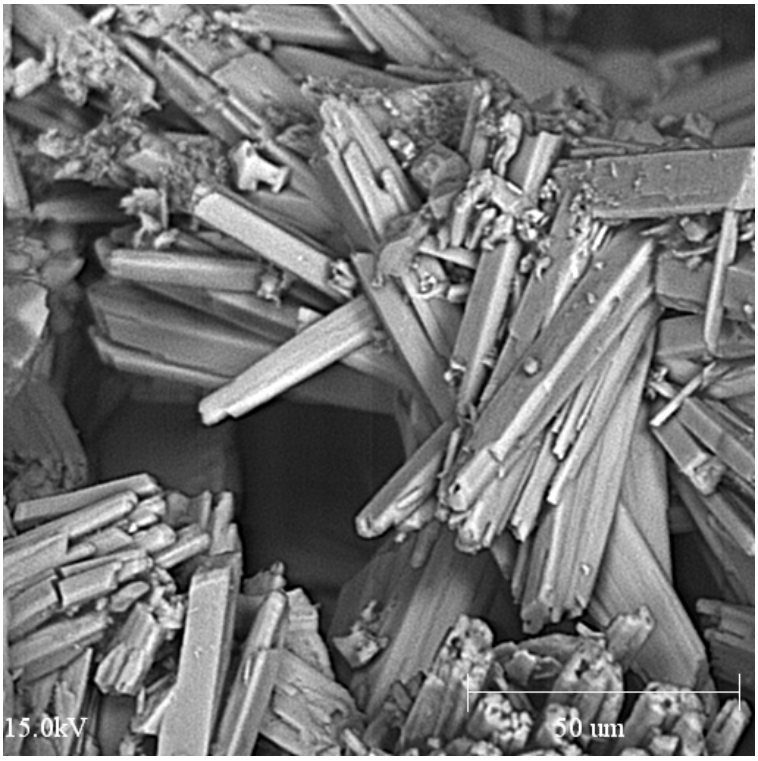

Figure 66: Backscattered electron image of prismatic whiteite-(CaMnMg) crystals from core margin sample P2-CM-30 from Palermo #2.

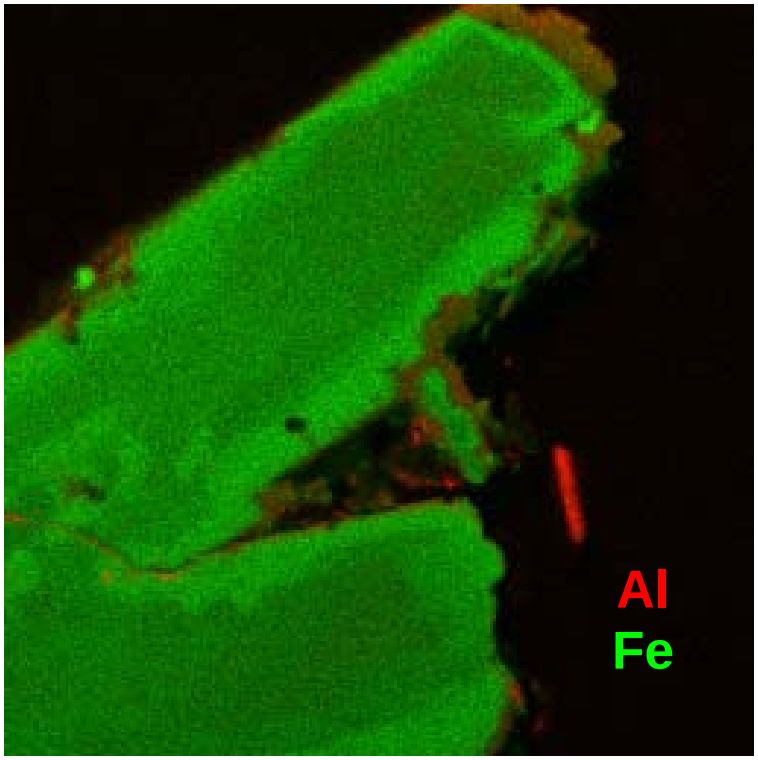

Figure 67: Energy dispersive X-ray map of zoned jahnsite-whiteite from sample P2-CM-27 from Palermo #2. Al-rich whiteite-(CaFeMg) (red) occurs as an overgrowth on Fe-rich jahnsite-(CaMnMn) (green).

Paravauxite group:

Laueite – $Mn^{2+}Fe^{3+}_2(PO_4)_2(OH)_2 \cdot 8\ H_2O$

Stewartite – $Mn^{2+}Fe^{3+}_2(PO_4)_2(OH)_2 \cdot 8\ H_2O$

Paravauxite – $Fe^{2+}Al_2(PO_4)_2(OH)_2 \cdot 8\ H_2O$

Ushkovite – $MgFe^{3+}_2(PO_4)_2(OH)_2 \cdot 8\ H_2O$

Gordonite – $MgAl_2(PO_4)_2(OH)_2 \cdot 8\ H_2O$

Paravauxite group minerals are widespread in the low temperature secondary phosphate assemblages at Palermo #2. Laueite and ushkovite form yellowish to reddish orange prisms to 2 mm that are longitudinally striated, possess diamond-shaped cross-sections and have steeply angled terminations (Figure 69). Stewartite is rare at Palermo #2 and occurs as bright yellow bladed crystals exhibiting extremely steep angled terminations that converge to a point. The presence of stewartite was confirmed via X-ray diffraction. Laueite, stewartite and ushkovite are generally found in oxidizing environments and are generally associated with rockbridgeite-frondelite, strunzite, beraunite, jahnsite-(CaMnFe), jahnsite-(CaMnMn), mitridatite and whitmoreite. Paravauxite and gordonite occur as colorless to white to pale yellow-orange prisms that are longitudinally striated, possess diamond-shaped cross-sections and have steeply angled terminations (Figure 68). Gordonite principally occurs in non-oxidizing environments, whereas paravauxite may occur in non-oxidizing to slightly oxidizing conditions. Paravauxite and gordonite are typically associated with scorzalite-lazulite, fairfieldite-messelite, gormanite-souzalite, whiteite-(MnFeMg), whiteite-(CaMnMg) and siderite. Like minerals of the whiteite group, members of the paravauxite group may display compositional zonation. Zoned crystals of paravauxite-gordonite and

paravauxite-laueite have been observed from Palermo #2. Representative electron microprobe analyses of laueite, ushkovite, paravauxite and gordonite are given in Table 25.

Table 25: Representative electron microprobe analyses of paravauxite group minerals from Palermo #2. Low analytical totals are due to the presence of OH^- and H_2O.

	Laueite P2-CM-32	Paravauxite P2-CM-27	Ushkovite P2-CM-09	Gordonite P2-CM-27
P_2O_5	26.68	30.12	29.40	31.87
Al_2O_3	2.22	21.46	0.10	22.55
Fe_2O_3	24.68	11.23	26.18	1.35
Mn_2O_3	0.00	0.00	7.14	0.00
FeO	0.80	0.00	0.00	0.00
MnO	8.05	1.89	0.00	0.54
CaO	0.00	0.03	3.51	0.23
MgO	2.88	1.16	6.56	9.08
Na_2O	0.00	0.00	0.10	0.00
SiO_2	0.01	0.10	0.04	0.50
TiO_2	0.00	0.12	0.01	0.05
Total	67.25	66.09	73.04	66.17
	Cations based on 9 oxygen atoms			
	Fe^{3+} and Mn^{3+} calculated by stoichiometry			
Mn^{2+}	0.600	0.125	0.000	0.033
Mg	0.377	0.135	0.773	0.981
Fe^{2+}	0.060	0.736	0.000	0.000
Ca	0.000	0.002	0.298	0.018
Na	0.000	0.000	0.015	0.000
Σ	1.037	0.998	1.086	1.032
Fe^{3+}	1.764	0.000	1.558	0.073
Mn^{3+}	0.000	0.000	0.429	0.000
Al	0.230	1.982	0.009	1.927
Σ	1.994	1.982	1.986	2.000
P	1.988	1.999	1.968	1.956
Si	0.001	0.008	0.003	0.036
Ti	0.000	0.007	0.000	0.003
Σ	1.989	2.014	1.971	1.995

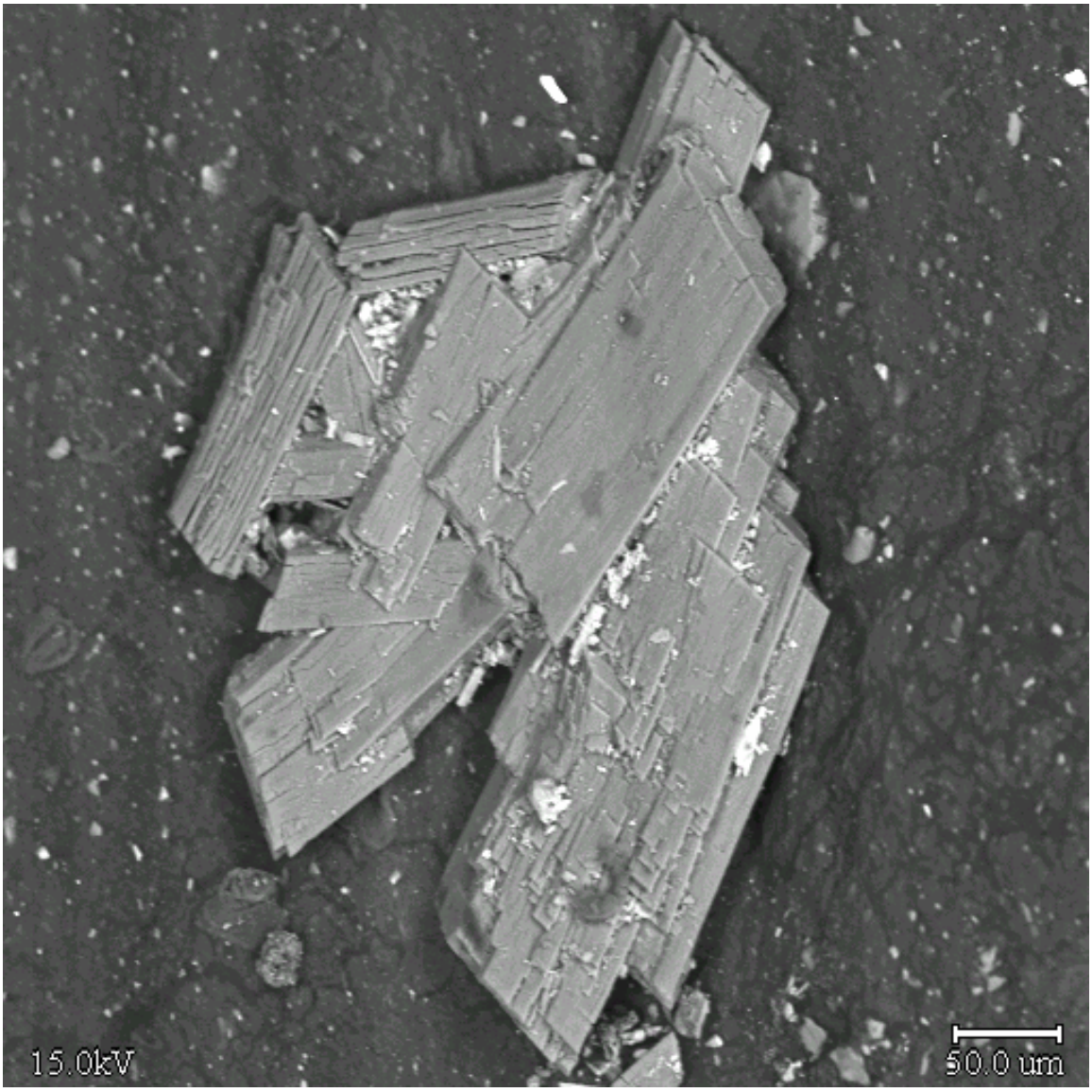

Figure 68: Backscattered electron image of compositionally zoned paravauxite-gordonite crystals from the Palermo #2 pegmatite (sample P2-CM-27).

Figure 69: Laueite crystals from the Palermo #2 pegmatite, field of view is approximately 3 mm.

Fairfieldite group:

Messelite – $Ca_2(Fe^{2+},Mn^{2+})(PO_4)_2 \cdot 2\ H_2O$

Fairfieldite – $Ca_2(Mn^{2+},Fe^{2+})(PO_4)_2 \cdot 2\ H_2O$

Collinsite – $Ca_2(Mg,Fe^{2+})(PO_4)_2 \cdot 2\ H_2O$

Members of the fairfieldite group present at Palermo #2 include messelite, fairfieldite and collinsite. Fairfieldite group minerals are usually colorless to white to pale blue in color and form platy, bladed and feathery sheaf-like crystals to 1.5 mm in size (Figure 70 and 71). Fairfieldite group minerals may display slight compositional zoning within crystals and typically form in a non-oxidizing environment. Fairfieldite and

messelite are often associated with childrenite-eosphorite, vivianite, ludlamite, hydroxylapatite and carbonates (siderite), whereas collinsite is associated with siderite, fluorapatite/hydroxylapatite and plumbogummite group minerals. Representative electron microprobe analyses of messelite, fairfieldite and collinsite are given in Table 26.

Table 26: Representative electron microprobe analyses of fairfieldite group minerals from Palermo #2. Low analytical totals are due to the presence of H_2O.

	Messelite P2-CM-05	Fairfieldite P2-CM-21	Collinsite P2-CM-05
P_2O_5	40.78	38.56	41.32
SiO_2	0.00	0.12	0.01
TiO_2	0.15	0.19	0.06
Al_2O_3	0.16	0.12	0.15
FeO	9.93	7.92	8.68
MnO	0.80	11.17	0.88
CaO	31.89	30.44	30.32
MgO	5.54	0.22	7.69
Na_2O	0.00	0.09	0.00
Total	89.25	88.83	89.10
Cations based on 5 oxygen atoms			
P	1.998	1.986	2.002
Si	0.000	0.007	0.000
Ti	0.006	0.009	0.002
Σ	2.004	2.002	2.004
Fe	0.481	0.403	0.415
Mn	0.039	0.576	0.042
Mg	0.478	0.020	0.533
Al	0.011	0.008	0.010
Σ	1.009	1.007	1.000
Ca	1.978	1.985	1.859
Mg	0.000	0.000	0.123
Na	0.000	0.011	0.000
Σ	1.978	1.996	1.982

Figure 70: Backscattered electron image of fairfieldite-messelite crystals lining a cavity in siderite from Palermo #2.

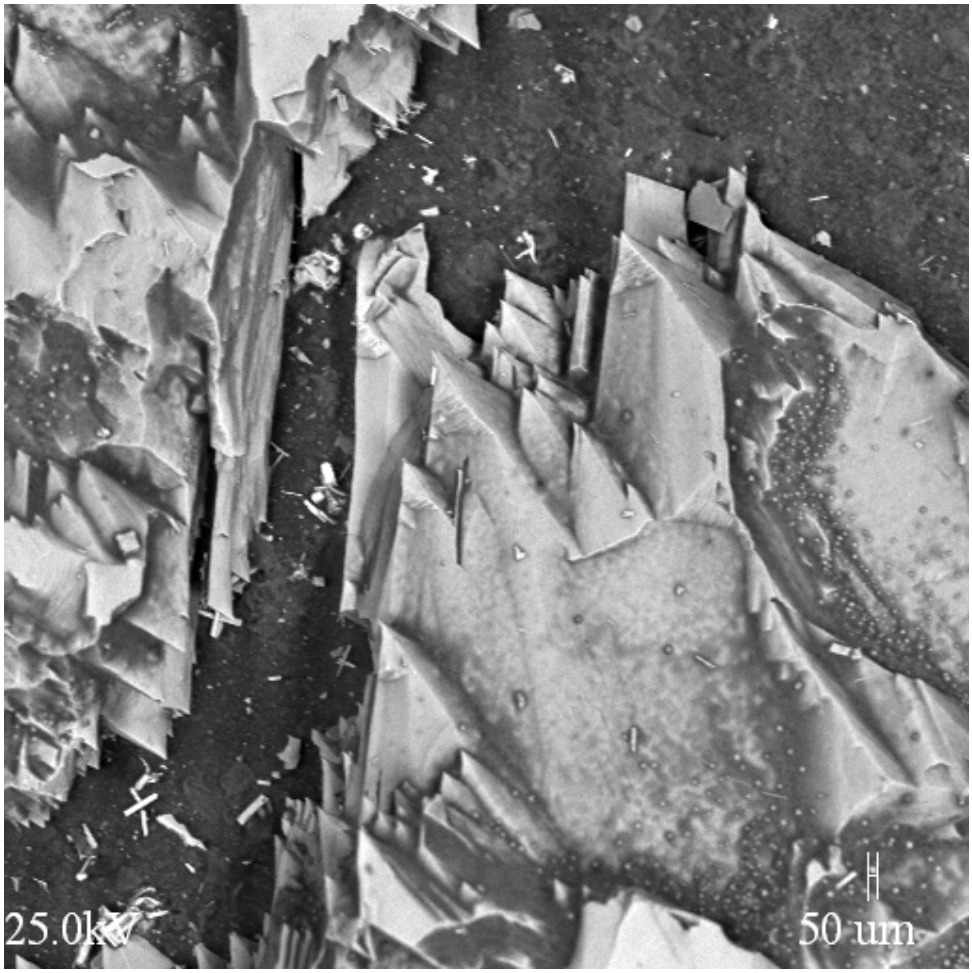

Figure 71: Backscattered electron image of collinsite from core margin sample P2-CM-05 of the Palermo #2 pegmatite.

Plumbogummite group:

Crandallite – $CaAl_3(PO_4)_2(OH,H_2O)_6$

Goyazite – $SrAl_3(PO_4)_2(OH,H_2O)_6$

Goyazite and crandallite are found as platy laths forming alteration rims on montebrasite or as pseudohexagonal platy crystals associated with fluorapatite/hydroxylapatite in cavities in siderite (Figure 72 and 73). Goyazite and crandallite exhibit compositional zonation in some cases (i.e. crandallite transitioning to goyazite). Goyazite-crandallite also occurs with vivianite as a possible alteration product

of “arrojadite”. Representative electron microprobe analyses of goyazite and crandallite are shown in Table 27.

Table 27: Representative electron microprobe analyses of plumbogummite group minerals from the Palermo #2 pegmatite. Low analytical totals are due to the presence of OH^- and H_2O.

	Crandallite P2-CM-05	Goyazite P2-CM-05
P_2O_5	31.87	29.62
SiO_2	0.21	0.41
TiO_2	0.00	0.00
Al_2O_3	34.79	32.62
Fe_2O_3	0.96	0.08
CaO	6.68	2.14
SrO	10.42	18.88
BaO	0.02	0.32
MnO	0.27	0.04
Na_2O	0.07	0.00
Total	85.29	84.11
Cations based on 10.5 oxygen atoms		
P	1.968	1.955
Si	0.015	0.032
Ti	0.000	0.000
Σ	1.983	1.987
Al	2.990	2.998
Fe^{3+}	0.053	0.005
Σ	3.043	3.003
Ca	0.522	0.179
Sr	0.441	0.853
Ba	0.001	0.010
Mn	0.017	0.002
Na	0.009	0.000
Σ	0.990	1.044

Goyazite and “arrojadite” are the only species present at Palermo #2 that contain Sr and Ba as major to minor constituents. In contrast, the nearby Palermo #1 pegmatite contains numerous phases (bjarebyite, kulanite, goyazite, goedkenite, palermoite) that contain substantial amounts of Ba and Sr (Nizamoff *et al.* 2004).

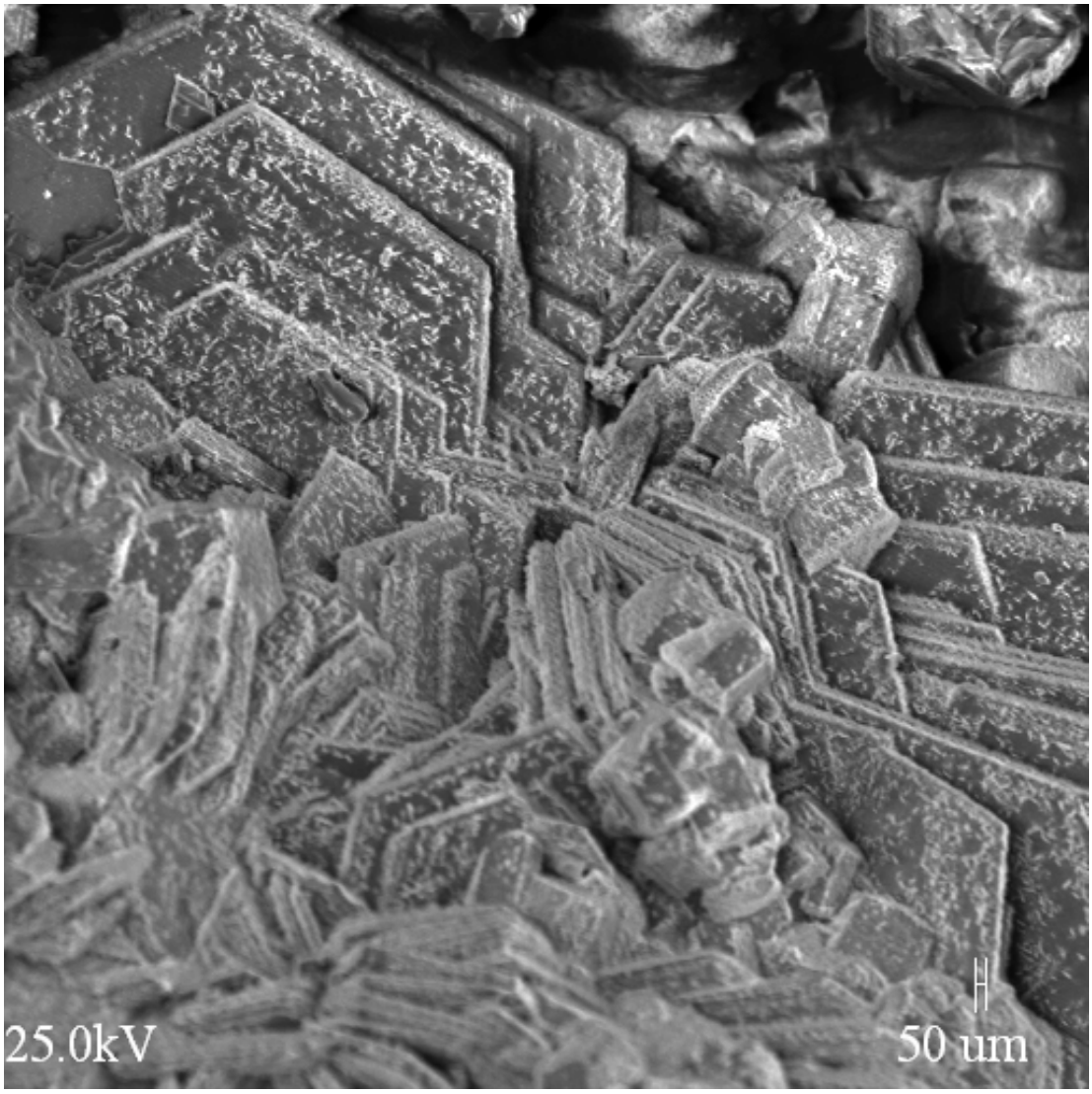

Figure 72: Backscattered electron image of crandallite from the core margin of the Palermo #2 pegmatite.

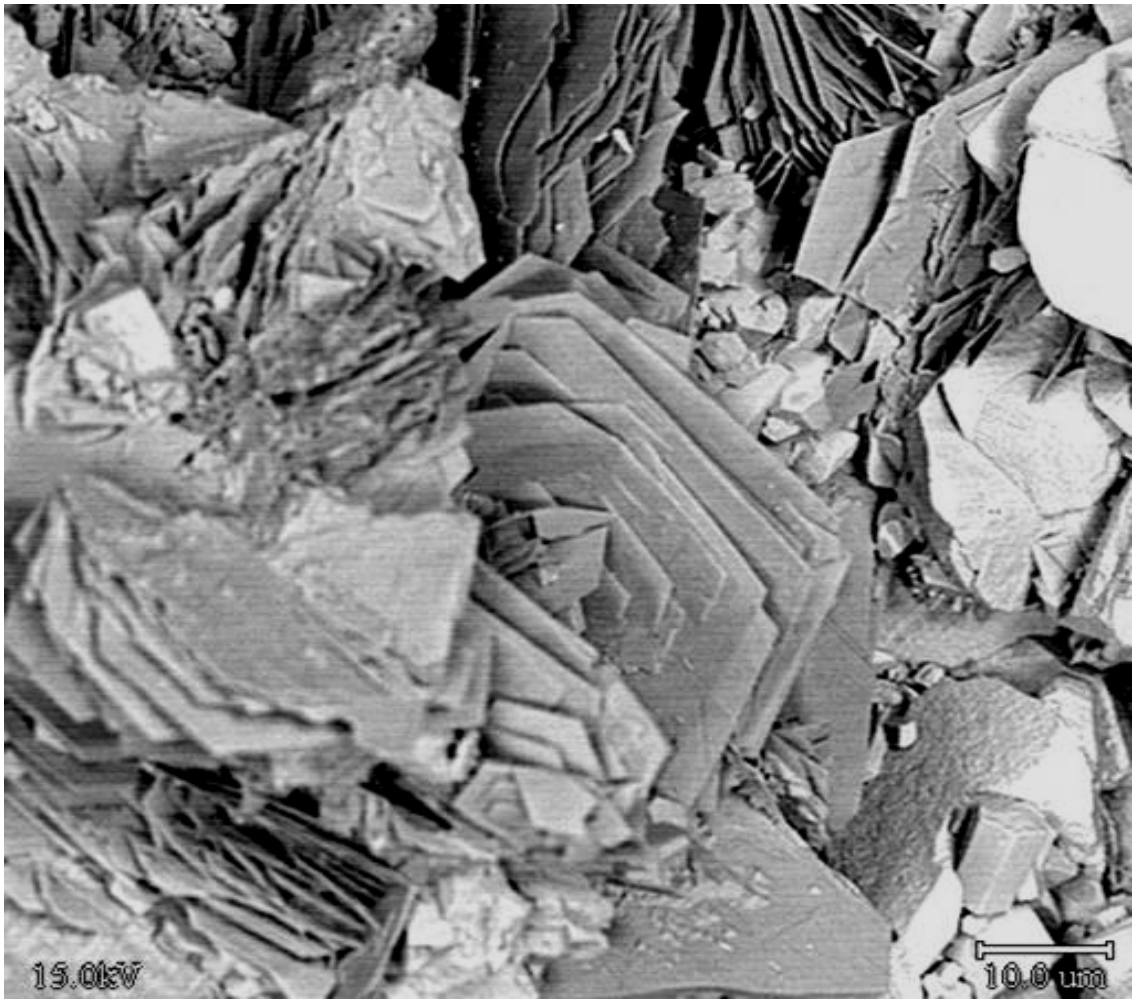

Figure 73: Secondary electron image of pseudohexagonal platy goyazite crystals from Palermo #2.

Autunite – $Ca(UO_2)_2(PO_4)_2 \cdot 10\text{-}12\ H_2O$

Autunite occurs as small (< 1 mm) yellow to greenish yellow tabular crystals in the core margin at Palermo #2. Autunite may occur on joint and fracture surfaces or in small cavities and is often associated with quartz, muscovite, torbernite, pyrite, and goethite. Autunite is a product of low temperature oxidative alteration of primary uranium-bearing minerals (uraninite) in the presence of Ca ions leached from Ca-bearing minerals (apatite group, carbonates, etc.).

Torbernite – $Cu^{2+}(UO_2)_2(PO_4)_2 \cdot 8\text{-}12\ H_2O$

Torbernite forms small (< 1 mm) yellow greenish to green tabular crystals in the core margin at Palermo #2. Torbernite may occur on joint and fracture surfaces or small cavities and is often associated with quartz, muscovite, autunite, pyrite, and goethite. Torbernite is a typical product of low temperature oxidative alteration of primary uranium-bearing minerals (uraninite) in the presence of Cu-bearing sulfides.

Strengite – $Fe^{3+}PO_4 \cdot 2\ H_2O$

Phosphosiderite – $Fe^{3+}PO_4 \cdot 2\ H_2O$

Strengite and its dimorph phosphosiderite occur as small (< 1 mm) pinkish to red crystals in association with rockbridgeite, pyrite/pyrrhotite and gypsum. Strengite and phosphosiderite typically form at low temperatures (< 250ºC) in an oxidizing environment. Strengite and phosphosiderite may also occur as products of the weathering environment as these phases have been identified from materials collected from the mine tailings dump. Interaction of altered primary phosphates and the resulting secondary species with meteoric water may be a possible mechanism for a weathering origin of strengite and phosphosiderite.

Phosphate Paragenesis

Approximately two hundred secondary phosphate species have been reported from granitic pegmatites. Most secondary phosphates are formed by subsolidus metasomatism of primary phosphates by aqueous fluids (Moore 1973). This alterative process takes place over a temperature range from ~600 to <100°C under both oxidative and reducing conditions (Moore 1973). Fransolet et al. (1985) suggested a lower temperature range for this process: ~400 to 25ºC for the phosphate assemblage present at the Angarf Sud pegmatite, Anti-Atlas, Morocco. Experimental work by Shigley and Brown (1986) found that lithiophilite crystallizes from a hydrous pegmatitic melt containing ~ 2 wt.% P_2O_5 over a temperature range of ~ 500 to 400ºC. It should be noted that these temperature ranges may be subject to some degree of variability depending on the volatile content (H_2O, F^-, Cl^-, CO_3^{2-}, BO_3^{3-}, Li^+ and PO_4^{3+}) of the pegmatitic melt. Assuming crystallization of primary phosphates between ~ 600 to 500ºC, and akin to Moore (although with slight differences in temperature), this author has chosen to split the metasomatic alterative process into two stages: high temperature metasomatic alteration (from ~500-300°C) and low temperature metasomatic alteration (from ~300-100°C) (Figure 74). The 300ºC boundary is proximal to the approximate temperature (~250ºC) where mineral structures can accommodate bonded water molecules in a stable arrangement (Moore 1973). Fransolet *et al*. (1985) suggested that secondary phosphates can form at ambient temperatures in the near-surface/surface environment and this phenomenon should not be discounted.

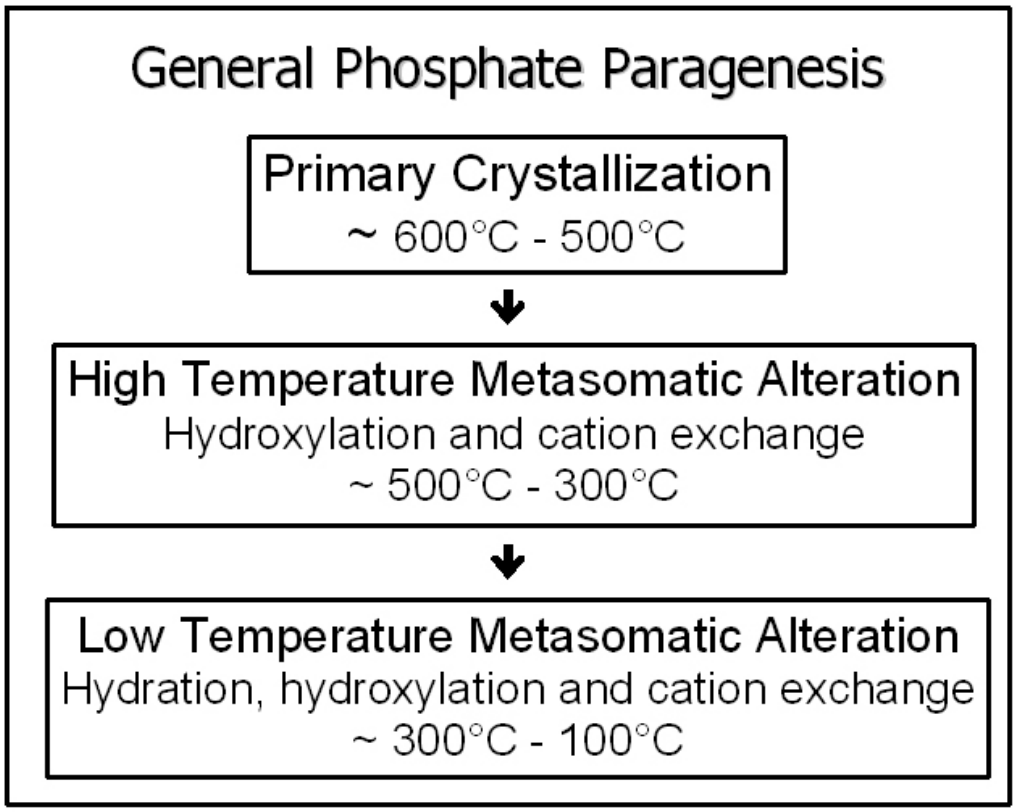

Figure 74: Generalized phosphate paragenesis and temperature conditions for primary and secondary species from LCT-type granitic pegmatites.

Triphylite, montebrasite and fluorapatite/hydroxylapatite are the main primary phases that facilitate the formation of secondary phosphates at Palermo #2. The fluids responsible for the alterative process are thought to be post-magmatic and aqueous with varying acidity/alkalinity (Moore, 1973; Hawthorne, 1998). The presence of Fe^{2+}-, Fe^{3+}-, Mn^{2+}- and Mn^{3+}-bearing secondary phosphates can provide insight regarding oxygen fugacity and the redox conditions during formation of the secondary phosphate suites. Large scale replacement of primary phosphates by siderite/rhodochrosite provides evidence that secondary phosphate-forming aqueous fluids can have a substantial carbonate (CO_3^{2-}) component.

In addition to the primary phosphates that are being altered, the minerals in contact with and proximal to the primary phosphate may contribute cations and /or

anions to the aqueous metasomatic fluids. The ensuing combination of cations and/or anions results in a complicated geochemical/mineralogical environment that may yield a large number of secondary species. In addition to the deposition of secondary phosphate species at the site of the parental primary phosphate, secondary phosphates may be deposited along fractures and joint surfaces radiating outward from the primary phosphate masses. Consequently, secondary phosphates can be found many meters away from their primary source. The metasomatic alteration schemes that follow are meant to illustrate observed assemblages with the caveat that these schemes show some degree of overlap (i.e. – certain species can occur in multiple environments and environmental constancy (T, pH, fO_2, etc.) cannot be assured).

High Temperature Metasomatic Alteration of Triphylite-lithiophilite:

The high temperature alteration of triphylite at the Palermo #2 pegmatite occurs during a temperature interval between ~500 to 300º C and involves cation exchange, leaching of Li^+ and may include hydroxylation (Figure 75). The main alteration sequence observed is the Mason-Quensel sequence (Quensel, 1937; Mason, 1941), involving the oxidative alteration sequence: triphylite → ferrisicklerite → heterosite. Divalent Fe in triphylite is oxidized to trivalent Fe yielding ferrisicklerite (Figure 76). Leaching of Li^+ from ferrisicklerite produces heterosite and its diagnostic purple hue. Addition of Na^+ and Ca^{2+} in the oxidizing environment may yield members of the alluaudite group (not observed at Palermo #2). High temperature alteration of triphylite-lithiophilite in the presence of non-oxidizing conditions may yield wolfeite-triploidite, griphite, scorzalite, whitlockite or natrophilite. At Palermo #2, scorzalite is the sole high temperature alteration product of triphylite in non-oxidizing conditions. Scorzalite

occurring proximally to triphylite is often intimately associated with altered muscovite of a greenish color. Muscovite likely donates the Al^{3+} required for the formation of scorzalite as Al^{3+} is typically present in only trace amounts in triphylite, although there are numerous minerals (schorl, almandine, feldspars) present in the core margin that could be possible sources of Al^{3+}. Moore (1973) noted a significant mass of scorzalite as an alteration product of triphylite at the Palermo #1 pegmatite.

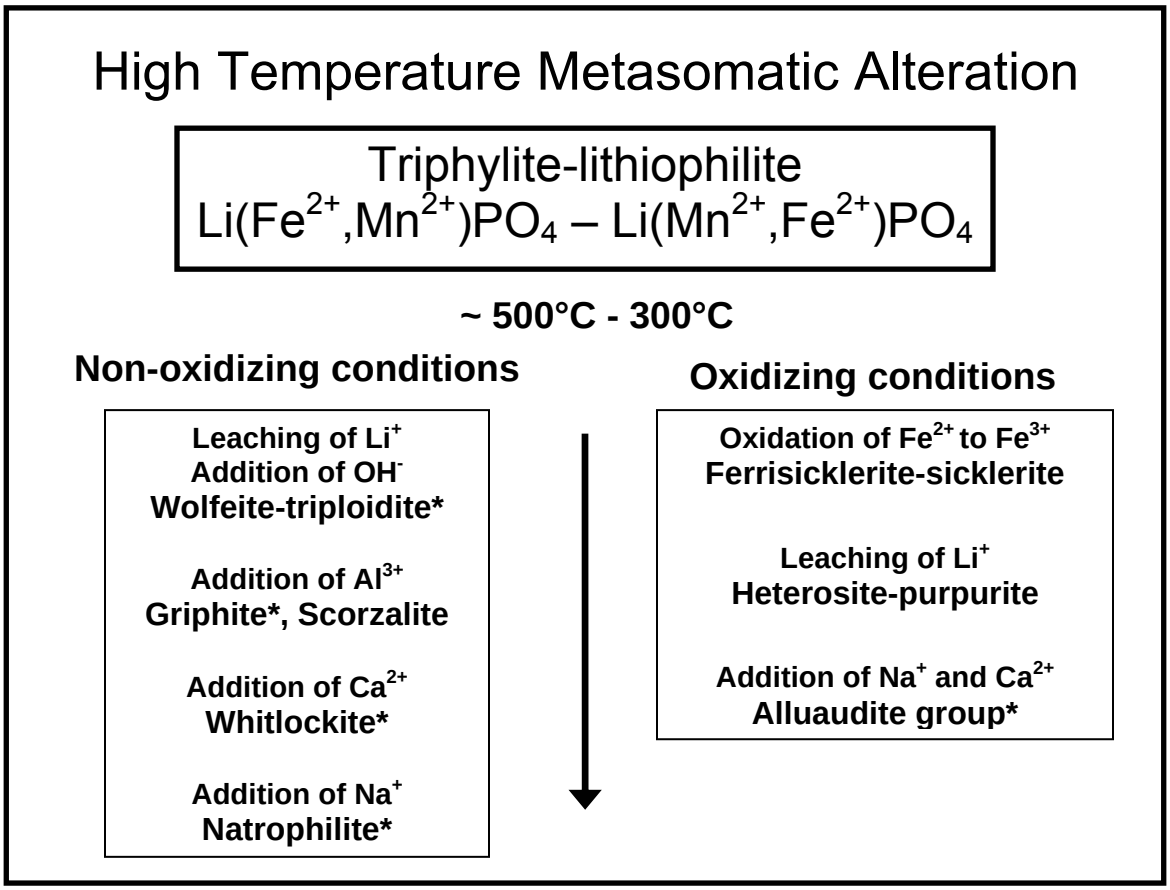

Figure 75: Typical high temperature metasomatic alteration conditions and products for the triphylite-lithiophilite series. *Species occurring at other localities and not found at Palermo #2.

Figure 77 illustrates the major cation content (Fe, Mn and Mg) in the primary phosphates triphylite, wolfeite, graftonite and sarcopside. Also plotted are compositions of selected high temperature metasomatic alteration products of triphylite (ferrisicklerite and heterosite); low temperature metasomatic phosphates (oxidizing conditions):

beraunite, rockbridgeite, and whitmoreite; and low temperature metasomatic phosphates (non-oxidizing conditions): kryzhanovskite, ludlamite and vivianite. Little compositional variation is evident between primary triphylite and its secondary products ferrisicklerite and heterosite suggesting that cations are mainly being exchanged and that additional cations are not likely being introduced to the system from other species at Palermo #2. Secondary phosphates forming in an oxidizing environment contain significantly less Mg in comparison with secondary phosphates forming in non-oxidizing conditions.

Figure 76: Triphylite mass (blue, 5 cm) exhibiting a rind of ferrisicklerite (dark brown) from the Palermo #2 pegmatite, North Groton, NH.

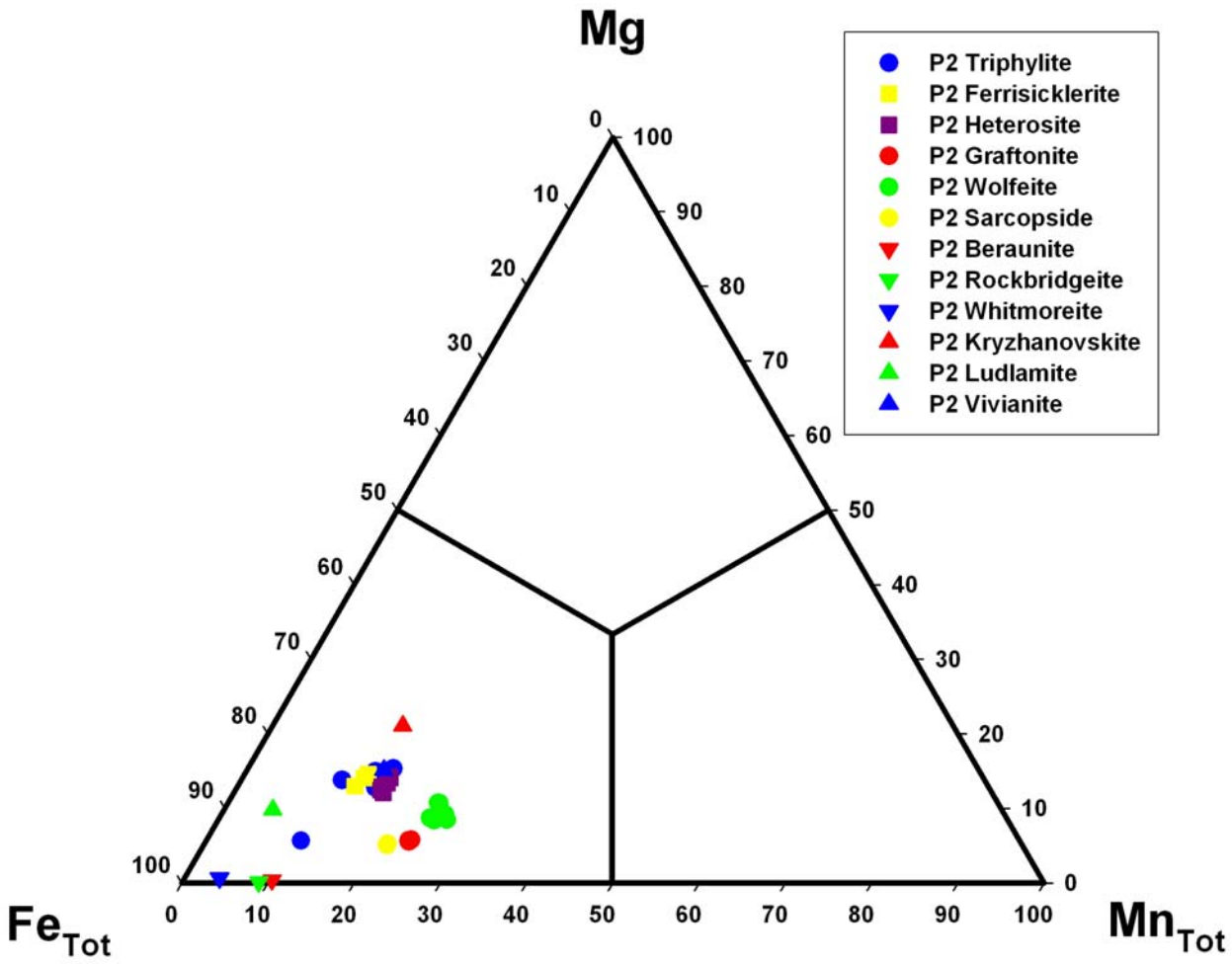

Figure 77: $Fe_{tot}Mn_{tot}Mg$ (apfu) plot of primary phosphates: triphylite, graftonite, wolfeite and sarcopside (circles); high temperature metasomatic phosphates: ferrisicklerite and heterosite (squares); low temperature metasomatic phosphates - oxidizing conditions: beraunite, rockbridgeite, and whitmoreite (triangles-down); and low temperature metasomatic phosphates - non-oxidizing conditions: kryzhanovskite, ludlamite and vivianite (triangles-up) from the Palermo #2 pegmatite.

Low Temperature Metasomatic Alteration of Triphylite-lithiophilite (oxidizing):

The low temperature alteration of triphylite at the Palermo #2 pegmatite occurs during a temperature interval between ~300 to 100º C and under oxidizing conditions is shown in Figure 78. In addition to cationic exchange and hydroxylation occurring in the high temperature alteration scheme, hydration and additional hydroxylation may take place in the ~300 to 100ºC temperature range. At Palermo #2, the major cations involved in the formation of secondary phosphates include: Fe^{2+}, Fe^{3+}, Mn^{2+}, Ca^{2+} and

Mg^{2+}. The exchange/addition of Fe^{2+}, Fe^{3+}, Mn^{2+}, Ca^{2+} and Mg^{2+} in combination with hydroxylation and hydration has resulted in the formation of rockbridgeite-frondelite, strunzite, laueite, stewartite, ushkovite, beraunite, jahnsite-(CaMnFe), jahnsite-(CaMnMn), jahnsite-(CaMnMg), kryzhanovskite, mitridatite and whitmoreite. At other phosphate-bearing pegmatites additional cations (mainly alkalis and transition metals) can be added to the system resulting in the formation of numerous secondary species (Figure 78).

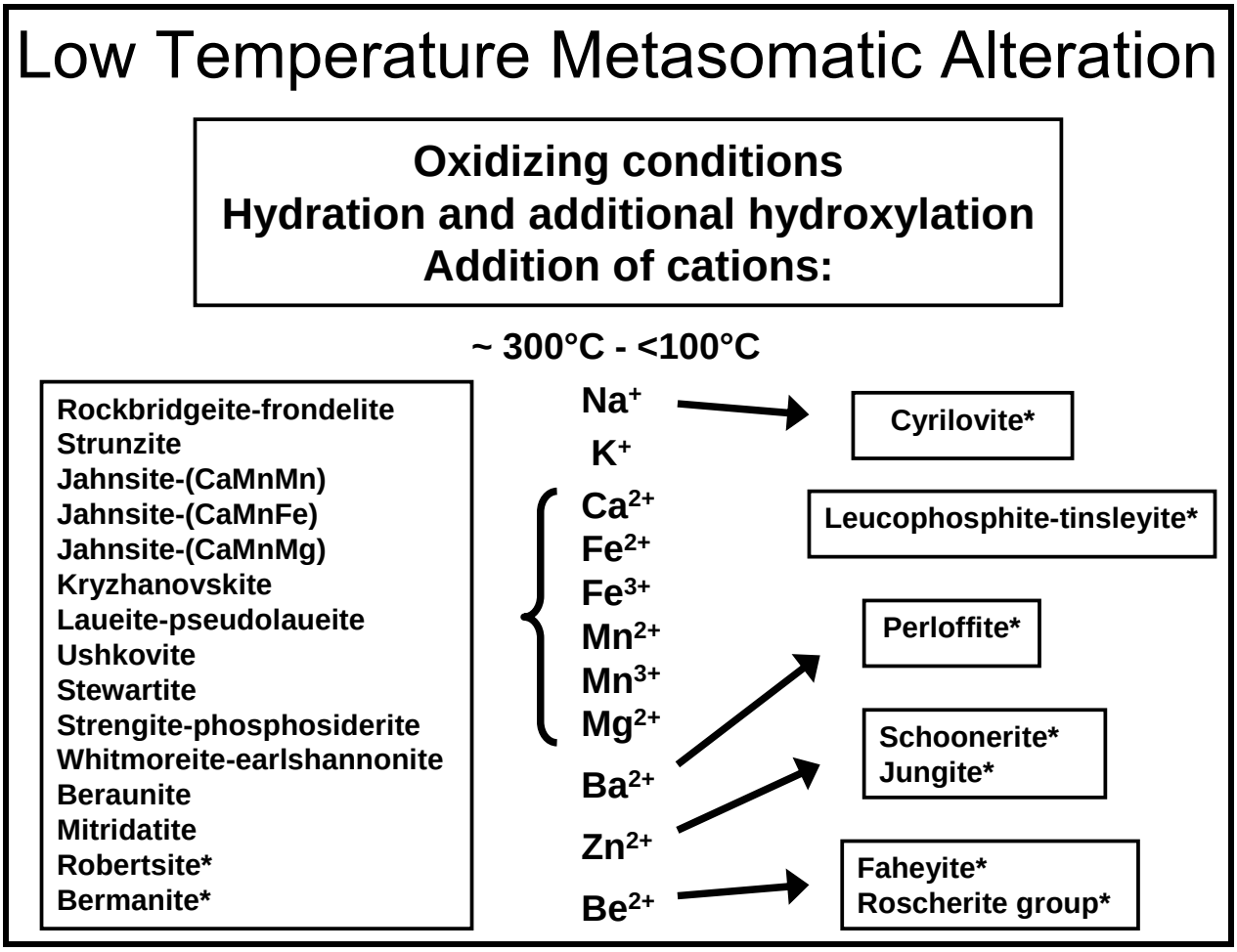

Figure 78: Possible low temperature metasomatic alteration products resulting from oxidizing conditions for the triphylite-lithiophilite series. *Denotes species not occurring at Palermo #2.

Low Temperature Metasomatic Alteration of Triphylite-lithiophilite (non-oxidizing):

The low temperature alteration of triphylite at the Palermo #2 pegmatite occurs during a temperature interval between ~300 to 100º C and under non-oxidizing conditions (Figure 79). In addition to cationic exchange and hydroxylation occurring in the high temperature alteration scheme, hydration and additional hydroxylation may take place in the ~300 to 100ºC temperature range. At Palermo #2, the major cations involved in the formation of secondary phosphates include: Fe^{2+}, Mn^{2+}, Ca^{2+} and Mg^{2+}. The exchange/addition of Fe^{2+}, Mn^{2+}, Ca^{2+} and Mg^{2+} in combination with hydroxylation and hydration has resulted in the formation of vivianite, ludlamite, fairfieldite-messelite and childrenite-eosphorite.

Additional cations involved in the formation of secondary phosphates include: Al^{3+} and Sr^{2+}. The exchange/addition of Al^{3+}, Fe^{2+}, Mn^{2+}, Ca^{2+} and Mg^{2+} in combination with hydroxylation and hydration has resulted in the formation of whiteite group species, paravauxite group species and childrenite-eosphorite. The exchange/addition of Al^{3+} and Sr^{2+} in combination with hydroxylation and hydration has resulted in the formation of crandallite and goyazite.

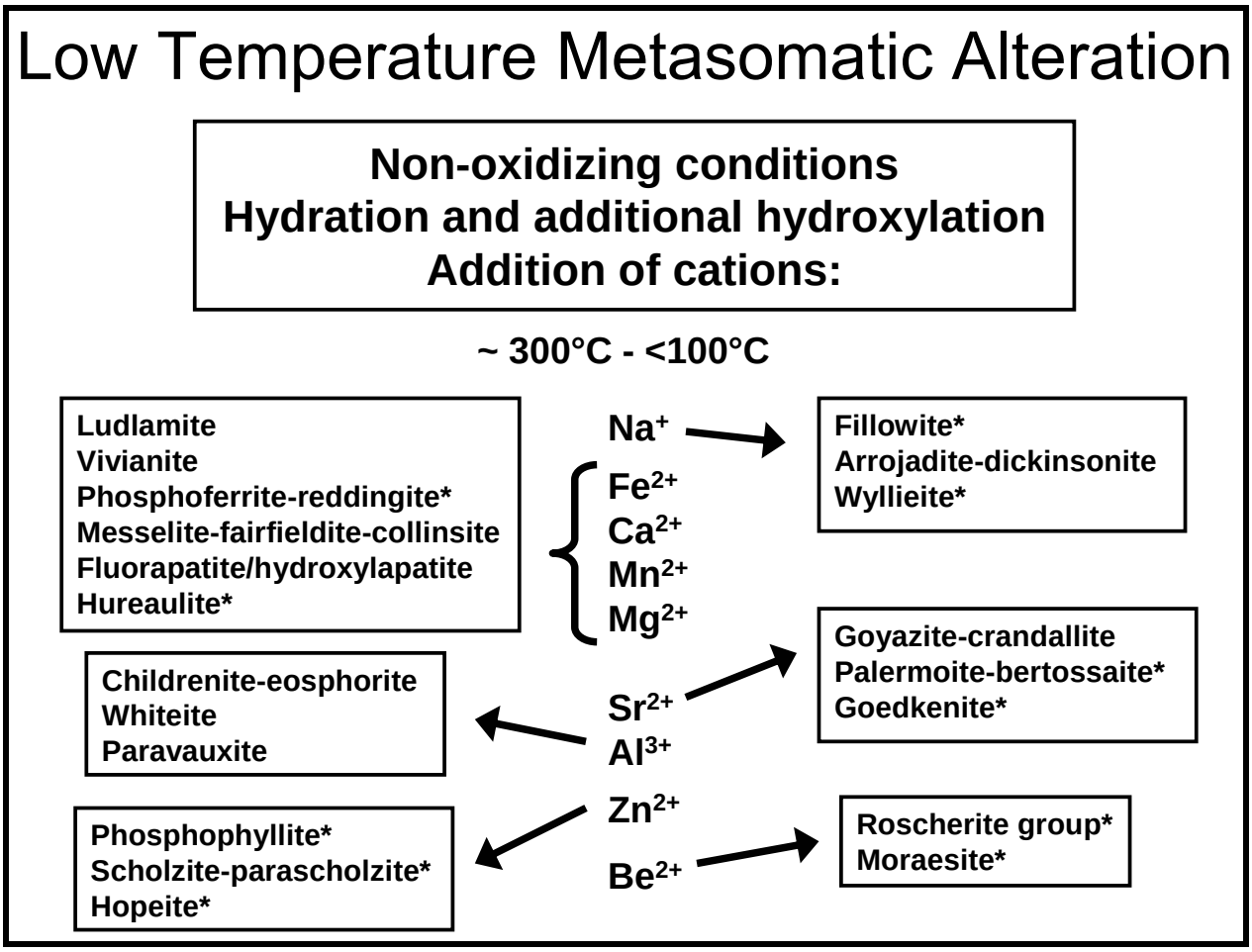

Figure 79: Possible low temperature metasomatic alteration products resulting from non-oxidizing conditions for the triphylite-lithiophilite series. *Species occurring at other localities and not found at Palermo #2.

Secondary Phosphate Alteration Sequence for Montebrasite-amblygonite:

Like triphylite-lithiophilite, montebrasite-amblygonite follows a two stage metasomatic alteration sequence and occurs in both oxidizing and non-oxidizing conditions. High temperature metasomatic alteration of montebrasite-amblygonite occurs over a temperature range of ~500 to 300º C and involves cation exchange, leaching of Li^+ and F^-, and hydroxylation (Figure 80). The high temperature alteration sequence observed at Palermo #2 is montebrasite → scorzalite-lazulite ± augelite. Leaching of Li^+ and F^- from montebrasite in combination with the addition of Fe^{2+}, Mg^{2+}

and OH^-, result in the formation of scorzalite-lazulite ± augelite (Figure 81). Scorzalite-lazulite is quite prevalent at Palermo #2 whereas augelite is more sporadic in occurrence.

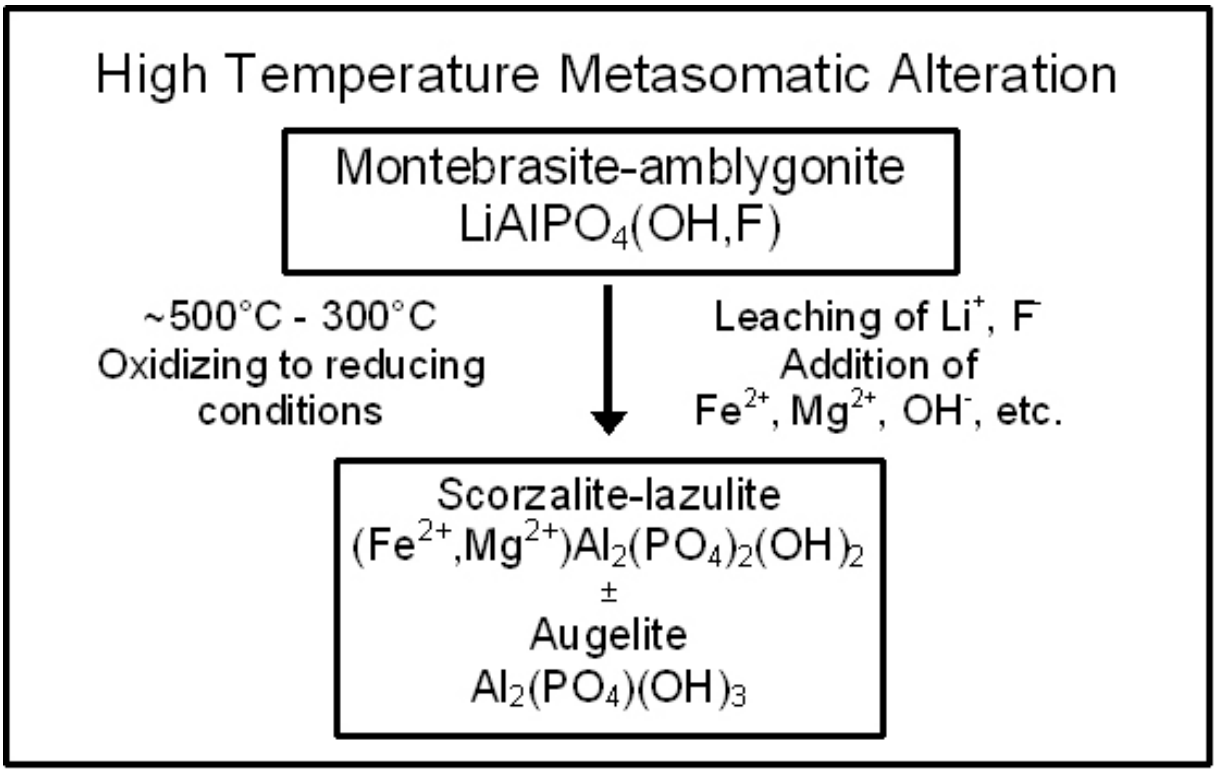

Figure 80: Typical high temperature metasomatic alteration conditions and products for montebrasite-amblygonite (modified from Nizamoff *et al.* 2002).

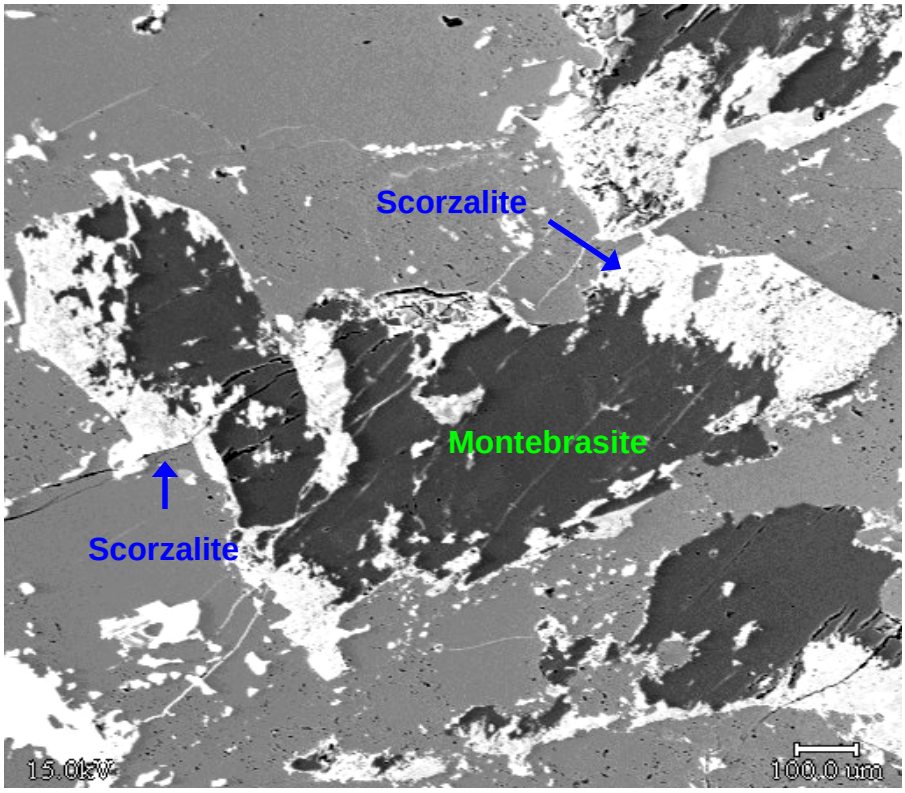

Figure 81: Backscattered electron image showing incipient alteration of montebrasite (very dark gray) to scorzalite (white) from Nizamoff *et al.* 2003.

Low Temperature Metasomatic Alteration of Montebrasite-amblygonite:

The low temperature alteration of montebrasite at the Palermo #2 pegmatite occurs during a temperature interval between ~300 to 100º C and under oxidizing to non-oxidizing conditions (Figure 82). In addition to cation exchange and hydroxylation occurring in the high temperature alteration scheme, hydration and additional hydroxylation may take place in the ~300 to 100ºC temperature range. At Palermo #2, the major cations involved in the formation of secondary phosphates include: Fe^{2+}, Mn^{2+}, Ca^{2+}, Mg^{2+} and Al^{3+}. The exchange/addition of Fe^{2+}, Mn^{2+}, Ca^{2+}, Mg^{2+} and Al^{3+} in combination with hydroxylation and hydration has resulted in the formation of gormanite-souzalite, augelite, goyazite-crandallite, chlorapatite-hydroxylapatite, paravauxite-gordonite, whiteite-(MnFeMg), whiteite-(CaMnMg), fairfieldite-messelite-

collinsite and childrenite-eosphorite. The overall alteration sequence of montebrasite from Palermo #2 displays some similarity to the alteration of montebrasite from pegmatites in the Karibib region of Namibia. Baldwin *et al.* (2000) report natromontebrasite, brazilianite, lazulite-scorzalite, goyazite-gorceixite-crandallite and hydroxylapatite as typical alteration products of montebrasite forming at temperatures below ~450ºC. The assemblage present at Palermo #2 suggests a lack of reactivity of Na^+ in the alterative fluids as no brazilianite or other Na-bearing phosphates are present.

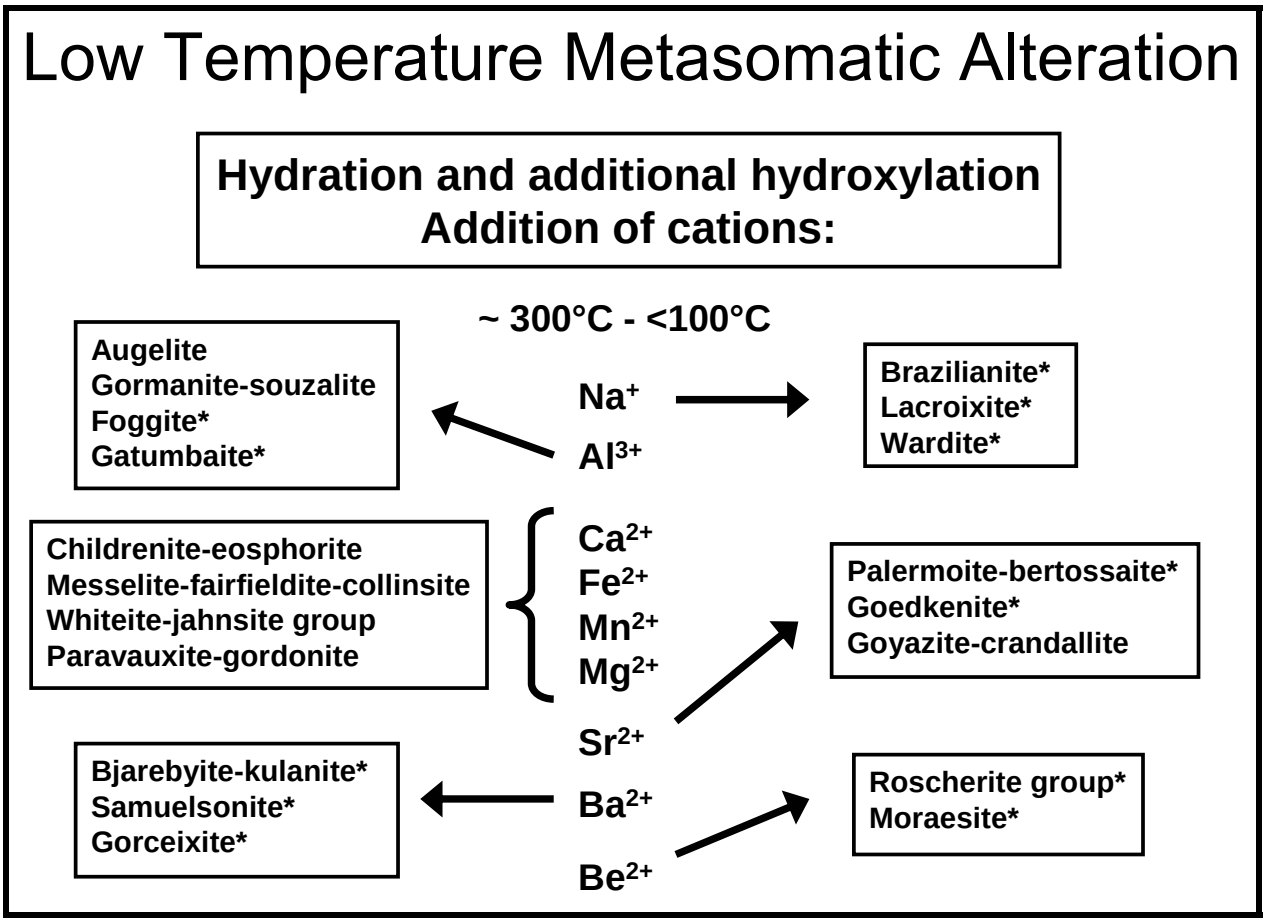

Figure 82: Low temperature metasomatic alteration products for montebrasite-amblygonite (modified from Nizamoff *et al.* 2002). *Species occurring at other localities and not found at Palermo #2.

Secondary Phosphate Alteration Sequence for "Arrojadite":

The low temperature alteration of "arrojadite" at the Palermo #2 pegmatite occurs between ~300 to 100º C in a non-oxidizing environment (Figure 83). Metasomatic alteration of primary "arrojadite" appears to have involved the leaching of leaching of Na^{+}, F^{-}, K^{+}, Ca^{2+} and possibly some Fe^{2+}. Hydroxyl and H_2O were added as well as possibly some Fe^{2+}. The alterative process yields mainly vivianite as a low temperature product although goyazite-crandallite occurs in one sample. It is uncertain if the goyazite-crandallite is a direct alteration product of "arrojadite" or an alteration product of a proximal primary phosphate such as montebrasite. Additional specimens of "arrojadite" should be examined to better understand this process.

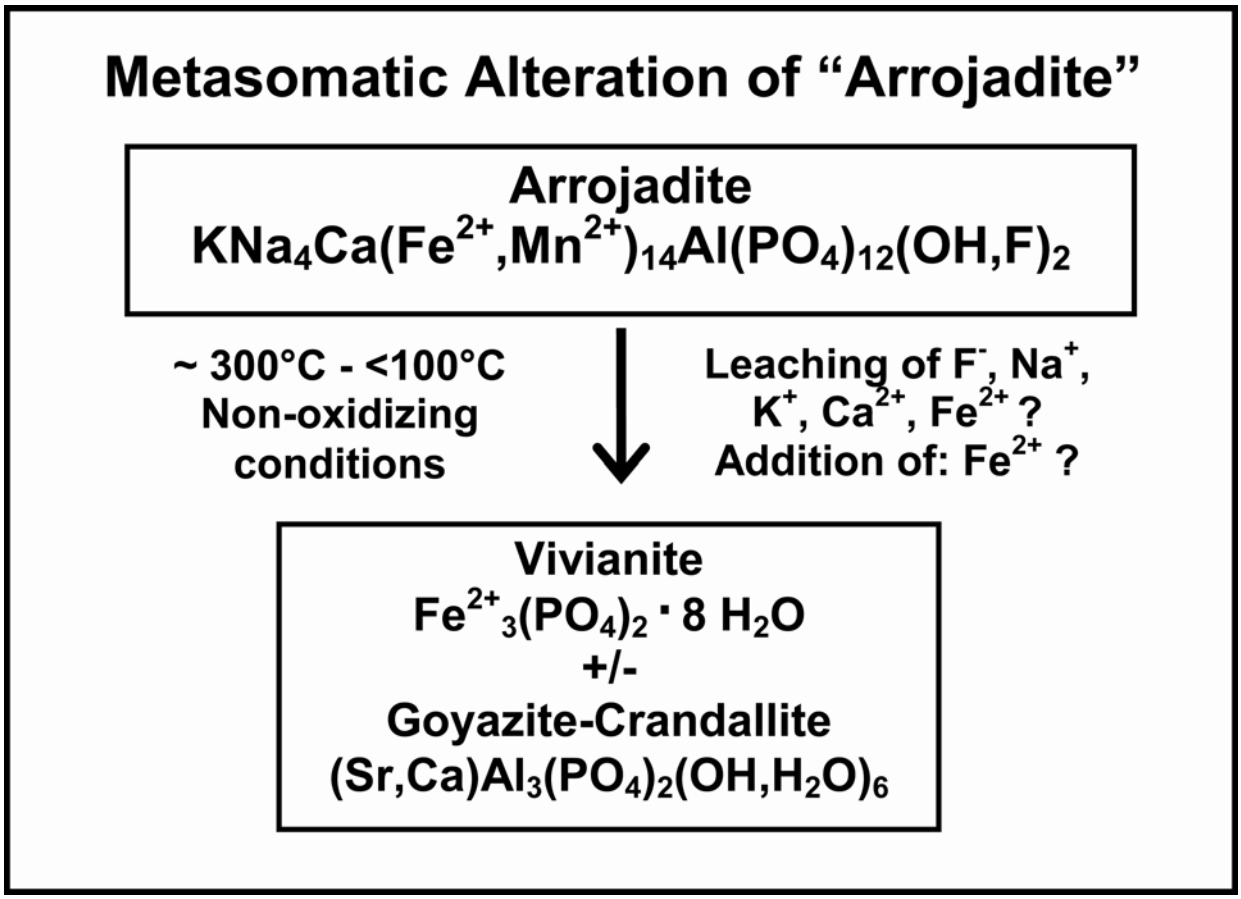

Figure 83: Low temperature metasomatic alteration products for "arrojadite" from the Palermo #2 pegmatite, North Groton, NH (Nizamoff *et al.* 2004).

Selected Phosphate Paragenesis for Sample P2-CM-42

The paragenetic sequence of phosphate minerals from sample P2-CM-42 from the core margin of the Palermo #2 pegmatite is presented in Figure 84. Sample P2-CM-42 is an interesting sample due to the presence of multiple primary phosphates (triphylite, fluorapatite and hydroxylapatite) that have undergone metasomatic alteration to secondary products. Alteration of triphylite under non-oxidizing conditions produces a suite of secondary phosphates including: ludlamite, vivianite and messelite-fairfieldite. Alteration of triphylite under non-oxidizing conditions in the presence of muscovite can produce a suite of secondary phosphates including: scorzalite and gormanite. Alteration of fluorapatite ± hydroxylapatite under non-oxidizing conditions produces a suite of secondary species including: siderite (two generations), childrenite and hydroxylapatite (colorless). At some point below ~ 250ºC, the alterative environment became more oxidizing, resulting in a suite of secondary phosphates including: rockbridgeite, strunzite, laueite, jahnsite, mitridatite, whitmoreite and beraunite. These phases occur on both the earlier triphylite-derived phosphates and fluorapatite ± hydroxylapatite-derived products.

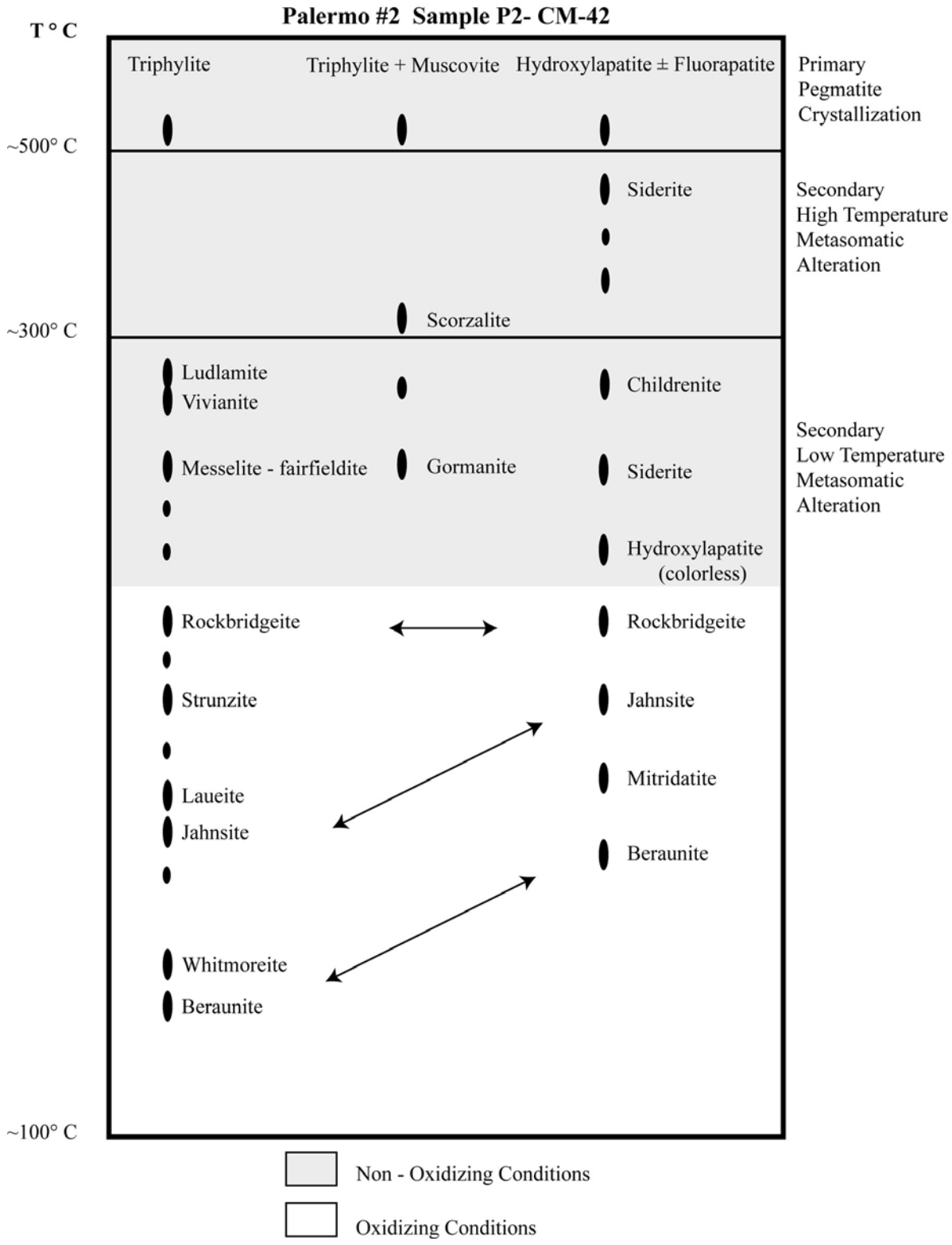

Figure 84: Paragenetic sequence for Palermo #2 sample P2-CM-42. Arrows indicate that the origin of the denoted species may identical.

Summary of Paragenetic Results for the Palermo #2 Pegmatite:

The approximately 40 secondary phosphates that occur at Palermo #2 are the result of alteration of primary phosphates and associated silicate, carbonate, sulfide, arsenide and oxide minerals locally present in the core margin of the pegmatite. Post-magmatic, aqueous fluids caused the concomitant alteration of many of the minerals occurring in core margin resulting in the formation of the diverse suite of secondary phosphates observed at Palermo #2. Unlike the nearby Palermo #1 pegmatite, secondary phosphates from the Palermo #2 pegmatite have resulted from the low temperature metasomatic exchange of Fe^{2+}, Fe^{3+}, Mn^{2+}, Al^{3+}, Ca^{2+}, Mg^{2+}, OH^- and H_2O (Figure 85).

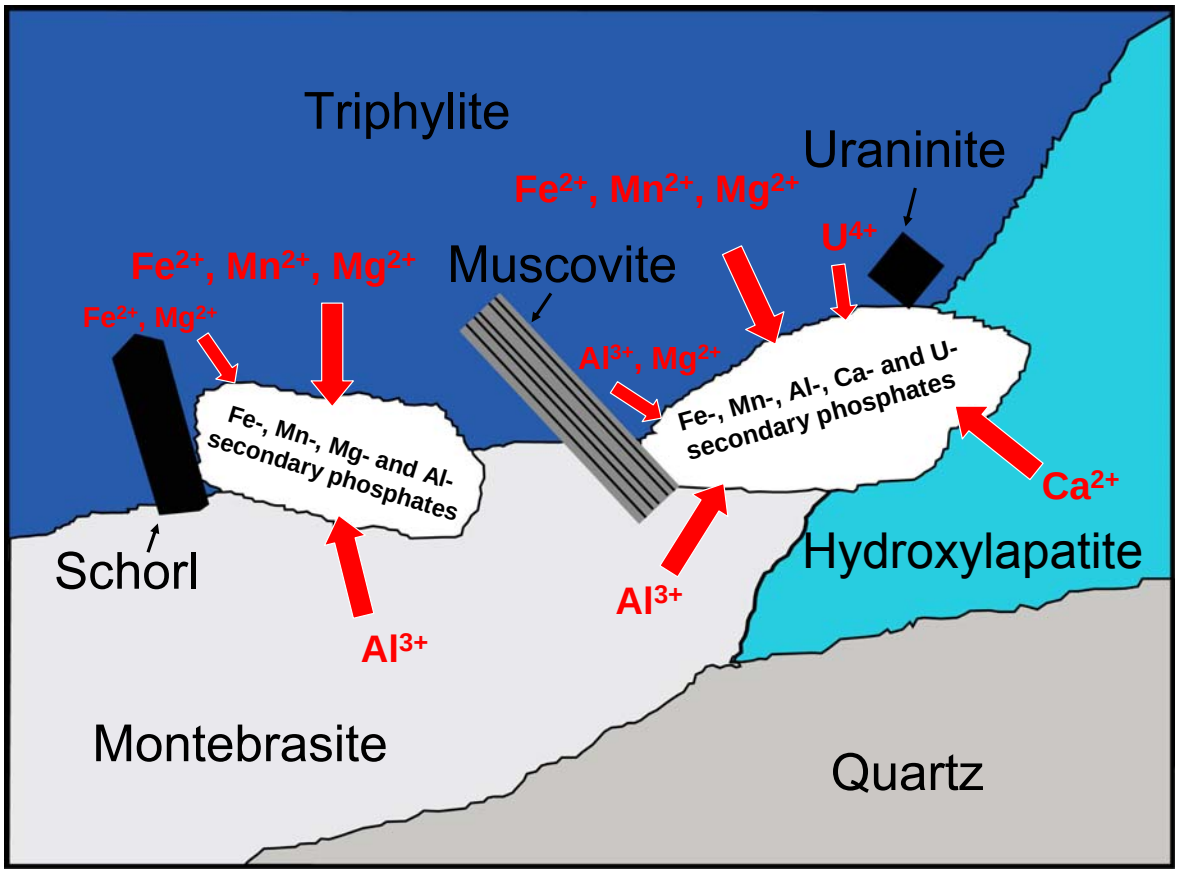

Figure 85: Diagram illustrating how primary phosphates as well as non-phosphate species donate cations to the alterative fluids producing metasomatic secondary phosphates.

In comparison with Palermo #2, the larger variety of secondary phosphates exhibited by the Palermo #1 pegmatite can probably be attributed to a combination of the presence of more significant amounts of accessory minerals (Zn-, Pb-, Cu-sulfides) and greater amounts of primary phosphates such as arrojadite group minerals that may contribute Ba and Sr to alterative fluids.

Conclusions

The Palermo #2 is a rare-element pegmatite of the beryl-phosphate subtype located in the Grafton pegmatite field of west-central New Hampshire. Geochemically, the Palermo #2 displays fractionation trends (Mn/Fe ratios in garnet and triphylite, Ta/Nb and Mn/Fe ratios in ferrocolumbite, Zr/Hf ratios in zircon) consistent with those reported by other researchers for beryl-phosphate and/or beryl-columbite-phosphate subtype granitic pegmatites.

Several notable trends are evident from the examination of geochemical data from Palermo #2. Three apatite group minerals (fluorapatite, hydroxylapatite and chlorapatite) occur in the pegmatite and exhibit an evolutionary trend of high F^- and low to moderate OH^- in apatite from the wall zone to low F^- and progressively higher OH^- and Cl^- in apatite in the core margin zone of the pegmatite. To the author's knowledge, this is the first time a trend of this nature has been seen in apatite group minerals in granitic pegmatites.

Montebrasite from Palermo #2 contains relatively low amounts of F^- (from 1.04 to 2.48 wt.%). Low F^- montebrasite and the presence of abundant hydroxylapatite in the core margin of the pegmatite suggest a decrease in the activity of F^- in late-stage magmatic fluids.

The primary phosphates triphylite, fluorapatite, hydroxylapatite and montebrasite have been metasomatically altered by late-stage, carbonate-bearing aqueous fluids. Interaction between the primary phosphates and late-stage aqueous fluids has produced a diverse suite of nearly 40 species of secondary phosphate minerals and associated carbonates.

References

Baldwin, J.R. & von Knorring, O. (1983) Compositional range of Mn-garnet in zoned granitic pegmatites. *Canadian Mineralogist*, 21, 683-688.

Baldwin, J.R., Hill, P.G., von Knorring, O., and Oliver, G.J.H. (2000) Exotic aluminum phosphates, natromontebrasite, brazilianite, goyazite, gorceixite and crandallite from rare-element pegmatites in Namibia. *Mineralogical Magazine*, 64, 6, 1147-1164.

Barreiro, B. and Aleinikoff, J.N. (1985) Sm-Nd and U-Pb isotopic relationships in the Kinsman Quartz Monzonite, New Hampshire. Geological Society of America Abstracts with Programs, V. 17, p.3.

Cameron, E.N., Larrabee, D.M., McNair, A.H., Page, J.J, Stewart, G.W. and Shainin, V.E. (1954) Pegmatite investigations 1942-45 New England. *U.S.G.S. Professional Paper* 255, 352 pp.

Campbell, T.J. and Roberts, W.L. (1986) Phosphate minerals from the Tip Top mine, Black Hills, South Dakota. *Mineralogical Record*, 17, 237-254.

Černá, I., Černý, P. and Ferguson, R.B. (1972) The Tanco pegmatite at Bernic Lake, Manitoba. III. Amblygonite-montebrasite. *Canadian Mineralogist*, 11, 643-659.

Černý, P. (1991a) Rare-element granitic pegmatites. Part 1: Anatomy and internal evolution of pegmatite deposits. *Geoscience Canada*, 18, 49-67.

Černý, P. (1991b) Rare-element granitic pegmatites. Part 2: Regional to global environments and petrogenesis. *Geoscience Canada*, 18, 68-81.

Černý, P. (2002) Mineralogy of beryllium in granitic pegmatites. *In*: Grew, E.S. (ed.) Beryllium: Mineralogy, petrology and geochemistry. Reviews in Mineralogy, V. 33. *Mineralogical Society of America*, 691 p.

Černý, P. and Ercit, T.S. (1989) Mineralogy of niobium and tantalum: crystal chemical relationships, paragenetic aspects and their economic implications. *In* Lathanides, Tantalum and Niobium (P. Möller, P. Černý and F.Saupé, eds.). Springer-Verlag, Berlin, Germany (27-79).

Černý, P. and Ercit, T.S. (2005) The classification of granitic pegmatites revisited. *Canadian Mineralogist*, 43, 2005-2026.

Černý, P. and Hawthorne, F.C. (1982) Selected peraluminous minerals. *In* Granitic Pegmatites in Science and Industry (P.Černý ed.). *Mineralogical Association of Canada*, Short Course Handbook 8, 163-186.

Černý, P., Goad, B.E., Hawthorne, F.C. & Chapman, R. (1986) Fractionation trends of the Nb- and Ta-bearing oxide minerals in the Greer Lake pegmatitic granite and its pegmatite aureole, southern Manitoba. *American Mineralogist*, 71, 501-517.

Černý, P., Meintzer, R.E., and Anderson, A.J. (1985) Extreme fractionation in rare-element granitic pegmatites: selected examples of data and mechanisms. *Canadian Mineralogist*, 23, 381-421.

Černý, P., Trueman, D.L., Ziehlke, D.V., Goad, B.E. & Paul, B.J. (1981) The Cat Lake – Winnipeg River and Wekusko Lake pegmatite fields, Manitoba. *Manitoba Mineral Resources Division, Economic Geology Report* ER80-1.

Clark, R.G., Jr. and Lyons, J.B. (1986) Petrogenesis of the Kinsman Intrusive Suite: Peraluminous granitoids of western New Hampshire. *Journal of Petrology*, 27, 1365-1393.

Dorais, M.J. (2003) The petrogenesis and emplacement of the New Hampshire plutonic suite. *American Journal of Science*, 303, 447-487.

Eusden, Jr., J. D. and Barreiro, B. (1989) The timing of high-grade metamorphism in central-eastern New England. *Maritime Sediments and Atlantic Geology*, 24, 241-255.

Eusden, Jr., J. D. and Lyons, J. B. (1993) The sequence of Acadian deformations in central New Hampshire. *Geological Society of America Special Paper* 275, 55-66.

Foord, E.E. (1976) *Mineralogy and Petrogenesis of Layered Pegmatite-Aplite Dikes in the Mesa Grande District, San Diego County, California*. Ph.D. Thesis, Stanford Univ., Stanford, CA.

Francis, C.A., Wise, M.A., Kampf, A.R., Brown, C.D., and Whitmore, R.W. (1993) Granitic pegmatites in northern New England, E1-E24. In: Field Trip Guidebook for the Northeastern United States: 1993 Boston GSA, Volume 1, Eds. Cheney, J.T. and Hepburn, J.C., Contribution No. 67, Department of Geology and Geography, University of Massachusetts, Amherst, Massachusetts.

Fransolet, A.M. (1975) On scorzalite from the Angarf-Sud pegmatite, Zenaga Plain, Anti-Atlas, Morocco. *Fortschritt der Mineralogie*, 52, 285-291.

Fransolet, A.M., Abraham, K. and Speetjens, J. (1985) Genetic evolution and significance of the phosphate mineral assemblages in the Angarf-Süd pegmatite, Tazenakht Plain, Anti-Atlas, Morocco. *Bulletin de Mineralogie*, 108, 3-4, 551-574.

Fransolet, A.M., Keller, P. and Fontan, F. (1986) The phosphate mineral associations of the Tsaobismund pegmatite, Namibia. *Contributions to Mineralogy and Petrology*, 92, 502-517.

Frondel, C. (1949) Wolfeite, xanthoxenite and whitlockite from the Palermo mine, New Hampshire. *American Mineralogist*, 34, 692-705.

Ginsburg, A.I. (1960) Specific geochemical features of the pegmatitic process. *21st International Geologic Congress (Norden)*, 17, 111-121.

Hawthorne, F.C. (1998) Structure and chemistry of phosphate minerals. *Mineralogical Magazine*, 62, 2, 141-164.

Hildreth, W. (1979) The Bishop Tuff: evidence for the origin of compositional zonation in silicic magma chambers. *Geological Society of America Special Paper* 180, 43-75.

Hildreth, W. (1981) Gradients in silicic magma chambers: implications for lithospheric magmatism. *Journal of Geophysical Research*, 86, 10153-10192.

Hurlbut, C.S., Jr. (1965) Detailed description of sarcopside from East Alstead, New Hampshire. *American Mineralogist*, 50, 1698-1707.

Hurlbut, C.S., Jr. and Aristarain, L.F. (1968) Beusite, a new mineral from Argentina, and the graftonite-beusite series. *American Mineralogist*, 53, 1799-1814.

Keller, P. (1991) The occurrence of Li-Fe-Mn phosphate minerals in granitic pegmatites of Namibia. *Communications of the Geological Survey of Namibia*, 7, 21-34.

Keller, P. and von Knorring, O. (1989) Pegmatites at the Okatjimukuju farm, Karibib, Namibia Part 1: Phosphate mineral associations of the Clementine II pegmatite. *European Journal of Mineralogy*, 1, 567-593.

Lathrop, A.S., Blum, J.D. and Chamberlain, C.P. (1996) Nd, Sr and O isotopic study of the petrogenesis of two members of the New Hampshire Plutonic Series. *Contributions to Mineralogy and Petrology*, 124, 126-138.

London, D., Černý, P., Loomis, J.L., and Pan, J.Y. (1990) Phosphorus in alkali feldspars of rare-element granitic pegmatites. *Canadian Mineralogist*, 28, 771-786.

London, D. and Burt, D.M. (1982) Alteration of spodumene, montebrasite and lithiophilite in pegmatites of the White Picacho District, Arizona. *American Mineralogist*, 67, 87-113.

Lyons, J.B., Bothner, W.A., Moench, R.H., and Thompson, J.B., Jr. (1997) Bedrock geologic map of New Hampshire. U.S. Geological Survey.

Mahood, G.A. (1981) Chemical evolution of a Pleistocene rhyolitic center: Sierra la Primavera, Jalisco, Mexico. *Contributions to Mineralogy and Petrology*, 77, 129-149.

Malinconico, M. (1982) *Stratigraphy and structure of the Southeastern Rumney 15 minute Quadrangle, New Hampshire*. M.S. Thesis. Dartmouth College, Hanover, New Hampshire, 234 pp.

Mason, B. (1941) Minerals of the Varuträsk pegmatite. XXIII. Some iron-manganese phosphate minerals and their alteration products, with special reference to material from Varuträsk. *Geologiska Föreningeni Förhandlingar*, 63, 2, 117-175.

Mason, R.A. (1982) Trace element distributions between the perthite phases of alkali feldspars from pegmatites. *Mineralogical Magazine*, 45, 101-106.

Masau, M., Staněk, J., Černý, P. and Chapman, R. (2000) Metasomatic wolfeite and associated phosphates from the Otov I granitic pegmatite, western Bohemia. *Journal of the Czech Geological Society*, 45, 1-2, 159-173.

McNair, A.H. (1943) Palermo number two mica mine, Groton, New Hampshire. USGS unpublished report. US Department of the Interior, 4 pp.

Moore, P.B. (1971) The $Fe^{2+}_3(H_2O)_n(PO_4)_2$ homologous series: crystal-chemical relationships and oxidized equivalents. *American Mineralogist*, 56, 1-17.

Moore, P.B. (1973) Pegmatite phosphates: descriptive mineralogy and crystal chemistry. *Mineralogical Record*, 4, 103-130.

Moore, P.B. (1982) Pegmatite minerals of P (V) and B (III). *In* Granitic Pegmatites in Science and Industry (P.Černý ed.). *Mineralogical Association of Canada*, Short Course Handbook 8, 267-291.

Moore, P.B. (2000) Analyses of Primary Phosphates from Pegmatites in Maine and Other Localities, *in* King, V.T., Tucker, R.D. and Marvinney, R.G. (editors), *Mineralogy of Maine: Volume 2 –mining history, gems and geology*: Maine Geological Survey, p. 333-336.

Moore, P.B., Irving, A.J. and Kampf, A.R. (1975) Foggite, goedkenite, and samuelsonite: three new species from the Palermo #1 pegmatite, North Groton, New Hampshire. *American Mineralogist*, 60, 957-964.

Moore, P.B., Araki, T., and Kampf, A.R. (1980) Nomenclature of the phosphoferrite structure type: refinements of landesite and kryzhanovskite. *Mineralogical Magazine*, 43, 789-795.

Mücke, A. (1981) The parageneses of the phosphate minerals of the Hagendorf pegmatite--a general view. *Chemie der Erde*, 40, 217-234.

Nizamoff, J. W, Simmons, W.B. and Falster, A.U. (2004) Phosphate mineralogy and paragenesis of the Palermo # 2 pegmatite, North Groton, New Hampshire. *Geological Society of America National Meeting, Denver. Abstract Vol. p. 115, #41-3.*

Nizamoff, J. W., Whitmore, R.W., Falster, A. U., Simmons, W. B., and Webber, K. L. (1998) Secondary Phosphate Minerals from the Palermo #2 Mine, North Groton, New Hampshire. *25th Annual Rochester Academy of Sciences Mineralogical Symposium, Abstracts with Program, 18.*

Nizamoff, J. W., Whitmore, R.W., Falster, A.U. and Simmons, W.B. (2002) Montebrasite and associated secondary phosphates from the Palermo No. 2 mine, North Groton, New Hampshire. *29th Annual Rochester Mineralogical Symposium, Abstracts with Program, 14-15.*

Nizamoff, J.W., Whitmore, R.W., Falster, A.U. and Simmons, W.B. (2003) Montebrasite and associated secondary phosphates from the Palermo #2 mine, North Groton, New Hampshire: *Rocks and Minerals*, 78, 122-123.

Nizamoff, J.W., Whitmore, R.W., Falster, A.U. and Simmons, W.B. (2004) Parascholzite, keckite, gormanite and other previously unreported secondary species and new data on kulanite and phosphophyllite from the Palermo #1 mine, North Groton, New Hampshire. *31st Annual Rochester Mineralogical Symposium, Abstracts with Program, 11-13.*

Osberg, P.H., Tull, J.F., Robinson, P., Hon, R., and Butler, J.R. (1989) The Acadian orogen. *In* The Appalachian-Ouachita Orogen in the United States (Hatcher, R.D., Jr., Thomas, W.A., and Viele, G.W., eds.). The Geology of North America, v. F-2, Geological Society of America, Boulder, Colorado, 179-232.

Page, L.R. (1937) *The geology of the Rumney quadrangle, New Hampshire*. Unpublished Ph.D. thesis, University of Minnesota.

Peacor, D.R. and Garske, D. (1964) Sarcopside from Deering and East Alstead, New Hampshire. *American Mineralogist*, 49, 1149-1150.

Plimer, I.R. and Bucher, I.D. (1979) Wolfeite and barbosalite from Thackaringa, Australia. *Mineralogical Magazine*, 43, 505-507.

Quensel, P. (1937) Minerals of the Varuträsk pegmatite. I. The lithium-manganese phosphates. *Geologiska Föreningeni Förhandlingar*, 59, 1, 77-96.

Roda, E., Pesquera, A., Fontan, F. and Keller, P. (2004) Phosphate mineral associations in the Cañada pegmatite (Salamanca, Spain): paragenetic relationships, chemical compositions and implications for pegmatite evolution. *American Mineralogist*, 89, 110-125.

Segeler, C.G., Ulrich, W., Kampf, A.R., and Whitmore, R.W. (1981) Phosphate minerals of the Palermo No.1 pegmatite. *Rocks and Minerals*, 56, 196-214.

Shigley, J.E. and Brown, G.E., Jr. (1985) Occurrence and alteration of phosphate minerals at the Stewart pegmatite, Pala district, San Diego County, California. *American Mineralogist*, 70, 395-408.

Shigley, J.E. and Brown, G.E., Jr. (1986) Lithiophilite formation in granitic pegmatites: a reconnaissance experimental study of phosphate crystallization from hydrous aluminosilicate melts. *American Mineralogist*, 71, 356-366.

Smeds, S-A., Uher, P., Černý, P., Wise, M.A., Gustafsson, L. and Penner, P. (1998) Graftonite-beusite in Sweden; primary phases, products of exsolution, and distribution in zoned populations of granitic pegmatites. *Canadian Mineralogist*, 36, Part 2; 377-394.

Smith, J.V. (1974) *Feldspar Minerals. 2. Chemical and Textural Properties*. Springer Verlag, New York.

Smith, J.V. (1983) Some chemical properties of feldspars. *In* Feldspar Mineralogy (2nd edition, P.H. Ribbe, ed.). *Reviews in Mineralogy*, 2, 281-296.

Spear, F.S., Kohn, M.J., Cheney, J.T., and Florence, F. (2002) Metamorphic, thermal, and tectonic evolution of Central New England. *Journal of Petrology*, 43, 2097-2120.

Trueman, D.L. and Černý, P. (1982) Exploration for rare-element granitic pegmatites. *In* Granitic Pegmatites in Science and Industry (P.Černý ed.). *Mineralogical Association of Canada*, Short Course Handbook 8, 463-493.

Whitmore, R.W. (2002) Personal communication.

Whitmore, R.W. and Lawrence, R.C., Jr. (2004) *The Pegmatite Mines Known as Palermo*. Friends of Palermo mines, 213 pp.

Wise, M.A and Černý, P. (1990) Beusite-triphylite intergrowths from the Yellowknife pegmatite field, Northwest Territories. *Canadian Mineralogist*, 28, 133-139.

Wise, M.A and Rose, T.R. (2000) The Bennett pegmatite, Oxford County, Maine. *In* King, V.T., Tucker, R.D. and Marvinney, R.G. (editors), *Mineralogy of Maine: Volume 2 –mining history, gems and geology*: Maine Geological Survey, p. 323-332.

Appendix I -- Whole-Rock Geochemistry

Appendix Table 1: XRF and INAA analyses of pegmatite wall zone from the Palermo #2 (JNWZ-1, JNWZ-2 and JNWZ-3) pegmatite and pegmatite (JNPG-1) a several km to the southwest.

Sample #	JNWZ-1	JNWZ-2A	JNWZ-3	JNPG-1
SiO_2 (wt. %	72.70	71.16	68.44	71.94
TiO_2	bdl	bdl	0.03	bdl
Al_2O_3	15.71	17.10	17.99	17.09
Fe_2O_3	0.29	0.31	0.44	0.32
FeO	bdl	bdl	bdl	bdl
MnO	bdl	bdl	bdl	0.03
MgO	bdl	bdl	0.20	bdl
CaO	0.47	0.44	0.12	0.54
Na_2O	6.71	6.30	2.81	7.22
K_2O	1.91	3.09	7.65	1.21
P_2O_5	0.28	0.29	0.28	0.24
L.O.I.	1.00	0.78	1.45	1.09
Totals	99.12	99.57	99.42	99.77
Rb (ppm)	51	102	524	54
Cs	22.1*	2.5*	22.1*	bdl
Sr	19	20	43	32
Ba	bdl	bdl	96	bdl
Sc*	0.1	0.6	0.6	n/a
V	bdl	bdl	bdl	bdl
Cr	bdl	bdl	bdl	bdl
Co	bdl	bdl	bdl	bdl
Ni	bdl	bdl	2	bdl
Cu	bdl	bdl	bdl	bdl
Zn	7	12	21	15
Ga	11	15	21	17
As	bdl	bdl	bdl	bdl
Y	13	19	57	14
Zr	6	bdl	bdl	38
Nb	8	8	18	10
Mo*	6.3	4.5	bdl	n/a
Sn	bdl	bdl	37.0	bdl
Sb*	bdl	0.1	bdl	n/a
Hf*	bdl	0.1	0.1	n/a
Ta*	4.2	0.9	4.2	n/a
W	bdl	bdl	bdl	bdl
Pb	38	48	69	36
Tl	bdl	bdl	bdl	bdl
Th*	bdl	0.3	bdl	n/a
U*	9.5	7.4	1.1	n/a
La*	0.8	0.9	bdl	n/a
Ce*	bdl	3.3	bdl	n/a
Nd*	bdl	6.1	bdl	n/a
Sm*	0.2	0.8	0.1	n/a
Eu*	0.1	0.1	0.1	n/a
Tb*	bdl	0.2	bdl	n/a
Yb*	bdl	0.4	bdl	n/a
Lu*	bdl	0.1	bdl	n/a

* - INAA (ppm) detection
bdl – Below Detection Limit
n/a – Not Analyzed

Appendix Table 2: XRF and INAA analyses of granitoids proximal to the Palermo #2 pegmatite. Sample designations are as follows: Concord granite: JNCOG-1 and JNCOG-2A; Bethlehem granodiorite: JNBG-1A and JNBG-2; Kinsman quartz monzonite: JNKQM-A.

Sample #	JNCOG-1	JCOG-2A	JNBG-1A	JNBG-2	JNKQM-A
SiO_2 (wt. %)	72.27	75.90	64.15	63.33	67.43
TiO_2	0.26	0.16	0.94	1.00	0.72
Al_2O_3	15.03	14.87	16.09	16.20	15.95
Fe_2O_3	1.59	1.04	6.24	6.69	4.56
FeO	bdl	bdl	bdl	bdl	bdl
MnO	0.03	0.01	0.09	0.08	0.06
MgO	0.36	0.25	1.70	1.73	1.43
CaO	0.59	1.02	2.94	2.71	1.57
Na_2O	3.39	2.93	2.69	2.68	2.52
K_2O	4.99	2.41	3.49	3.65	4.23
P_2O_5	0.18	0.14	0.23	0.20	0.21
L.O.I.	1.24	1.41	0.83	1.23	1.38
Totals	99.93	100.14	99.39	99.51	100.06
Rb (ppm)	204	62	133	135	158
Cs*	2.4	2.3	5.7	5.5	4.3
Sr	270	267	170	164	135
Ba	823	396	755	826	693
Sc*	1.3	2.7	16.9	17.9	5.7
V	14	bdl	99	105	81
Cr	bdl	bdl	55	45	34
Co	bdl	bdl	18	20	13
Ni	bdl	bdl	19	20	19
Cu	bdl	4	20	18	22
Zn	54	17	101	102	79
Ga	25	19	24	26	21
As	bdl	bdl	bdl	bdl	bdl
Y	31	19	52	53	35
Zr	126	71	313	329	219
Nb	6	8	17	20	18
Mo*	bdl	7.3	bdl	bdl	6.5
Sn	bdl	bdl	bdl	bdl	bdl
Sb*	0.1	bdl	bdl	bdl	0.4
Hf*	3.1	2.0	10.5	9.5	4.8
Ta*	0.4	2.1	1.3	1.1	1.1
W	bdl	bdl	bdl	bdl	bdl
Pb	44	34	18	18	25
Tl	bdl	bdl	bdl	bdl	bdl
Th*	12.0	4.8	20.3	17.4	15.0
U*	1.9	6.9	1.6	2.2	4.9
La*	41.4	22.4	56.8	63.2	36.1
Ce*	73.6	40.6	119.3	118.9	68.2
Nd*	24.3	17.5	50.2	55.3	28.1
Sm*	5.2	2.0	11.8	12.7	4.4
Eu*	0.7	0.8	2.0	1.9	1.0
Tb*	0.3	0.4	1.6	1.6	0.4
Yb*	0.2	0.8	4.8	3.6	1.4
Lu*	0.1	0.2	0.6	0.5	0.2

* - INAA (ppm) detection
bdl – Below Detection Limit

Appendix Table 3: XRF and INAA analyses of the host rock (Littleton schist) of the Palermo #2 pegmatite. Sample designations are as follows: JNLS-1A – collected 12 m from hanging wall contact; JNLS-2A – collected 1 m from hanging wall contact; JNLS-3A – collected at hanging wall contact; JNLS-4A – collected 10 m from footwall contact; JNLS-5 – collected 1 m from footwall contact; JNLS-7 – Littleton schist from Palermo #1 contact.

Sample #	JNLS-1A	JNLS-2A	JNLS-3A	JNLS-4A	JNLS-5	JNLS-7
SiO_2 (wt. %	63.77	62.60	62.36	62.63	76.54	73.25
TiO_2	0.87	0.94	0.83	1.01	0.59	0.61
Al_2O_3	17.39	17.39	17.69	18.27	9.44	13.08
Fe_2O_3	6.66	7.24	6.37	7.08	3.57	4.22
FeO	bdl	bdl	bdl	bdl	bdl	bdl
MnO	0.14	0.11	0.18	0.09	0.04	0.08
MgO	2.46	2.47	2.60	2.25	1.13	1.36
CaO	0.39	0.33	0.61	0.30	0.18	0.33
Na_2O	1.17	1.21	0.40	1.23	0.25	1.09
K_2O	3.76	4.20	5.14	3.66	2.82	3.85
P_2O_5	0.15	0.13	0.47	0.13	0.15	0.25
L.O.I.	2.65	3.08	2.93	3.18	2.26	2.14
Totals	99.41	99.70	99.59	99.83	96.96	100.27
Rb (ppm)	165	242	327	135	152	371
Cs	13.9*	18.9*	25.7*	7.5*	14.8*	54
Sr	85	98	32	109	20	22
Ba	566	637	609	579	296	192
Sc*	17.1	18.1	16.3	18.3	8.4	10.9
V	120	128	117	131	69	75
Cr	138	160	135	139	114	87
Co	20	25	22	22	10	12
Ni	58	74	74	50	34	36
Cu	9	9	8	15	bdl	4
Zn	101	130	127	101	57	113
Ga	24	22	23	27	9	13
As	28	bdl	bdl	bdl	bdl	bdl
Y	44	54	60	44	36	60
Zr	188	269	157	243	287	213
Nb	13	19	12	22	11	11
Mo*	bdl	13.0	bdl	bdl	bdl	bdl
Sn	bdl	bdl	22	bdl	bdl	bdl
Sb*	bdl	bdl	bdl	bdl	bdl	bdl
Hf*	5.5	7.6	4.6	6.6	9.7	7.1
Ta*	1.2	1.2	1.2	1.4	0.9	1.2
W	bdl	bdl	bdl	bdl	bdl	bdl
Pb	19	16	bdl	19	bdl	bdl
Tl	bdl	bdl	bdl	bdl	bdl	bdl
Th*	12.1	13.9	10.0	12.7	7.2	7.5
U*	3.1	12.0	4.4	2.8	2.4	3.5
La*	46.8	49.8	38.8	45.0	27.3	27.8
Ce*	90.3	98.6	77.8	90.3	54.9	56.6
Nd*	27.7	37.6	18.8	22.1	25.5	19.6
Sm*	7.9	8.0	6.8	7.8	4.9	5.3
Eu*	1.4	1.6	1.3	1.6	0.9	0.8
Tb*	1.2	1.2	0.8	1.1	0.7	0.6
Yb*	3.6	3.6	2.9	3.5	2.6	2.5
Lu*	0.5	0.6	0.5	0.5	0.4	0.4

* - INAA (ppm) detection
bdl – Below Detection Limit

Vita

Jim Nizamoff was born in Putnam, Connecticut on December 13, 1971. After discovering his mother's college introductory geology rock and mineral set at the age of 7, it became clear that he would be forever afflicted with a chronic case of mineral fever. Jim graduated from Putnam High School in 1990 and decided to attend the University of Maine at Farmington (UMF) to attain an undergraduate degree in geology. While attending UMF, Jim learned about a short course on granitic pegmatites offered by Dr. Michael Wise of the Smithsonian Institution. During the short course, Jim realized that pegmatites are by far the coolest rocks and decided that he should study them in greater detail. After completing his undergraduate degree in geology/chemistry at the University of Maine at Farmington in 1996, Jim came to UNO to pursue a master's degree in pegmatology. Skip Simmons provided Jim the opportunity to work on the Palermo #2 pegmatite in North Groton, NH. With the assistance of Bob Whitmore of Weare, NH (owner of the Palermo #2), Jim began his master's research in the summer of 1997. In addition to his master's project, Jim took full advantage of opportunities to work on many other research projects; attend numerous international scientific meetings and field trips: Madagascar (1998 and 2001), Brazil (2000), Namibia (2003) and Italy (2005); and work part-time as a petrologist/mineralogist at Crescent Technology, Inc. in Belle Chasse, LA. Finally, nearly ten years after he arrived in New Orleans, Jim received his Master of Science in Geology from the University of New Orleans in August 2006.